

Manuscript Number: JCIS-18-1315R1

Title: Controllable internal mixing in coalescing droplets induced by the solutal Marangoni convection of surfactants with distinct headgroup architectures

Article Type: Full length article

Section/Category: B. Surfactants and Soft Matter

Keywords: Marangoni flow; convection; mixing; coalescence

Corresponding Author: Professor Kendra A. Erk, PhD

Corresponding Author's Institution: Purdue University

First Author: Jerome J Nash

Order of Authors: Jerome J Nash; Patrick T Spicer, PhD; Kendra A Erk, PhD

Abstract: Through several complementary experiments, an investigation of the bulk and interfacial flows that emerged during the coalescence of two water-in-oil droplets with asymmetric compositional properties was performed. By adding surfactant to one of the coalescing droplets and leaving the other surfactant-free, a strong interfacial tension gradient (i.e., solutal Marangoni) driving energy between the merging droplets generated pronounced internal mixing. The contributions of two distinct types of surfactant, anionic ammonium lauryl sulfate (ALS) and cationic cetyltrimethylammonium bromide (CTAB) on the rate of coalescence bridge expansion and on the generation of opposing flows during coalescence were investigated. All coalescence experiments supported the power law relation between the radius of the expanding connective liquid bridge and time, $r_b \propto t^{1/2}$. However, the presence of surfactant decreased the magnitude of the prefactor in this relationship due to induced interfacial solutal Marangoni convection. Experiments showed that packing efficiency, diffusivity, and bulk concentration of the selected surfactant are vital in solutal Marangoni convection and thus the degree and timescale of internal mixing between merging droplets, which has yet to be adequately discussed within the literature. Denser interfacial packing efficiency and lower diffusivity of CTAB produced stronger opposing bulk and interfacial flow as well as greater bulk mixing. A discussion of how optimized surfactant selection and solutal Marangoni convection can be used for passively inducing convective mixing between coalescing drops in microfluidic channels when viscosity modulation is not feasible is provided.



SCHOOL OF MATERIALS ENGINEERING

June 4, 2018

Dear Prof. Boyd,

This letter accompanies the revised submission of our manuscript entitled, “Controllable internal mixing in coalescing droplets induced by the solutal Marangoni convection of surfactants with distinct headgroup architectures” by Jerome J. Nash, Patrick T. Spicer, and myself, which we are submitting for consideration as a research paper in the *Journal of Colloids and Interface Science*.

This manuscript seeks to demonstrate that varying degrees of internal mixing between coalescing droplets can be passively induced through asymmetric droplet compositions and optimized surfactant selection. As is often observed in microfluidic experiments, encouraging mixing of immiscible fluids can be quite challenging due to the low Reynolds number flows encountered within microchannels. This unique hurdle is compounded when traditional methods for circumventing such difficulties (e.g., modulating bulk fluid viscosities) are not feasible due to various material constraints. This research therefore illustrates a simple alternative processing technique for encouraging pronounced internal mixing during droplet coalescence. Here, mixing between merging millimeter-scale water-in-oil drops was obtained by induced solutal Marangoni motion, and the development of opposing bulk and interfacial flows. Our experimental results indicated that interfacial packing efficiency, diffusivity, and bulk concentration of the selected surfactant are vital in solutal Marangoni flow and thus the degree and timescale of internal mixing obtained between merging droplets, which has yet to be adequately discussed within the literature.

Our new results are important to fundamental colloidal science because the physicochemical relationships elucidated here may aid both academic and industrial formulators that seek alternative techniques for passively encouraging mixing of fluid droplets in a surrounding immiscible fluid, when modulating bulk fluid viscosities is not a viable option. This manner of internal droplet mixing is directly relevant to many applications including microfluidic reactors and functional microparticle synthesis. A fundamental understanding of the governing criteria that would enable optimized surfactant selection and bulk mixing of coalescing drops obtained through solutal Marangoni flow may prove to be extremely useful in such applications.

This manuscript (including all contents) has not been published previously by any of the authors and is not under consideration for publication in another journal. All authors have seen and approved the submission of this manuscript. I will act as the corresponding author for all future communications. Please consider all figures for online publishing in color and black-and-white in print.

Sincerely,

Kendra A. Erk, Ph.D.
Assistant Professor of Materials Engineering

erk@purdue.edu, 765-494-4118

Responses to Reviewers

Point-by-Point Responses to Reviewers' Comments – Due June 20th, 2018

The authors would like to extend their sincerest appreciation to both the reviewer and the editor for their careful reading of the manuscript and for taking the time to provide insightful feedback on how the manuscript could be improved. Changes incorporated have been discussed here directly, and have also been highlighted in yellow within the revised text. With the following responses and updates to the manuscript, the authors hope that both the reviewer's and the editor's concerns have been sufficiently addressed. Again, thank you both very much for your time and helpful feedback. –JJN, PTS, and KAE

Reviewer #2: The paper "Controllable internal mixing in coalescing droplets induced by the solutal Marangoni convection of surfactants with distinct headgroup architectures" investigates the interfacial and bulk liquid droplet flows that occur when two droplets of symmetrical or asymmetrical compositions are coalesced. Due to the presence of surfactant, it is found that the gradient of interfacial tension induces Marangoni flows during coalescence, and these flows are imaged using a high-speed camera. Two surfactant systems are studied: ALS (anionic) and CTAB (cationic), and the differences in the flow patterns arising from these two types of surfactant are explained. It is found that the presence of surfactant modifies the prefactor in the power law scaling relation between the radius of the expanding liquid bridge and time. The authors posit that by selecting the optimum surfactant concentration with the desired properties i.e. head group architecture and diffusivity, microfluidic mixing techniques can be enhanced through these Marangoni flows. This is the most important and novel contribution of this paper. Although previous microfluidic mixing techniques have looked at surface tension gradients or viscosity gradients via temperature or other types of control, none have considered Marangoni convection as an effective mixing strategy. Overall, this manuscript is well written, with clear and concise language, and is very thorough. However, there are a number of clarifications and edits are required before publication, which are listed below:

1) Graphical abstract: The images on the right depict a planar interface. Can these be changed to depict curved interfaces, since this is the scenario of interest?

Response: We agree that illustrating curved interfaces would more accurately represent the scenario of interest. The graphical abstract in the revised manuscript has been updated to depict curved interfaces.

2) Introduction:

* Lines 32-33: While it is obvious that this is the main point of this paper, it would be interesting to know how there can be droplets with asymmetric properties in any of these applications. In most cases one would expect the surfactant to be present in one or the other phase and would be somewhat uniformly distributed among the droplets/ interfaces.

Response: One of the most advantageous applications of using the controlled coalescence of droplets with asymmetric properties is in the synthesis of functional nanoparticles. Recently, Frenz et al. [1] demonstrated that magnetic iron oxide nanoparticles could be precipitated in a highly reproducible reaction following the fusion of droplet pairs comprised of different reagents in a hydrodynamically coupled, single-nozzle microfluidic device. Controlled pairwise mixing of aqueous droplets in oil was produced by electrocoalescence and the droplets were prevented from fusing prematurely by using a surfactant that was essentially uniformly distributed at the interfaces of both droplets. The methodology developed by these researchers could be readily adapted to incorporate the findings of the present manuscript by isolating the surfactant to one of the inlet droplet flows, while leaving the other surfactant-free. Upon merging, Marangoni-induced flows would produce pronounced bulk mixing between the drops, reminiscent of those explored here. Moreover, enhanced control over the degree of mixing obtained between the drops at different timescales could be explored with the surfactant selection criteria discussed within this manuscript. This example has been added to the Summary and Conclusion section of the revised text (Lines 408-422) to provide additional relevance for interested readers.

* Line 33: Microfluidic reactors are not really an industrial application.

Response: The phrase that the reviewer is referring to has been rewritten to be more inclusive of other scientific areas of interest (pg. 3, Line 33)

* Line 48: Too few or none? If too few, which ones (cite)?

Response: To the best of the authors knowledge, no experimental studies have investigated the role of appropriate surfactant selection on the magnitude of opposing bulk and interfacial flows in the coalescence of droplets with asymmetric compositional properties in a surrounding fluid. This clarification has been provided in pg. 3, Line 48-50 of the revised manuscript.

* Line 51: Reference for Gibbs-Marangoni effect is recommended.

Response: A citation for the original mathematical analysis of solutal Marangoni instabilities established by Sternling & Scriven [2,3] has been added to pg. 3, Line 51-52 and the References section (refs. 19,20) of the revised manuscript.

* Line 54: 'induced' rather than 'imposed'.

Response: The word ‘imposed’ has been replaced by ‘induced’ in pg. 3, Line 54 of the revised manuscript.

* Line 67: Reference for nonuniform surfactant distribution is recommended.

Response: A relevant literature citation by D. T. Wasan [4] on the development of a non-uniformly distributed surfactant monolayers between two merging, surfactant-stabilized emulsion droplets has been added to pg. 4, Line 66-68 and the References section [ref. 21] of the revised text.

* Line 80: Nature of 'its' not 'is'.

Response: This correction has been added to pg. 4, Line 79 of the revised manuscript.

* Line 84: What does 'within surface tension-driven droplet coalescence' mean? Overall, this sentence should be reworded to improve readability.

Response: We agree with the confusing wording of this section of the manuscript and it has been rewritten in pg. 4, Lines 80-86 of the revised text.

* Line 92: It is unclear why the early-stage coalescence behavior is not being investigated. Has this already been studied before?

Response: Many detailed experimental and theoretical analyses have been performed regarding the early-stage coalescence phenomena of uniform liquid droplets both in air and an external liquid, [5–9]. However, fully developed mixing behaviors in the later stages of coalescence (i.e., several milliseconds following the onset of coalescence) are often a primary concern in microfluidic reactor applications. [1,10] Therefore, to aid in the design of such systems, the specific aims of this work were to (1) investigate the late-stage coalescence behavior of binary liquid droplets with an induced surfactant concentration gradient along the connective liquid bridge, and (2) illustrate how controlling equilibrium adsorption and solutal Marangoni motion through appropriate surfactant selection can encourage varying degrees of bulk fluid mixing. This clarification has been added to the revised manuscript (pg. 5, Lines 94-98).

3) Materials and Experimental methods:

* Materials - provide CAS numbers for all chemicals used.

Response: The CAS numbers for each material used are provided below, and have been incorporated into relevant areas of the revised manuscript. Medium-chain triglyceride Oil – CAS # 73398-61-5; cetyltrimethylammonium bromide – CAS # 57-09-0, chromatographic alumina CAS # 1344-28-1; hollow glass spheres, CAS # 65997-17-3

* How is the viscosity of the oil measured?

Response: The viscosity of the triglyceride oil was not measured directly in this study, but was reported by the manufacturer, Stepan Company, as 25 mPa·s at 25 °C in the accompanying Safety Data Sheet (SDS) upon purchasing the chemical. This clarification has been added to pg. 6, Line 114 of the revised manuscript.

* Where were the metal capillaries obtained from? Mention source.

Response: Metal capillaries (18-gauge x 1.0" Pink Blunt Tip Dispensing Fill Needles) were obtained from CML Supply, Lexington, KY. This corrected information has been incorporated into the text of the revised text (pg. 6, Lines 124-125).

* Figure 1: Indicate surfactants in left-most droplet in schematic.

Response: The schematic in Figure 1 has been revised to illustrate that surfactant was present in the leftmost droplet during coalescence studies.

* Line 132: The relevant data for determining the CMC's mentioned in this line are included in a section further into the manuscript. Consider mentioning that these will be referenced later in the manuscript.

Response: A sentence indicating that, "relevant data used in determining the CMC's for each surfactant is provided in Section 2.3" has been added to pg. 7, Line 141-142 of the revised manuscript.

* Line 152: Remove 'that' after 'force balance...'.

Response: This suggested revision has been incorporated into pg. 9, Line 167 of the revised manuscript.

* Lines 162-164: What were the literature values? Please mention them explicitly in the statement.

Response: The literature value for the CMC of ALS in aqueous solution at 25 °C has been reported as 6.25×10^{-3} mol L⁻¹ [11] and literature values for the CMC of CTAB have been reported as ranging from 0.9×10^{-3} mol L⁻¹ [12] to 1×10^{-3} mol L⁻¹. [13] These values have been added to the text of revised manuscript (pg. 10, Lines 179-181), accompanied with their corresponding references.

* Are the Marangoni-induced flows less pronounced if a surfactant concentration lower than the CMC is used in the surfactant-laden droplet?

Response: Yes, Marangoni-induced flows would be less pronounced for bulk concentrations far below the CMC in the case of coalescing droplets with asymmetric compositions. This is because as the bulk and interfacially adsorbed surfactant concentrations (simultaneously) approach zero in the surfactant-laden droplet, the timescale of solutal Marangoni convection, given by $\tau_M = \frac{\Gamma_m^2}{Dc^2}$, would also tend toward zero. For small solutal Marangoni convection timescales, gradients in the interfacial tension at the interface are short-lived, and relaxation toward an equilibrated state occurs rapidly. For longer timescales, interfacial tension gradients persist for extended periods, enabling pronounced opposing flows to develop between the interface (acting in the direction of high surfactant concentration to low interfacial tension) and the bulk (acting in the direction of high capillary pressure to low capillary pressure). Thus, the driving energy for Marangoni-induced flows would decrease for very dilute surfactant concentrations, as both the flows generated at the interface and within the bulk would be reduced. Supporting evidence for this mechanism can be found in the non-existent bulk and interfacial flows that developed in Figure 5a for droplets of the same initial diameter containing no surfactant in comparison to the pronounced flows that emerge for droplets with asymmetric solute composition in Figures 5b and 5c. This explanation has been added to the revised manuscript (pg. 7, Lines 142-146).

* Line 175: What does 'linear fit of the slope' mean? (the word 'slope' is confusing). Consider using 'linear fit of the portion of the curve near the point of interfacial saturation...' of the sloping region of the curve' or something similar.

Response: We agree with the confusing wording in this sentence. Thus, this portion of the text has been rewritten (pg. 10, Lines 189-192) to improve the overall readability of the revised manuscript.

* Table 1: How is the minimum area per molecule calculated?

Response: Substituting the slope value of the best-fitting straight line in the low surfactant concentration regime from the interfacial tension versus log of surfactant concentration curve for $\frac{dy}{d \log c}$ in the Gibbs adsorption equation, Γ_m was calculated for ALS and CTAB at the triglyceride oil-water interface. The minimum molecular area, A_{min} ($\text{\AA}^2 \text{ molecule}^{-1}$), was then determined from the equation, $A_{min} = \frac{1 \times 10^{20}}{\Gamma_m N_A}$, where N_A is Avogadro's number. This clarification has been added to the revised manuscript (pg. 10, Lines 192-193).

* Section 2.4: Why is the interfacial spreading velocity determined for a planar interface instead of a droplet? Would any difference be expected between the two? Please clarify.

Response: The motion of tracer particles was measured at a planar oil-water interface because this experimental scheme specifically enabled the measurement of Marangoni-induced flow rates under the effect of a surfactant concentration gradient at the oil-water interface. Ensuring that measured flow rates were obtained for tracer particles located solely at the oil-water interface and not within one of the subphases was most directly accomplished with a droplet coalescing with a planar oil-water interface. Moreover, isolating the initial motion of the 9-13 μm tracer particles caused by gravitational effects from the motion resulting from Marangoni-induced interfacial flows would be experimentally challenging from a droplet-droplet coalescence frame of reference, as the curvature of the droplet interfaces would cause the tracer particles to naturally migrate to a central point. The primary difference between the two experimental setups would be the direction of the generated bulk flow between the aqueous droplet and planar water reservoir upon coalescence. In the case of the droplet-planar interface study, the capillary pressure ratio, $\Delta P_2/\Delta P_1$ (where ΔP_1 and ΔP_2 are the capillary pressures for the surfactant-laden droplet and planar water reservoir, respectively), would approach zero due to the near infinite radius of curvature of the planar water reservoir. This would in turn produce a driving energy for bulk fluid motion to propagate from the surfactant-laden droplet into the surfactant-free, planar reservoir. This bulk fluid behavior stands in contrast to the bulk flows observed and quantified within the manuscript, where bulk fluid motion was driven from the surfactant-free droplet into the surfactant-laden droplet due to the capillary pressure gradient. However, Marangoni-induced interfacial flows always act in the direction of the interfacial solute concentration gradient [2] and occur on a shorter timescale than bulk flows. Thus, the measured values for the interfacial spreading velocities (i.e. the Marangoni-induced interfacial flowrates) would presumably be minimally influenced by bulk flows. This clarification has been added directly to the revised manuscript (pg. 11, Lines 201-206).

* Figure 3b: Indicate particles at the interface.

Response: A statement which explicitly states that particles exist at the interface under investigation has been incorporated into the caption for Figure 3b of the revised manuscript.

* Line 197: Would the slight aggregation have an effect on your measurements versus no aggregation? Please justify.

Response: Indeed, very large aggregates would be expected to display lower interfacial spreading velocities due to their larger mass in comparison to unaggregated primary particles and could therefore introduce some degree of uncertainty into the measured interfacial spreading velocity, which would increase with increasing aggregate size. However, the largest aggregates observed in this study consisted of 2-3 primary particles, and measurements of the steady-state, fully developed displacement rates for these aggregates were indistinguishable from the measured displacement rates of unaggregated, interfacially adsorbed primary particles. Care was taken to measure the interfacial spreading velocities of at least 5 distinct interfacially adsorbed tracer particles from two separate coalescence experiments for each system containing either CTAB or ALS. This justification has been added to the revised version of the manuscript (pg. 12, Lines 220-227).

4) Results and Discussion:

* Figure 4: Figure captions (in general) need to be more detailed. Please mention what is being plotted here. Define D_0 . etc.

Response: The caption of Figure 4 has been revised to provide additional information on what is being shown and the meaning of relevant parameter. The updated caption is provided below, as well as in the revised manuscript. Moreover, the captions for each figure in the manuscript have been revised to provide greater detail for the displayed data.

Figure 4. Kinetics of expansion for the connective bridge separating spherical droplets with an equivalent initial diameter, $2R$ (= 2 mm). The data represent the increase in the connective bridge diameter, D_b , relative to $2R$, as a function of the square-root-of-time, $t^{1/2}$, succeeding the onset of droplet coalescence.

* Line 226: Remove "in" from "...influenced by in the presence of ALS."

Response: This suggested revision has been incorporated into pg. 14, Line 254 of the revised text.

* What is the exact value of equilibrium interfacial tension in each of the surfactant-laden droplets? This is mentioned at the very end, but should to be stated earlier.

Response: At the chosen bulk concentration, the equilibrium interfacial tension of the oil-water interface was $3.40 \pm 0.48 \text{ mN m}^{-1}$ for ALS and $3.01 \pm 0.41 \text{ mN m}^{-1}$ for CTAB. These exact values were added to an earlier section of the revised manuscript (pg. 8, Lines 146-148).

* Again, not very clear why only the loading close to CMC is being studied. What happens at lower concentrations?

Response: For dilute surfactant solutions far below the CMC, the surfactant's chemical potential increases logarithmically, while near and above the CMC, the chemical potential of the surfactant negligibly changes, and as a result conditions at the interface do not change. [14] Thus, an initial bulk concentration near the CMC for the surfactant-laden droplet in this study was chosen because it approximates an interfacial monolayer near saturation equilibrium. Interfacial diffusional flows induced by the Marangoni effect were therefore anticipated to be highest near and above the CMC because the starting conditions of the surfactant-laden interface was near its equilibrium state. This clarification has been added to the revised text (pg. 7, Lines 142-146).

* Line 256: 'droplets', not 'droplet.

Response: This suggested revision has been incorporated into pg. 16, Line 275 of the revised text.

* What are the actual diameters used?

Response: The initial diameter of droplets in coalescence experiments with equally sized drops was 2 mm. To further aid in illustrating the marked influence of surfactant in the jetting behavior observed for binary droplet systems, the initial diameters of the two merging droplets were modulated by increasing the initial diameter of the leftmost droplet to 2.2 mm and decreasing the initial diameter of the rightmost droplet to 1.0 mm. These experimental parameters have been added to the revised manuscript in pg. 7, Lines 130-131 and pg. 17, Lines 296-298.

* Figure 6 caption: Caption needs to be reworded slightly. In the plain water case, there is no surfactant in the leftmost droplet.

Response: The caption of Figure 6 has been revised to reflect the appropriate compositions for each droplet.

* Figure 7: Mention what the scale bars represent in the caption

Response: The caption for Figure 7 has been revised to include an explicit statement that describes the length of the scale bars in each image.

* Section 3.3: What is the reason, according to the authors, for the presence of the Rayleigh-Taylor-like instability in the CTAB case? A short discussion on this interfacial instability would be extremely helpful.

Response: The variation in the shape of the jetted fluid stemmed from the magnitudes of the convective mixing that was generated by the opposing bulk and interfacial flows during droplet coalescence. As the fluid from the dyed droplet flowed through the coalescence neck, an interfacial diffusional flux developed in the opposite direction, as interfacially adsorbed surfactant molecules in the surfactant-laden droplet migrated from regions of high concentration to low concentration. This in turn generated eddy currents within the bulk of the merging droplets, just beneath the interface. In the case of CTAB, the driving energy for interfacial flux appeared to be sustained for a longer time than in the case of ALS, which led to more pronounced eddy currents and the observed jetting behavior. This explanation for the observed jetting behavior in the case of CTAB has been added to the revised text (pg. 19, Lines 314-324).

* Line 369 : "This behavior matches what would be expected of each system..."

Response: This sentence has been rewritten to improve clarity both below, as well as in the revised manuscript (pg. 24, Lines 402-404).

These calculations for the characteristic timescales of interfacial deformation under and induced surfactant concentration gradient provide additional evidence that ALS molecules express a lower driving force for solutal Marangoni-driven convection in comparison to CTAB molecules.

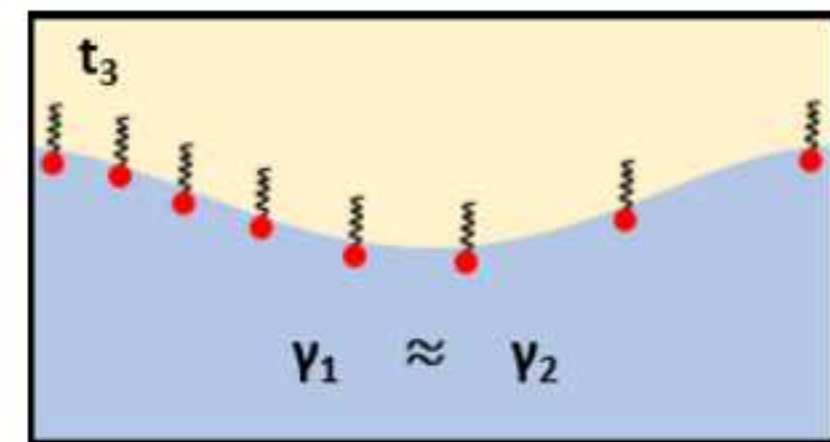
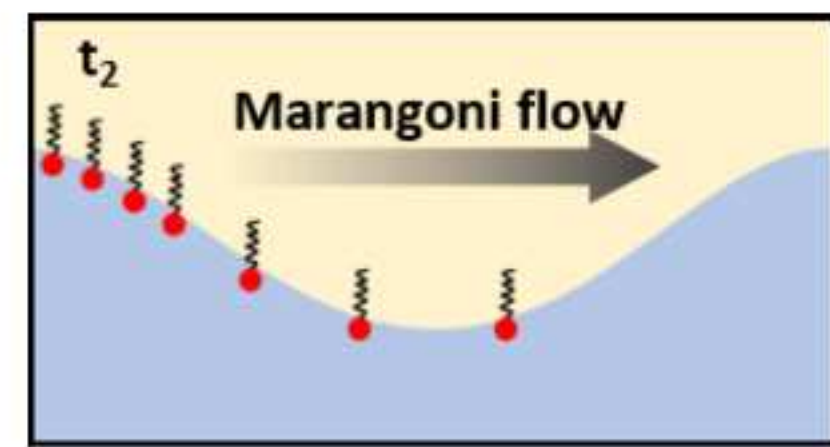
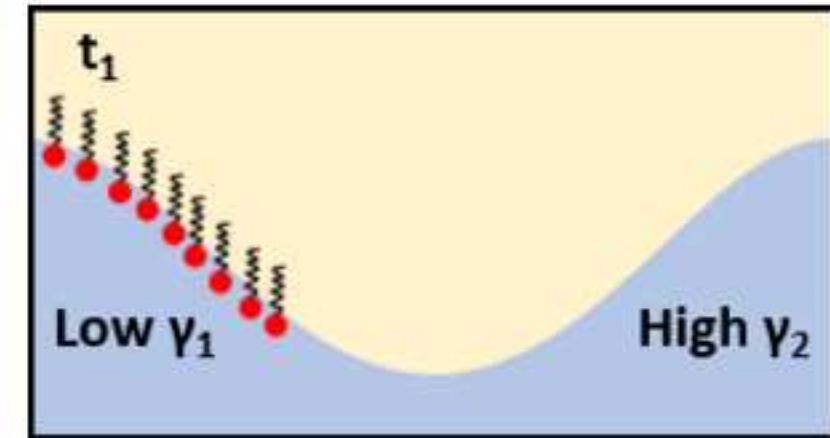
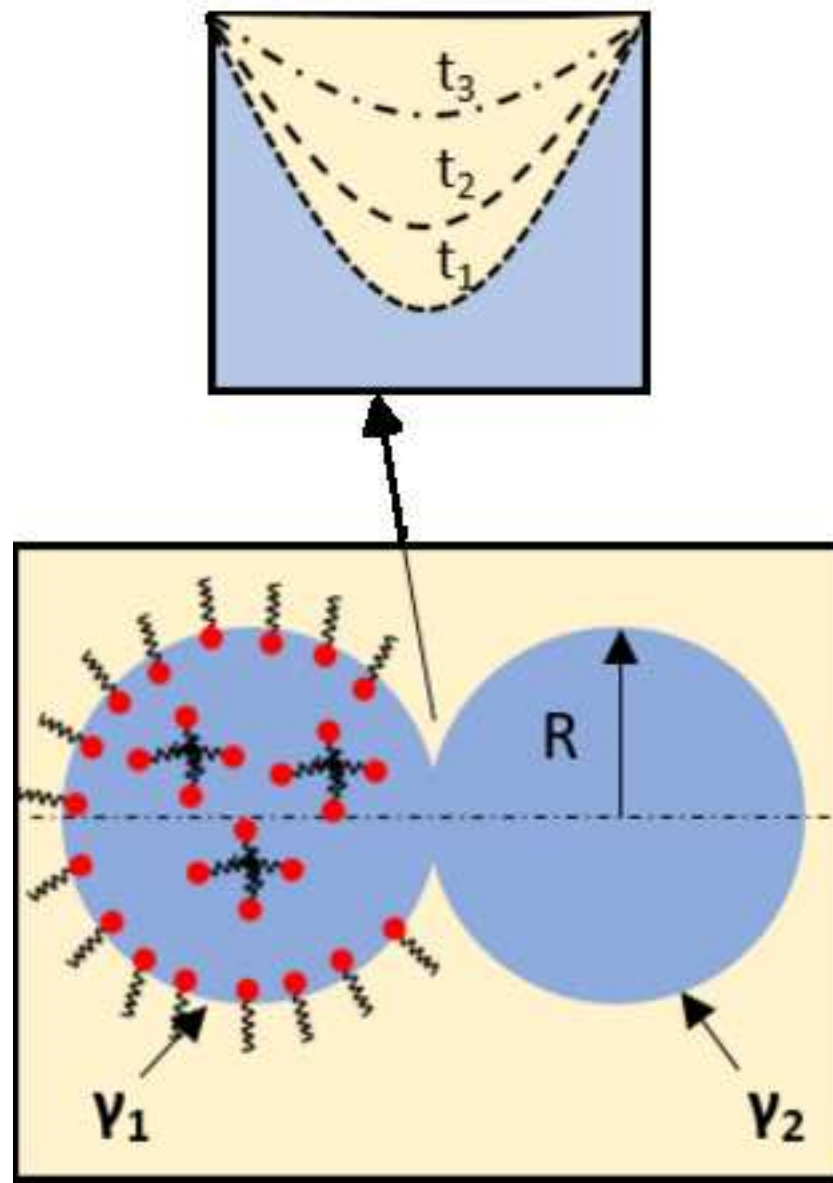
* Does the approach velocity affect the observed behavior?

Response: In the present study, the approach velocity did not affect the observed coalescence behavior. Droplets were made to contact at very low approach velocities ($\sim 0.01 \text{ mm s}^{-1}$), and droplet merging did not occur immediately after the liquid droplets made contact. A residence time of 2-3 seconds for ALS and 8-10 seconds for CTAB was observed, which suggests that film drainage preceded coalescence, a well-known phenomenon in the literature. [4] Based on the three reproducibility experiments that were performed for every binary droplet coalescence experiment, neck expansion and fluid jetting all displayed consistently reproducible results. A discussion on the non-effect of droplet approach velocity has been added to pg. 7, Lines 132-133 of the revised text.

REFERENCES

- [1] L. Frenz, A. El Harrak, M. Pauly, S. Bégin-Colin, A.D. Griffiths, J.C. Baret, Droplet-based microreactors for the synthesis of magnetic iron oxide nanoparticles, *Angew. Chemie - Int. Ed.* 47 (2008) 6817–6820. doi:10.1002/anie.200801360.
- [2] C. V. Sternling, L.E. Scriven, Interfacial turbulence: Hydrodynamic instability and the marangoni effect, *AIChE J.* 5 (1959) 514–523. doi:10.1002/aic.690050421.
- [3] L.E. Scriven, C. V. Sternling, The Marangoni Effects, *Nature.* 187 (1960) 186–188. doi:10.1038/187186a0.
- [4] D.T. Wasan, Destabilization of Water-in-Oil Emulsions, in: *Emuls. - A Fundam. Pract. Approach*, 1992: pp. 283–295.
- [5] J.D. Paulsen, Approach and coalescence of liquid drops in air, *Phys. Rev. E - Stat. Nonlinear, Soft Matter Phys.* 88 (2013) 1–13. doi:10.1103/PhysRevE.88.063010.
- [6] J. Qian, C.K. Law, Regimes of coalescence and separation in droplet collision, *J. Fluid Mech.* 331 (1997) 59–80.
- [7] J.D. Paulsen, R. Carmignani, A. Kannan, J.C. Burton, S.R. Nagel, Coalescence of bubbles and drops in an outer fluid, *Nat. Commun.* 5 (2014) 3182. doi:10.1038/ncomms4182.
- [8] J. Eggers, J.R. Lister, H.A. Stone, Coalescence of Liquid Drops, (1999) 1–37. doi:10.1017/S002211209900662X.
- [9] L. Duchemin, J. Eggers, C. Josserand, Inviscid coalescence of drops, *J. Fluid Mech.* 487 (2003) 167–178. doi:10.1017/S0022112003004646.
- [10] A.M. Huebner, C. Abell, W.T.S. Huck, C.N. Baroud, F. Hollfelder, Monitoring a reaction at submillisecond resolution in picoliter volumes, *Anal. Chem.* 83 (2011) 1462–1468. doi:10.1021/ac103234a.
- [11] K.H. Kang, H.U. Kim, K.H. Lim, Effect of temperature on critical micelle concentration and thermodynamic potentials of micellization of anionic ammonium dodecyl sulfate and cationic octadecyl trimethyl ammonium chloride, *Colloids Surfaces A Physicochem. Eng. Asp.* 189 (2001) 113–121. doi:10.1016/S0927-7757(01)00577-5.
- [12] V. Mosquera, J.M. Del Río, D. Attwood, M. García, M.N. Jones, G. Prieto, M.J. Suarez, F. Sarmiento, A study of the aggregation behavior of hexyltrimethylammonium bromide in aqueous solution, *J. Colloid Interface Sci.* 206 (1998) 66–76. doi:10.1006/jcis.1998.5708.
- [13] T.G. Movchan, A.I. Rusanov, I. V Soboleva, N.R. Khlebunova, E. V Plotnikova, A.K. Shchekin, Diffusion Coefficients of Ionic Surfactants, *Colloid J.* 77 (2015) 492–499. doi:10.1134/S1061933X15040146.

[14] D.F. Evans, H. Wennerström, *The Colloidal Domain: Where Physics, Chemistry, Biology, and Technology Meet*, 2nd ed., 1999.



1 **Controllable internal mixing in coalescing droplets induced by the solutal Marangoni**
2 **convection of surfactants with distinct headgroup architectures**

3 Jerome J. Nash^a, Patrick T. Spicer^b, and Kendra A. Erk^{a*}

4 a. School of Materials Engineering, Purdue University, West Lafayette, IN 47907, USA;

5 b. School of Chemical Engineering, The University of New South Wales, Sydney 2052, Australia

6 *corresponding author, Email: erk@purdue.edu, Phone: (765) 494-4118

7 **Keywords:** Marangoni flow; convection; mixing; coalescence

8 **Abstract**

9 Through several complementary experiments, an investigation of the bulk and interfacial
10 flows that emerged during the coalescence of two water-in-oil droplets with asymmetric
11 compositional properties was performed. By adding surfactant to one of the coalescing droplets
12 and leaving the other surfactant-free, a strong interfacial tension gradient (i.e., solutal
13 Marangoni) driving energy between the merging droplets generated pronounced internal mixing.

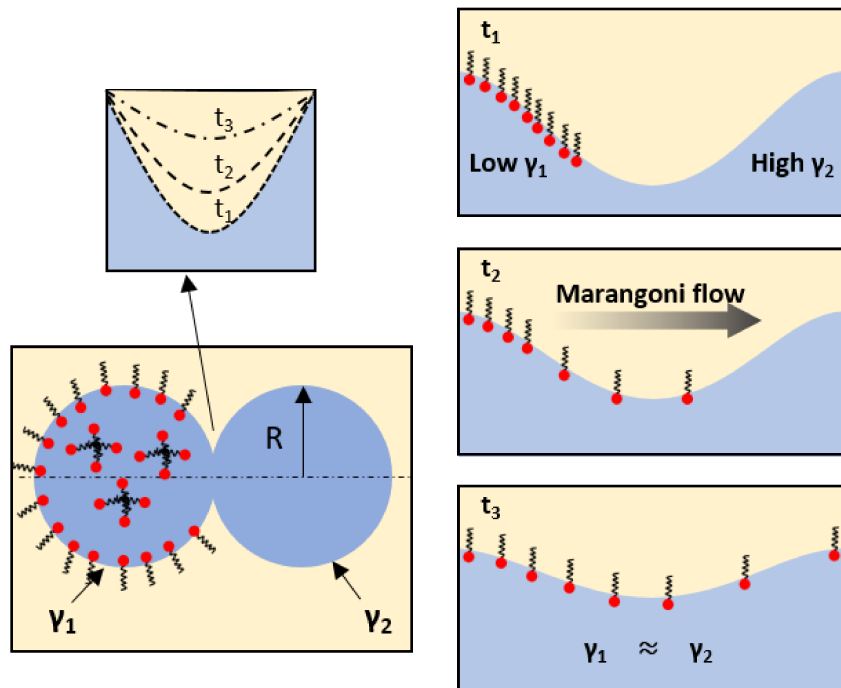
14 The contributions of two distinct types of surfactant, anionic ammonium lauryl sulfate (ALS) and
15 cationic cetyltrimethylammonium bromide (CTAB) on the rate of coalescence bridge expansion

16 and on the generation of opposing flows during coalescence were investigated. All coalescence
17 experiments supported the power law relation between the radius of the expanding connective
18 liquid bridge and time, $r_b \propto t^{1/2}$. However, the presence of surfactant decreased the magnitude of
19 the prefactor in this relationship due to induced interfacial solutal Marangoni convection.

20 Experiments showed that packing efficiency, diffusivity, and bulk concentration of the selected
21 surfactant are vital in solutal Marangoni convection and thus the degree and timescale of internal
22 mixing between merging droplets, which has yet to be adequately discussed within the literature.

23 Denser interfacial packing efficiency and lower diffusivity of CTAB produced stronger opposing

1
2
3
4 24 bulk and interfacial flow as well as greater bulk mixing. A discussion of how optimized
5 surfactant selection and solutal Marangoni convection can be used for passively inducing
6
7 25 convective mixing between coalescing drops in microfluidic channels when viscosity modulation
8
9 26 is not feasible is provided.
10
11
12



39 28 **Graphical Abstract**
40
41

42 29 **1. Introduction**
43
44

45 30 The coalescence of two identical droplets, and the corresponding bulk fluid flows that
46
47 31 emerge, has been studied at length in the literature. [1–5] However, far less attention has been
48
49 32 given to the coalescence of binary droplets with asymmetric physical properties, despite its
50
51 33 importance to many industrial and research applications including enhanced oil recovery [6],
52
53 34 emulsification [7], microfluidic reactors [8], and functional microparticle fabrication. [9–11]
54
55
56
57
58
59
60
61
62
63
64
65

1
2
3
4 35 Many additional examples can be found in the literature of microfluidic applications that
5
6 36 utilize the coalescence of droplets as a vital processing step in material fabrication. However,
7
8 37 mixing immiscible phases in microfluidic devices often proves difficult because of the low
9
10 38 Reynolds number flows encountered within microchannels. Several researchers have shown that
11
12 39 the combination of immiscible fluids in microchannels can be improved with modified channel
13
14 40 designs [12–14] or, quite often, by modulating the viscosity of one or both of the coalescing
15
16 41 fluids to achieve desired bulk convective mixing. [15,16] While several detailed coalescence
17
18 42 studies have investigated the effects of variable external oil phase viscosity on the generation of
19
20 43 bulk flows in coalescing water droplets [17,18], little attention was given to the potential
21
22 44 influence of polar surfactant headgroup architecture in the generation of the observed opposing
23
24 45 interfacial and bulk flows. Moreover, altering the viscosities of the bulk fluids is not always a
25
26 46 viable option in microfluidic applications (for example, when high throughput is a processing
27
28 47 requirement, or when a system is restricted to fluids with predetermined viscosities). Thus,
29
30 48 additional routes for inducing a similar degree of internal mixing under these restrictions are
31
32 49 necessary, and currently, no experimental studies in the literature have sought to provide insight
33
34 50 into how appropriate surfactant selection can influence this phenomenon.

44 51 Utilizing solutal Marangoni convection, also known as the Gibbs-Marangoni effect,
45
46 52 [19,20] provides a compelling avenue for inducing desired bulk flows in coalescing binary fluid
47
48 53 systems, without the need for modulating bulk fluid viscosity. The Gibbs-Marangoni effect can
49
50 54 be induced simply by adding a dilute concentration of a highly surface-active solute to one of the
51
52 55 fluid droplets, while keeping the second drop initially free of any surfactant, then bringing the
53
54 56 droplets into contact. When the two fluid droplets coalesce, a highly curved connective liquid
55
56 57 bridge forms between them and expands rapidly due to interfacial stresses. In the inertial regime,
58
59
60
61
62
63
64
65

1
2
3
4 58 a scaling relation derived from a simple physical argument can be used to describe the expansion
5
6 59 of the coalescence bridge. [4] This scaling law predicts linear proportionality between the radius
7
8 60 of the connective liquid bridge, r_b ($= D_b/2$), and the square root of the coalescence time, $t^{1/2}$,
9
10 61 given by the equation, $D_b/2 \propto (R\gamma/\rho_{out})^{1/4}t^{1/2}$, where R is the initial drop radius, γ is the
11
12 62 interfacial tension, and ρ_{out} is the density of the outer fluid.
13
14
15
16

17 63 As bridge expansion proceeds, the resulting fluid motion acts to pull the droplets together
18
19 64 to form a single, larger drop. However, in the presence of an induced surface tension (i.e.,
20
21 65 surfactant concentration) gradient between the droplets, opposing interfacial and bulk flows can
22
23 66 emerge. This is because surfactant molecules become nonuniformly distributed at the interface
24
25 67 along the highly curved, connective liquid bridge separating the surfactant-laden and surfactant-
26
27 68 free drops. [21] Relaxation to a homogenous surfactant coverage does not proceed primarily by
28
29 69 diffusion, but by a far more rapid process (i.e., the Gibbs-Marangoni effect) where the surfactant
30
31 70 molecules at the interface swiftly migrate toward regions of highest local interfacial tension. This
32
33 71 in turn generates interfacial motion in the direction of the surfactant concentration gradient that
34
35 72 acts tangentially to the merging droplets, which is accompanied by bulk motion in the adjacent
36
37 73 fluid layers. Consequently, bulk flows which drive the droplets together under the influence of a
38
39 74 favorable reduction in capillary pressure, $\Delta P = 2\gamma/R$, become unbalanced with interfacial flows.
40
41 75 This ultimately results in opposing interfacial and bulk convective motion and can lead to
42
43 76 pronounced bulk fluid mixing.
44
45
46
47
48
49
50
51

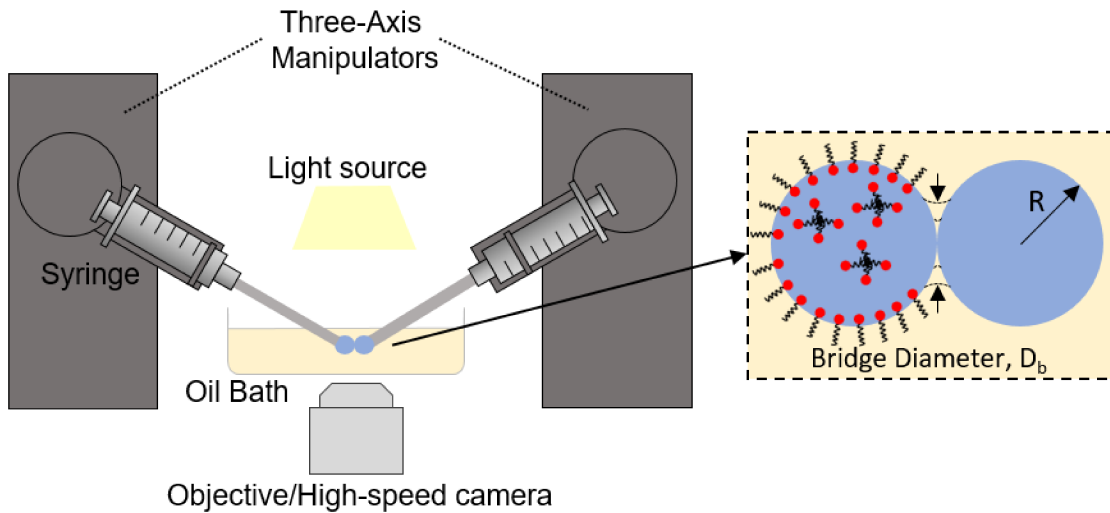
52 77 It has been shown that the mobility [22], as well as the degree of equilibrium interfacial
53
54 78 adsorption of low molecular weight surfactants [23,24], can vary substantially depending on the
55
56 79 nature of the surfactant's polar headgroup in a polar solvent such as water (i.e., whether it is
57
58 80 anionic, cationic, nonionic, or zwitterionic). These interfacial characteristics are also well-known
59
60
61
62
63
64
65

1
2
3
4 81 to have demonstrated importance in the occurrence of film rupture and coalescence for
5
6 82 surfactant-laden fluid interfaces. [25,26] Therefore, it would stand to reason that strategically
7
8 83 modulating the interfacial mobility, equilibrium saturation adsorption, and adsorption-desorption
9
10 84 kinetics of the added surfactant would enable interested parties to control coalescence related
11
12 85 phenomena, such as passively-induced internal mixing between emulsion droplets in the
13
14 86 presence of a surfactant concentration gradient. Optimized design of such small-scale processes
15
16 87 will require the ability to identify appropriate surfactants based on their physicochemical
17
18 88 properties and performance in applications like diagnostic chips and other microfluidics systems.
19
20 89 Thus, this work seeks to demonstrate several key mechanisms relating the adsorption of two
21
22 90 oppositely charged ionic surfactants and the manifested solutal Marangoni flows that drive bulk
23
24 91 mixing between coalescing aqueous droplets in a viscous surrounding oil. Generalized
25
26 92 relationships between the interfacial properties of low molecular weight surfactant and their
27
28 93 potential influence on bulk coalescing phenomena are also provided.
29
30
31
32
33
34
35
36
37 94 Many detailed experimental and theoretical analyses have been performed which
38
39 95 elucidate early-stage coalescence phenomena of uniform liquid droplets both in air and an
40
41 96 external liquid. [1–5] However, fully developed mixing behaviors in the later stages of
42
43 97 coalescence (i.e., several milliseconds following the onset of coalescence) are often a primary
44
45 98 concern in microfluidic reactor applications. [8,27] Therefore, to aid in the design of such
46
47 99 systems, the specific aims of this work were to (1) investigate the late-stage coalescence
50
51 100 behavior of binary liquid droplets with an induced surfactant concentration gradient along the
52
53 101 connective liquid bridge, and (2) illustrate how controlling equilibrium adsorption and solutal
54
55 102 Marangoni motion through appropriate surfactant selection can encourage varying degrees of
56
57 103 bulk fluid mixing. Through several complementary experiments, including equilibrium
58
59
60
61
62
63
64
65

36
37 94 Many detailed experimental and theoretical analyses have been performed which
38
39 95 elucidate early-stage coalescence phenomena of uniform liquid droplets both in air and an
40
41 96 external liquid. [1–5] However, fully developed mixing behaviors in the later stages of
42
43 97 coalescence (i.e., several milliseconds following the onset of coalescence) are often a primary
44
45 98 concern in microfluidic reactor applications. [8,27] Therefore, to aid in the design of such
46
47 99 systems, the specific aims of this work were to (1) investigate the late-stage coalescence
50
51 100 behavior of binary liquid droplets with an induced surfactant concentration gradient along the
52
53 101 connective liquid bridge, and (2) illustrate how controlling equilibrium adsorption and solutal
54
55 102 Marangoni motion through appropriate surfactant selection can encourage varying degrees of
56
57 103 bulk fluid mixing. Through several complementary experiments, including equilibrium
58
59
60
61
62
63
64
65

1
2
3
4 104 surfactant adsorption measurements, high-speed image processing, and concentration gradient-
5
6 105 induced interfacial velocity measurements via particle tracking, we provide new insights into the
7
8 106 fundamental relationships between optimized surfactant selection and bulk fluid mixing.
9
10 107 Considering that the adsorption and interfacial spreading behavior of surfactants can vary
11
12 108 dramatically depending on the electrostatic interactions of the surfactant present at the fluid
13
14 109 interface in the bulk aqueous solution [28], detailed investigations which further elucidate the
15
16 110 role of surfactant selection in the development of varying degrees of opposing flows within
17
18 111 coalescing binary droplets are essential.
19
20
21
22
23
24 112 **2. Materials and Experimental Methods**
25
26
27 113 *2.1. Materials*
28
29
30
31 114 The external liquid phase used during drop coalescence measurements was a triglyceride
32
33 115 oil (Stepan Company, **CAS # 73398-61-5**) with a **manufacturer reported viscosity of 25 mPa·s**
34
35 116 **and density of 0.95 g cm⁻³**, both at 25 °C. The oil was double-filtered through a chromatography
36
37 117 column containing alumina (Fisher, **CAS # 1344-28-1**) to remove trace surface-active impurities
38
39 118 prior to use. The droplets consisted of aqueous solutions prepared with water passed through a
40
41 119 Filmtec™ reverse osmosis membrane (total dissolved solids ≤ 15 ppm, Dow Chemical
42
43 120 Company). The two commercially available surfactants used in this study, ammonium lauryl
44
45 121 sulfate, ALS (anionic surfactant, 30% in water, **CAS # 2235-54-3**) and cetyltrimethylammonium
46
47 122 bromide, CTAB (cationic surfactant, ≥ 99%, **CAS # 57-09-0**), were obtained from Sigma-
48
49 123 Aldrich and used without further purification. The blue dye added to the surfactant-free droplet
50
51 124 in each binary droplet coalescence measurement as an aid for visualizing bulk motion was
52
53 125 purchased from Queen Fine Foods Pty Ltd. **The flat metal capillaries (18-gauge x 1.0" blunt tip**
54
55
56 126 **dispensing needles)** used in droplet coalescence experiments were obtained from CML Supply.
57
58
59
60
61
62
63
64
65

1
2
3
4 127 2.2. Visualizing rapid binary drop coalescence
5
6
7
8
9
10
11
12
13
14
15
16
17
18
19
20
21
22
23
24



25 **Figure 1.** An illustration of the experimental setup used to study coalescence phenomena between binary aqueous
26 droplets in a surrounding oil. The leftmost aqueous droplet was laden with surfactant and the rightmost droplet was
27 surfactant-free, yet contained a small concentration of dye to aid in flow visualization.

28 128 A schematic of the experimental setup used for visualizing binary liquid droplet
29 129 coalescence is shown in Figure 1. Experiments were performed using a pair of three-axis
30 130 micromanipulators (Sensapex) secured to z-axis translational stages (THORLABS) flanking an
31 131 inverted optical microscope (AE31, Motic Microscopes). Two water droplets with asymmetric
32 132 compositional properties, each having an initial diameter of 2 mm (unless otherwise specified)
33 133 were formed at the tips of 18-gauge metal capillaries and were made to contact at negligible
34 134 approach velocities ($\sim 0.01 \text{ mm s}^{-1}$) in a clear petri dish containing the low viscosity triglyceride
35 135 oil (5 mL working volume). Coalescence of the binary droplets was captured with a high-speed
36 136 camera (Phantom v7.3) at 11000 frames per second. Measurements of the bridge expansion
37 137 kinetics were performed via image processing using open-source ImageJ software. [29]

38 138 A concentration gradient along the connective liquid between the two merging water

39 139 drops was generated by adding the surfactant of interest to the leftmost coalescing droplet
40 140 (Figure 1), while keeping the rightmost droplet surfactant-free. The surfactant-loaded droplet in

41
42
43
44
45
46
47
48
49
50
51
52
53
54
55
56
57
58
59
60
61
62
63
64
65

1
2
3
4 141 each experiment contained either ALS or CTAB at a concentration of 2.5×10^{-3} mol L⁻¹, which
5
6 142 was near the experimentally determined critical micelle concentration (CMC) for each surfactant
7
8 143 type. The relevant data used in determining the CMC for each surfactant is provided in Section
9
10 144 2.3. This initial bulk surfactant concentration was chosen because near and above the CMC, the
11
12 145 chemical potential of the surfactant negligibly changes and as a result conditions at the interface
13
14 146 do not change. [30] Thus, the surfactant-laden droplet interface in this experimental setup
15
16 147 represents an interfacial monolayer near saturation equilibrium. At the chosen bulk
17
18 148 concentration, the equilibrium interfacial tension of the oil-water interface was 3.40 ± 0.48 mN
19
20 149 m⁻¹ for ALS and 3.01 ± 0.41 mN m⁻¹ for CTAB, as determined by the drop shape analysis
21
22
23 150 technique (Section 2.3).

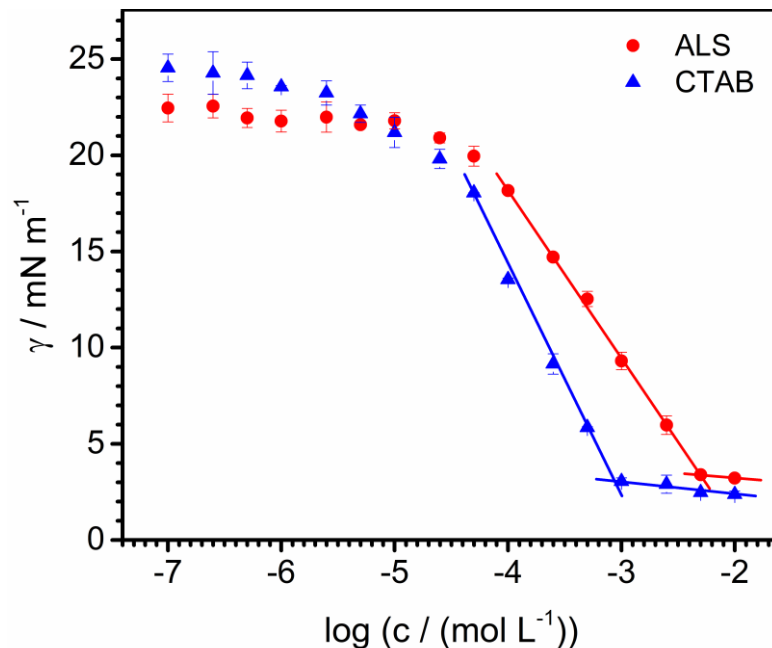
28
29 151 To help visualize the emergent bulk fluid motion during droplet coalescence, dye was
30
31 152 added to the surfactant-free droplet at a concentration of 0.1 g L⁻¹. The addition of dye did not
32
33 153 substantially affect the oil-water interfacial tension (surfactant-free, pure droplet: $\gamma = 23.67 \pm$
34
35 154 0.13 mN m⁻¹; surfactant-free, dyed droplet: $\gamma = 21.42 \pm 0.27$ mN m⁻¹), and thus its contribution to
36
37 155 the emergent coalescence flows was presumed to be negligible in comparison to the presence of
38
39 156 the highly surface-active molecules, ALS and CTAB.

43
44 157 *2.3. Determination of interfacial adsorptive properties at the oil-water interface*

47
48 158 Interpreting the relationship between the induced bulk flows and the contributing
49
50 159 interfacial Marangoni stresses of coalescing binary droplets requires knowledge of the
51
52 160 equilibrated interfacial adsorption for each surfactant-laden droplet prior to merging. The
53
54 161 effective interfacial tension values for pure and surfactant-laden oil-water interfaces were
55
56 162 obtained using axisymmetric drop shape analysis with a contact angle goniometer/tensiometer
57
58 163 (Ramé-Hart) following experimental procedures established in previous work by Nash and Erk.

61
62
63
64
65

1
 2
 3
 4 164 [31] The theory underpinning this technique and its corresponding application to study the
 5 effective interfacial tensions for air-liquid and liquid-liquid monolayers have been previously
 6 discussed in the literature. [32,33] In brief, the interfacial tension of each oil-water interface was
 7 determined by fitting the shape profile of an aqueous pendant drop suspended from the tip of a
 8 flat 12-gauge PTFE capillary immersed in oil to the theoretical profile prescribed by the Young-
 9 Laplace equation, $\Delta P = \gamma \left(\frac{1}{R_1} + \frac{1}{R_2} \right)$. This force balance relates the differential in pressure, ΔP ,
 10 across a curved interface to its principle radii of curvature R_1 and R_2 , and interfacial tension, γ .
 11
 12 170 As surface active solutes become adsorbed to the interface, there is a demonstrable reduction in
 13 the capillary pressure. For a known pressure and interfacial curvature, the effective interfacial
 14 tension of the surfactant-laden interface can be directly measured.
 15
 16
 17
 18
 19
 20
 21
 22
 23
 24
 25
 26
 27
 28
 29
 30 174 The equilibrium interfacial adsorption isotherms for dilute aqueous solutions of ALS or
 31
 32 175 CTAB in contact with triglyceride oil are provided in Figure 2. In each adsorption experiment,
 33
 34 176 the interfacial tension was measured over time for at least 45 minutes, or until a constant
 35
 36
 37
 38



61 **Figure 2.** Interfacial tension, γ , versus log of surfactant concentration, c , in aqueous solution at 23 °C at the
 62 triglyceride oil-water interface measured by the drop shape analysis technique. Lines represent best-fitting straight
 63 lines of the data in the low and high surfactant concentration regimes for each surfactant. The slope value of the
 64 best-fitting line in the low surfactant concentration regime was used in the determination of the surface excess
 65 concentration, Γ_m , for ALS and CTAB.

1
2
3
4 177 interfacial tension value was reached. The critical micelle concentration (CMC's) for each
5
6 178 surfactant was determined graphically from Figure 2 as the intersection of the linear fits to the
7
8 179 low and high concentration regimes for each surfactant. Experimental CMC values for ALS and
9
10 180 CTAB at 23 °C were ca. 5.5×10^{-3} mol L⁻¹ and 0.95×10^{-3} mol L⁻¹, respectively. The CMC value
11
12 181 obtained here for ALS closely corresponded to the value found in the literature, 6.25×10^{-3} mol L⁻¹
13
14 182 ¹. [34] Likewise, the CMC value obtained here for CTAB agreed well with previous observations
15
16 183 in the literature of 0.9×10^{-3} mol L⁻¹ [35] and 1×10^{-3} mol L⁻¹ [36].
17
18
19
20
21

22 184 The surface excess concentration, Γ_m , corresponds to the maximum concentration of
23
24 185 surfactant adsorbed to the oil-water interface of the surfactant-laden droplet at equilibrium and
25
26 186 was approximated for each surfactant using the Gibbs adsorption equation,
27
28
29 187 $\Gamma_m = -\frac{1}{mRT} \left(\frac{dy}{d \log c} \right)_{T,P}$, where γ is the interfacial tension (mN m⁻¹), c is the bulk surfactant
30
31 concentration (mol L⁻¹), R is the gas constant, T is the temperature (K), and the integer, m ,
32
33 accounts for the charge interactions within the polar head group of the surfactant. For dilute
34
35 189 aqueous solutions containing a single, 1:1 ionic surfactant in the absence of excess salt, $m =$
36
37 190 4.606, which was taken for both anionic ALS and cationic CTAB. [37,38] Substituting the slope
38
39 191 value of the best-fitting straight line in the low surfactant concentration regime from the
40
41
42 192 interfacial tension versus log of surfactant concentration curve for $\frac{dy}{d \log c}$ in the Gibbs adsorption
43
44
45 193 equation, Γ_m was calculated for ALS and CTAB at the triglyceride oil-water interface. The
46
47
48 194

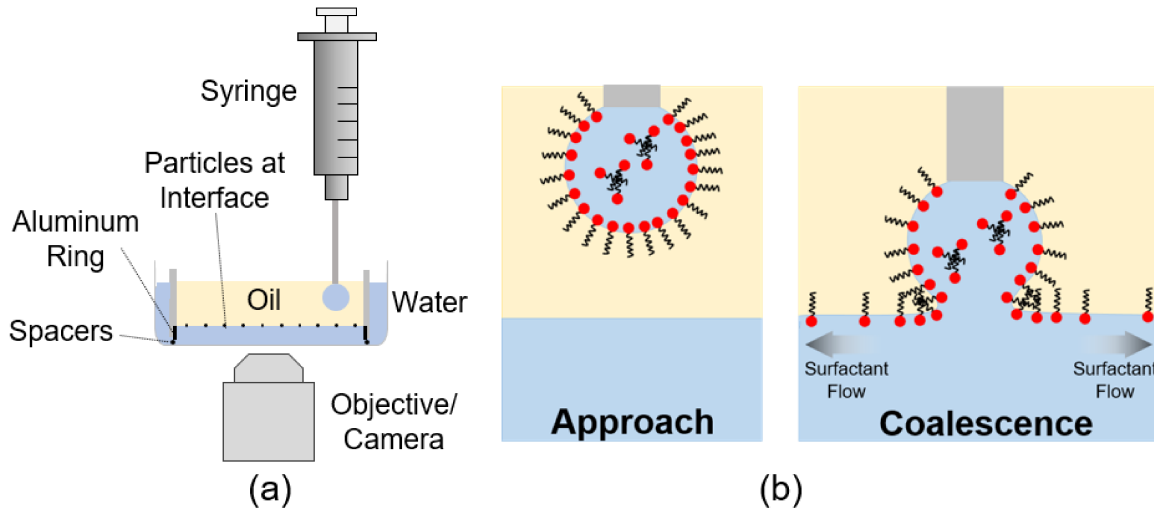
53
54 **Table 1.** Surface excess concentrations and minimum molecular areas calculated for ALS and CTAB at 23 °C at the
55 triglyceride oil-water interface.

57 58 59 60 61 62 63 64 65 Surfactant	Surface Excess Concentration, $\Gamma_m/(10^{-6}$ mol m ⁻²)	Minimum Molecular Area, $A_{min}/(\text{\AA}^2 \text{ molecule}^{-1})$
Ammonium Lauryl Sulfate (ALS)	0.76	218
Cetyltrimethylammonium bromide (CTAB)	1.07	156

1
2
3
4 195 minimum molecular area, A_{\min} ($\text{\AA}^2 \text{ molecule}^{-1}$), was then determined from the equation, $A_{\min} =$
5
6
7 196 $\frac{1 \times 10^{20}}{\Gamma_m N_A}$, where N_A is Avogadro's number. (Table 1).
8
9
10
11
12
13
14
15
16
17
18
19
20
21
22
23
24
25
26
27
28
29
30
31
32
33
34
35
36
37
38
39
40
41
42
43
44
45
46
47
48
49
50
51
52
53
54
55
56
57
58
59
60
61
62
63
64
65

1
2
3
4 197 2.4. Determination of surfactant-induced interfacial spreading velocity, U_s
5
6

7 198 The experimental setup used to study the interfacial spreading velocity, U_s , of each
8 surfactant when introduced into the pure triacylglyceride oil-water interface is shown in Figure 3.
9
10 199 The displacement of tracer particles (hollow glass spheres, 9-13 μm diameter, Sigma-Aldrich,
11
12 200 CAS # 65997-17-3) seeded at the pure oil-water interface initiated by the introduction of a
13
14 201 surfactant-loaded water droplet to the pure oil-water interface and driven by solutal Marangoni
15
16 202 surfactant-loaded water droplet to the pure oil-water interface and driven by solutal Marangoni
17
18
19
20



39 505 **Figure 3.** Schematic representation of the experimental setup used to quantify interfacial spreading velocities, U_s ,
40 under an induced interfacial tension gradient at the triglyceride oil-water interface. A side view depicting the
41 introduction of a surfactant loaded water droplet at the surfactant-free, oil-water interface (containing tracer
42 particles) is shown in (a) and an illustration of the surfactant diffusion mechanism, quantified by measuring the rate
43 of displacement for tracer particles attached to the interface, is shown in (b).

44 203 flow was measured.
45
46

47 204 The motion of tracer particles was measured at a planar oil-water interface because this
48
49 205 experimental scheme specifically enabled the measurement of Marangoni-induced flow rates
50 under the effect of a surfactant concentration gradient at the oil-water interface. Ensuring that the
51
52 206 measured flow rates were obtained for tracer particles located specifically at the oil-water
53
54 207 interface and not within one of the subphases was most directly accomplished with a droplet
55
56 208 coalescing with a planar oil-water interface.
57
58
59
60 209
61
62
63
64
65

1
2
3
4 210 Preparation of a planar triglyceride oil-water interface containing the seeded glass
5
6
7 211 spheres was performed using a modified optical microscopy cell and methodology adapted from
8
9 212 the work of Park et al. [39] The cell used here consisted of a polystyrene petri dish (height 1 cm,
10
11 213 outer diameter of 40 mm) and a concentric polystyrene cylinder (height 1 cm, outer diameters of
12
13 214 30 mm). An aluminum ring was inserted into the bottom of the inner polystyrene cylinder to pin
14
15 215 the contact line of the oil-water interface. The inner cylinder was secured to the polystyrene petri
16
17 216 dish using a fast curing epoxy and 0.1 mm glass spacers. This allowed for the oil-water system to
18
19 217 achieve hydrostatic equilibrium, ensuring that a planar oil-water interface could be attained via
20
21 218 the addition or removal of water from the outer portion of the sample cell.

22
23
24 219 After forming a planar oil-water interface free of any solutes, an oil droplet containing
25
26
27 220 tracer particles was directly added to the upper oil phase of the sample cell. This yielded a seeded
28
29 221 tracer concentration of $\sim 4 \times 10^6$ particles-cm⁻² at the interface, a concentration which was
30
31 222 necessary for accurate particle tracking measurements and quantifying the interfacial spreading
32
33 223 velocities resulting from the introduction of surfactant. It should be noted that at this
34
35 224 concentration, seeded tracer particles displayed slight aggregation. Very large aggregates would
36
37 225 be expected to display lower interfacial spreading velocities in comparison to unaggregated
38
39 226 primary particles due to their larger mass and could therefore introduce some degree of
40
41 227 uncertainty into the measured interfacial spreading velocities in this experimental setup.
42
43
44 228 However, the largest aggregates observed in this study consisted of 2-3 primary particles, and
45
46 229 measurements of the steady-state, fully developed displacement rates for these aggregates were
47
48 230 indistinguishable from the measured displacement rates of unaggregated, interfacially adsorbed
49
50 231 primary particles.

51
52
53
54
55
56
57
58
59
60
61
62
63
64
65

1
2
3
4 232 Following the seeding of tracer particles, the experimental cell was stabilized for 15
5 minutes, then a 10 μL droplet of either surfactant solution was formed at the tip of a metal
6 capillary within the oil layer. The droplet was equilibrated for an additional 30 minutes within
7 the upper oil layer prior to contact with the planar oil-water interface to allow for saturated
8 interfacial adsorption of the surfactant. Finally, the droplet was lowered slowly ($\sim 0.01 \text{ mm s}^{-1}$) to
9 contact the planar oil-water interface and the resulting isotropic tracer particle motion was
10 captured using an inverted microscope and high-speed camera (Photron Mini UX) at 2000
11 frames per second. Due to the remarkably high energy of attachment for micrometer-scale
12 particles at the oil-water interface, [40] particle motion was presumed to be approximately two-
13 dimensional for the duration of particle spreading. Care was taken to quantify the displacement
14 of at least five tracer particles from two separate experiments for each oil-water-surfactant
15 system, measured manually using ImageJ software.
16
17
18
19
20
21
22
23
24
25
26
27
28
29
30
31
32
33
34 244 **3. Results and Discussion**
35
36
37 245 *3.1. Effect of surfactant type on bridge expansion and bulk mixing during the coalescence of*
38
39 246 *equally sized drops*
40
41
42
43 247 Our investigation of surfactant contributions in the generation of opposing flows within
44
45 248 coalescing binary droplets begins with the consideration of two surfactant-free droplets sharing
46
47 249 an equivalent initial diameter, $2R$ ($= 2 \text{ mm}$), and approximately equal oil-water interfacial
48
49 250 tensions (surfactant-free, undyed droplet: $\gamma_1 = 23.67 \pm 0.13 \text{ mN m}^{-1}$; surfactant-free, dyed
50
51 251 droplet: $\gamma_2 = 21.42 \pm 0.27 \text{ mN m}^{-1}$). Analysis of bridge expansion for the two, equally sized
52
53 252 coalescing droplets with no added surfactant revealed that this system closely obeyed the
54
55 253 $D_b/2 \propto (R\gamma/\rho_{\text{out}})^{1/4}t^{1/2}$ scaling relation over the entire duration of droplet merging (Figure
56
57 254 4), agreeing well with the experimental observations of previous researchers. [17,18]

1
2
3
4
5
6
7
8
9
10
11
12
13
14
15
16
17
18
19
20
21
22
23
24
25
26
27
28
29
30
31
32
33
34
35
36
37
38
39
40
41
42
43
44
45
46
47
48
49
50
51
52
53
54
55
56
57
58
59
60
61
62
63
64
65

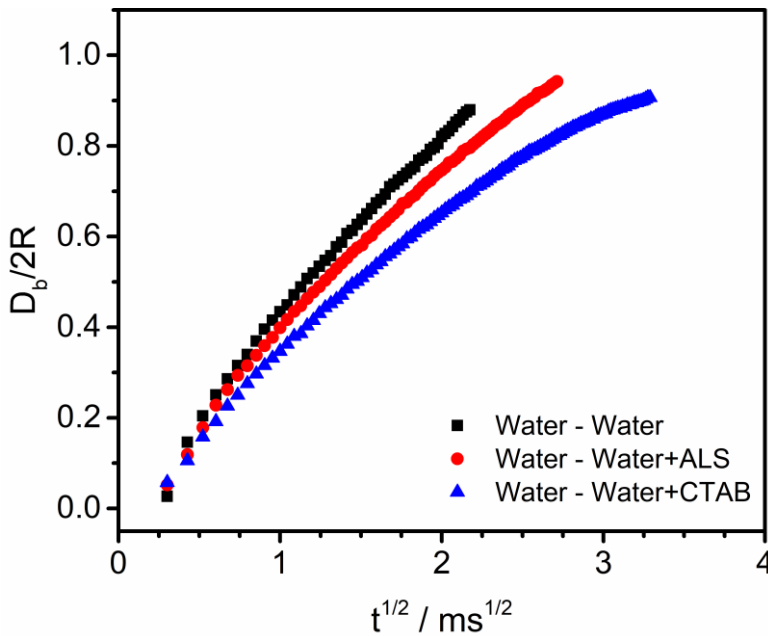


Figure 4. Kinetics of expansion for the connective bridge separating spherical droplets with an equivalent initial diameter, $2R$ ($= 2$ mm). The data represent the increase in the connective bridge diameter, D_b , relative to $2R$, as a function of the square-root-of-time, $t^{1/2}$, succeeding the onset of droplet coalescence.

For equally sized coalescing droplets, where one of the drops contained 2.5×10^{-3} mol L $^{-1}$

ALS, the $D_b/2 \propto t^{1/2}$ scaling relation was also closely obeyed, but a slightly reduced slope in the

experimental data was observed. This indicates that the value of the prefactor, $(R\gamma/\rho_{out})^{1/4}$, in

the coalescence scaling relation was influenced by the presence of ALS. Likewise, an even more

pronounced decrease in the slope of this scaling relationship became apparent at longer times for

systems containing 2.5×10^{-3} mol L $^{-1}$ CTAB. This further suggests that the gradient in interfacial

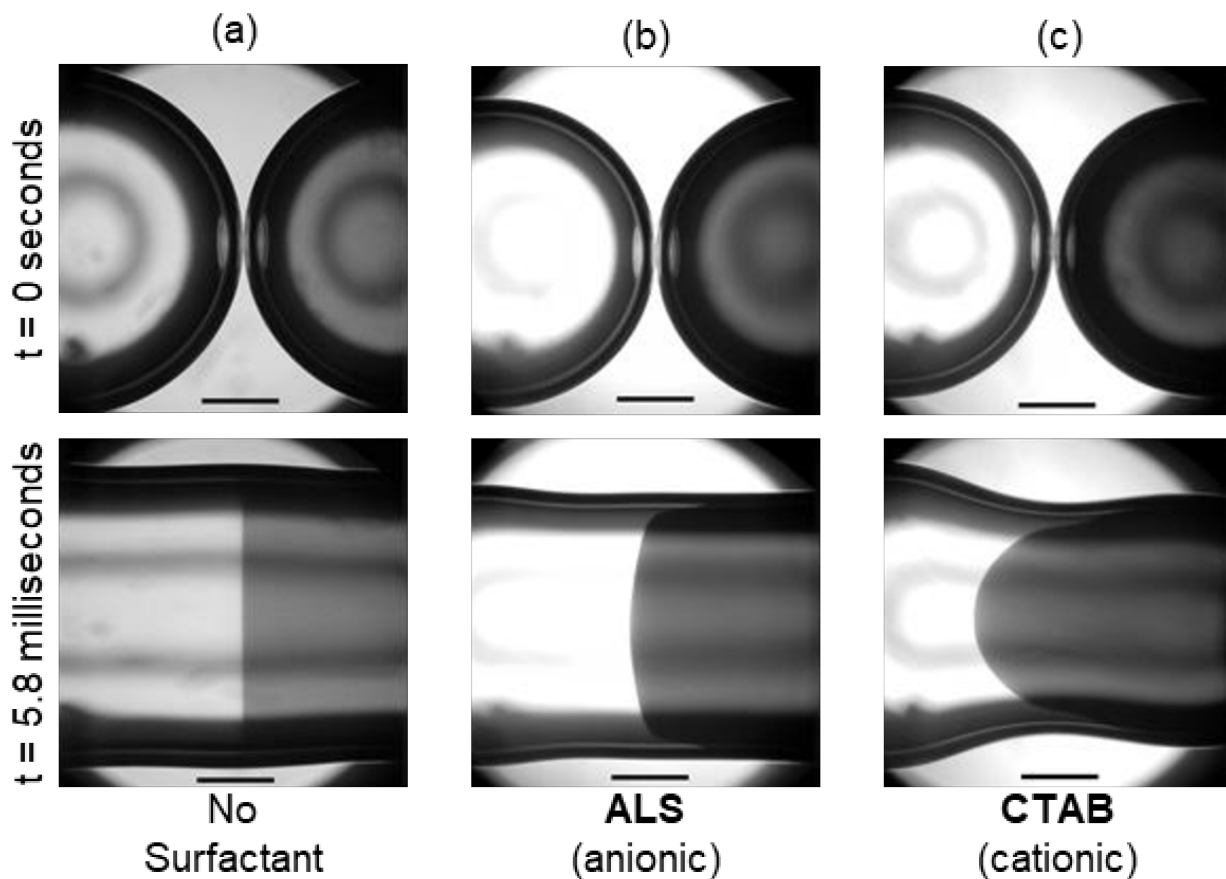
tension and timescale of solutal Marangoni flow of the chosen surfactant along the interface of

expanding liquid bridge has a demonstrable influence on the value of the prefactor in the scaling

relation, which was not explicitly accounted for or discussed in the derivation of this scaling

relation.

1
 2
 3
 4 265 The characteristic time scale for coalescence of two equally sized drops with equal
 5
 6 interfacial tensions in inviscid flow is set by $\tau_C = \sqrt{(\rho R^3)/\gamma}$. [41] For the merging of two 0.75-
 7 mm radius water drops in the inertial regime, with $\gamma = 23 \text{ mN m}^{-1}$, τ_C is $\sim 4.2 \text{ ms}$. This
 8
 9 267 characteristic relaxation time closely approximates the experimentally measured time required
 10
 11 268 for the expanding bridge between the surfactant-free water droplets to become equal to the initial
 12
 13 269 drop diameter for the system shown in Figure 5a. This approximation is less representative in the
 14
 15 270 presence of a surfactant concentration gradient, which can be seen from the data in Figure 5b and
 16
 17 271 5c, for ALS and CTAB, respectively. Each of these systems require a longer duration for the
 18
 19 272 diameter of the expanding bridge to be equal to the initial diameter of the drops. The observed
 20
 21 273
 22
 23
 24
 25
 26
 27



57 **Figure 5.** Temporal shape profiles of equally sized water droplets coalescing in triglyceride oil. The leftmost droplet
 58 in each image contained either (a) no surfactant, (b) $2.5 \times 10^{-3} \text{ mol L}^{-1}$ ALS, or (c) $2.5 \times 10^{-3} \text{ mol L}^{-1}$ CTAB, while the
 59 rightmost droplet in each image was surfactant-free, with dye added for flow visualization. The absence or presence
 60 of opposing flows at the interface and within the bulk of the merging droplets illustrate the effect of interfacially
 61 adsorbed surfactant molecules. Differences in the curvature of the jetted fluid following coalescence in (b) and (c)
 62 demonstrate the influence of surfactant headgroup architecture on the relative magnitude of these induced flows.
 63 The scale bars in each image are 0.5 mm in length.

1
2
3
4 274 increase in τ_C for systems containing ALS or CTAB, as well as the clear difference between their
5 corresponding τ_C values, suggests that interfacial adsorptive and convective properties of the
6 surfactant contribute to the decrease in the value of the prefactor in the coalescence scaling
7 relation. This observation is discussed in greater detail in Section 3.3.
8
9
10
11
12
13
14

15 278 Figure 5a illustrates that negligible internal mixing occurred during the merging of
16 surfactant-free droplets due to the generation of two balanced, plug-flow water jets which
17 converged at the propagating coalescence neck. In this instance, the interfacial tensions of the
18 280 converging droplets are balanced and thus no tangential stress was competing with the bulk fluid
19 281 motion of the merging drops. This behavior agreed well with experimental observations of
20 282 previous researchers. [17,18] Contrarily, coalescence of binary droplets with non-uniform
21 283 compositions of a surface-active species displayed pronounced internal convective mixing during
22 284 the coalescence process, the degrees of which strongly depended on the surfactant present at the
23 285 oil-water interface of the surfactant-laden droplet.
24
25
26
27
28
29
30
31
32
33
34
35
36

37 287 Distinct bulk fluid motion was observed in the presence of either anionic ALS or cationic
38 surfactant CTAB for equally sized droplet with a capillary pressure ratio of $\Delta P_2/\Delta P_1 \approx 5$ (where
39 288 ΔP_1 and ΔP_2 are the capillary pressures of the leftmost droplet and the rightmost droplet,
40 289 respectively) and are shown in Figures 5b and 5c. The presence of surfactant in the undyed,
41 290 leftmost drop led to the formation of a fluid jet which propagated from the bulk of dyed,
42 291 surfactant-free drop as direct result of this droplet's higher capillary pressure. For the binary
43 292 droplets system containing 2.5×10^{-3} mol L⁻¹ ALS, the motion of the jetted fluid appeared to
44 293 occur under near plug flow conditions, with some discernable curvature of the jetting dyed fluid
45 294 at later times. However, the internal mixing for the binary systems containing 2.5×10^{-3} mol L⁻¹
46
47
48
49
50
51
52
53
54
55
56
57
58
59
60
61
62
63
64
65

1
2
3
4 296 CTAB was demonstrably more pronounced, displaying a much higher curvature of the jetted
5
6
7 297 fluid at later stages of coalescence (i.e., after 5.8 milliseconds).
8
9
10 298 *3.2. Influence of surfactant type on the development of bulk fluid jetting*
11
12
13 299 To further aid in illustrating the marked influence of surfactant in the jetting behavior
14
15 300 observed for binary droplet systems, the initial diameters of the two merging droplets were
16
17 301 modulated by increasing the initial diameter of the leftmost droplet to 2.2 mm and decreasing the
18
19
20 302 initial diameter of the rightmost droplet to 1.0 mm. Figure 6a shows that for asymmetrically
21
22
23 303 sized droplets, both free of any added surfactant and of approximately equal interfacial tension,
24
25 304 droplet merging led to only slight jetting of the fluid within the smaller diameter, surfactant-free
26
27 305 droplet into the larger droplet as a direct result of the relatively small capillary pressure gradient
28
29
30 306 ($\Delta P_2/\Delta P_1 \approx 2$) originating from the difference in initial droplet sizes. However, the magnitude of
31
32
33 307 the capillary pressure gradient was insufficient to induce a great deal of internal mixing.
34
35
36
37
38
39
40
41
42
43
44
45
46
47
48
49
50
51
52
53
54
55
56
57
58
59
60
61
62
63
64
65

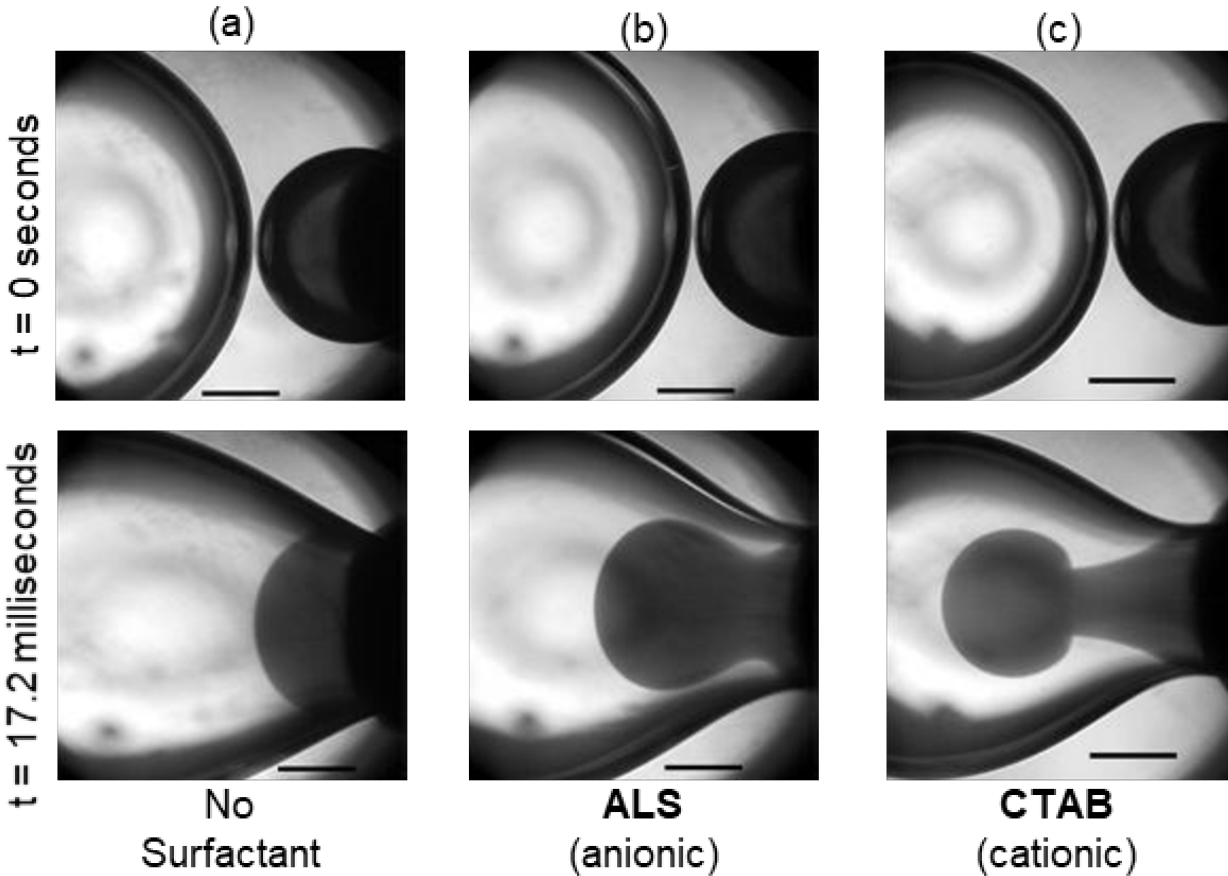


Figure 6. Flow profiles depicting the formation of fluid jets of different sizes for asymmetrically sized water droplets coalescing in triglyceride oil. The leftmost droplet in each image contained either (a) no surfactant, (b) 2.5×10^{-3} mol L⁻¹ ALS, or (c) 2.5×10^{-3} mol L⁻¹ CTAB, while the rightmost droplet in each image was surfactant-free, with dye added for flow visualization. The scale bars in each image are 0.5 mm in length.

308 In the case of binary droplet systems that contained a concentration gradient of either

409 ALS or CTAB, the difference in diameter and interfacial tension between the binary droplets

44 provided a much larger capillary pressure ratio ($\Delta P_2/\Delta P_1 \approx 11.5$) and thus a greater driving

48 energy for jetting of the fluid from the smaller droplet into the larger droplet containing

49 surfactant during coalescence. The late-stage flows that emerged under these experimental

51 conditions are shown in Figure 6b and 6c, respectively. For the binary droplet system with

53 2.5×10^{-3} mol L⁻¹ ALS present in the surfactant-laden droplet, the profile of the fluid jetted from

55 the smaller, surfactant-free droplet took the shape of a bulb-like plume with a relatively large

59 diameter forming near the apex of the jetted fluid and slightly narrower base. Similarly, for the

1
2
3
4 317 binary droplet system containing 2.5×10^{-3} mol L⁻¹ CTAB, the late-stage internal flow also
5
6 318 resulted in the formation of a fluid jet with a large bulb and narrow base. However, the jetting
7
8 319 that occurred in this case was demonstrably stronger, with the formation of a mushroom-shaped
9
10 320 plume of dyed water and a far narrower base.
11
12
13
14
15 321 The difference in the shape of the jetted fluid that emerged in systems containing ALS or
16
17 322 CTAB stemmed from the magnitudes of the convective mixing generated by the opposing bulk
18
19 323 and Marangoni interfacial flows upon droplet coalescence. As the fluid from the dyed droplet
20
21 324 flowed through the propagating coalescence neck, an interfacial diffusional flux developed in the
22
23 325 opposite direction, as interfacially adsorbed surfactant molecules in the surfactant-laden droplet
24
25 326 migrated from regions of high concentration to low concentration. This in turn generated eddy
26
27 327 currents within the bulk of the merging droplets, just beneath the interface. In the case of CTAB,
28
29 328 the driving energy for interfacial flux appeared to be sustained for a longer time than in the case
30
31 329 of ALS, which led to more pronounced eddy currents and thus the observed jetting behavior.
32
33
34
35
36
37 330 Furthermore, assessment of the displacement of the jetted fluid apex as a function of time
38
39
40
41
42
43
44
45
46
47
48
49
50
51
52
53
54
55
56
57
58
59
60
61
62
63
64
65

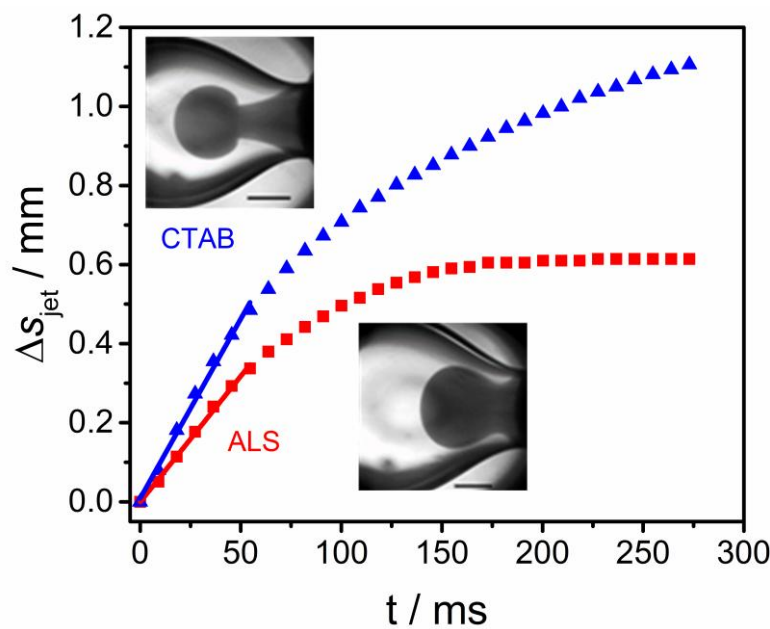


Figure 7. Displacement of the jetted fluid apex, Δs_{jet} , apex originating from the surfactant-free droplet into the surfactant-laden droplet as a function of time, t , succeeding droplet contact for asymmetrically sized droplet systems. Micrograph insets depict the position of the fluid jets 17.2 ms after the onset of coalescence. The scale bars in each image are 0.5 mm in length.

1
2
3
4 331 for asymmetrically sized binary droplet systems, containing either ALS or CTAB (Figure 7),
5
6 332 indicates a clear difference in the induced fluid motion. The rate of fluid jetting during the initial
7
8 333 stages of coalescence was roughly 30% faster for the droplet system containing cationic CTAB
9
10 334 compared to the analogous system containing anionic ALS (9.08 mm s^{-1} and 6.37 mm s^{-1} ,
11
12 335 respectively, from a linear regression fit to the initial data in Figure 7). In the following sections,
13
14 336 we discuss in detail our experimental basis for attributing differences in the emerged jetting
15
16 337 phenomena to differences in the magnitudes of the induced interfacial Marangoni flows
17
18 338 accompanying each surfactant. The jetting phenomena observed between merging drops with an
19
20 339 induced surfactant concentration gradient can also be explained by the induction of Marangoni
21
22 340 convection, where low interfacial tension liquid along the oil-water interface of the coalescing
23
24 341 neck is carried toward the higher interfacial tension regions in the surfactant-free droplet and
25
26 342 accumulates. A localized increase in the hydrostatic pressure of this region follows and the
27
28 343 development of a bulk flow of liquid from the surfactant-free droplet in the opposite direction of
29
30 344 the Marangoni flow.
31
32
33
34
35
36
37
38
39 345 *3.3. Comparison of adsorptive properties of ALS and CTAB at the triglyceride oil – water*
40
41 346 *interface*
42
43
44
45 347 Values for the surface excess concentration, Γ_m , in Table 1 indicate that CTAB molecules
46
47 348 pack more densely at the triglyceride oil-water interface than ALS molecules, which is in line
48
49 349 with previous experimental observations for the same or similar ionic surfactants at the oil-water
50
51 350 interface. [42,43] The negatively charged moiety of 1:1 anionic surfactants leads these molecules
52
53 351 to have a relatively large hydrodynamic diameter in comparison to cationic surfactants, which
54
55 352 have a comparably small hydrodynamic diameter surrounding their positively charged
56
57 353 headgroups. [44] These differences in the hydrodynamic volume surrounding the hydrophilic
58
59
60
61
62
63
64
65

347 Values for the surface excess concentration, Γ_m , in Table 1 indicate that CTAB molecules
348 pack more densely at the triglyceride oil-water interface than ALS molecules, which is in line
349 with previous experimental observations for the same or similar ionic surfactants at the oil-water
350 interface. [42,43] The negatively charged moiety of 1:1 anionic surfactants leads these molecules
351 to have a relatively large hydrodynamic diameter in comparison to cationic surfactants, which
352 have a comparably small hydrodynamic diameter surrounding their positively charged
353 headgroups. [44] These differences in the hydrodynamic volume surrounding the hydrophilic

1
2
3
4 354 portions of each surfactant molecule lead to differences in their corresponding equilibrium
5
6
7 355 adsorptive capabilities at immiscible fluid interfaces. As a direct result, anionic surfactants tend
8
9 356 to pack less efficiently at fluid interfaces than their cationic counterparts.
10
11

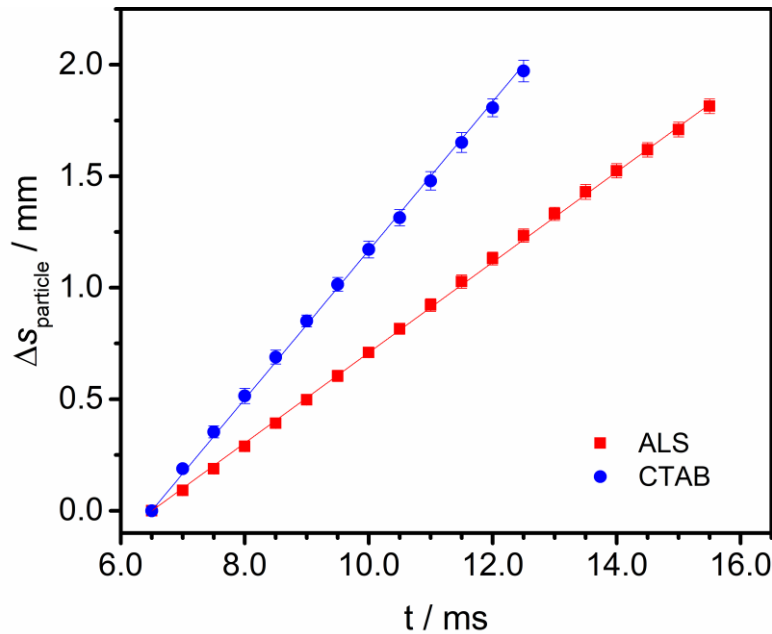
12 357 Each of the experimental observations of the differences in the magnitudes of solutal
13
14 358 Marangoni convection for ALS and CTAB would also suggest that Γ_m has a pivotal role in the
15
16 359 timescale of Marangoni interfacial flow. A more densely packed interfacial layer laden with
17
18 360 surfactant would be expected to behave more rigidly in response to interfacial tension and
19
20 361 surfactant concentration perturbations. This rigidity restricts lateral surface movements and
21
22 362 solutal Marangoni convention. Thus, the timescale for solutal Marangoni flow would increase, as
23
24 363 the interface overall would take longer to relax to a homogenous state (i.e., regions of high
25
26 364 interfacial tension and regions of low interfacial tension would exist longer for more densely
27
28 365 packed interfaces). Under these conditions, the high interfacial tension regions would apply a
29
30 366 high tangential surface stress over a longer duration.
31
32
33
34
35
36

37 367 Likewise, considering that both ALS and CTAB are soluble in the aqueous phase, and
38
39 368 can therefore adsorb and desorb from the bulk aqueous phase during droplet coalescence, both
40
41 369 the surfactant's diffusion coefficient, D , and bulk surfactant concentration, c , would be expected
42
43 370 to decrease the timescale of solutal Marangoni flow. A surfactant that can diffuse swiftly to the
44
45 371 interface from the bulk would be expected to decrease the lifetime of interfacial tension gradient,
46
47 372 (i.e., higher diffusion coefficients will favor a small concentration difference). Similarly, high
48
49 373 concentrations of surfactant in the bulk would be expected to increase the overall adsorption rate
50
51 374 of molecules near the interface, thus favoring small concentration gradients and reducing the
52
53 375 timescale of solutal Marangoni convection.
54
55
56
57
58
59
60
61
62
63
64
65

1
2
3
4 376 The timescale of solutal Marangoni convection, τ_M , was approximated using these
5
6
7 377 parameters in the equation, $\tau_M = \frac{\Gamma_m^2}{Dc^2}$. Incorporating the experimentally determined saturation
8
9
10 378 adsorption values from Table 1, a bulk surfactant concentration of 2.5×10^{-3} mol L⁻¹, and
11
12 379 diffusion coefficients of 5×10^{-10} m² s⁻¹ for ALS, [45] and 1×10^{-10} m² s⁻¹ [46] for CTAB, the
13
14 380 characteristic timescale of solutal Marangoni becomes ~ 0.2 ms for ALS and ~ 2 ms for CTAB.
15
16
17 381 The order of magnitude difference in τ_M implies that the time required for interfacially adsorbed
18
19 382 ALS molecules to respond and dampen interfacial tension fluctuation is far faster than that of
20
21
22 383 CTAB molecules.
23
24

25 384 Regarding the flows observed in the coalescence of binary droplets with asymmetric
26
27 385 compositions, the differences in interfacial motion between surfactants can be directly attributed
28
29
30 386 to the magnitudes of the surfactant molecule's corresponding τ_M values. The timescale of solutal
31
32 387 Marangoni convection is shorter than the characteristic coalescence timescale for two water
33
34 388 droplets of equal diameters and interfacial tensions in the inertial regime for ALS (i.e., $\tau_M < \tau_C$).
35
36
37 389 The driving energy for solutal Marangoni-driven convection is therefore relatively low because
38
39 390 interfacial relaxation toward a homogenous interfacial tension along the coalescing bridge occurs
40
41 391 faster than the time required for droplets to completely merge. In contrast, these timescales are
42
43 392 very close in magnitude for systems containing CTAB (i.e., $\tau_M \approx \tau_C$). Thus, for CTAB molecules,
44
45 393 relaxation toward homogenous interfacial tension takes much longer and is on the order of the
46
47 394 time required for droplets to merge, which leads to the development of strong Marangoni-driven
48
49 395 convection and competing bulk and interfacial flows.
50
51
52
53
54
55 396 *3.3. Surfactant interfacial spreading properties under an induced concentration gradient*
56
57
58
59
60
61
62
63
64
65

1
2
3
4 397 Figure 8 shows the distance tracer particles travel as a function of time at the (initially)
5
6 398 pure triglyceride oil-water interface following the introduction of a 2.5×10^{-3} mol L⁻¹ aqueous
7
8 399 droplet solution of either anionic ALS or cationic CTAB. These data represent the fully-
9
10 400 developed motion of the particles, starting 6.5 ms after the introduction of surfactant into the
11
12
13
14
15



37
38
39
40
41
42
43
44
45
46
47 398 Seeded tracer particle displacement, $\Delta s_{\text{particle}}$, versus time, t , following the introduction of a 2.5×10^{-3} mol
48 L⁻¹ aqueous droplet solution of anionic ALS or cationic CTAB surfactant at a planar triglyceride oil-water
49 interface. Motion of the interfacially seeded tracer particles resulted directly from the induced surfactant
50 concentration gradient of either ALS or CTAB. Data are shown for fully developed particle displacement rates, 6.5
51 milliseconds after initial contact between the surfactant-laden drop and the planar oil water interface.
52
53
54
55
56
57
58
59
60
61
62
63
64
65

401 pure oil-water interface.

402 These data show a clear difference in the steady-state spreading velocities, U_s , of seeded
43 glass spheres under the induced concentration gradient (i.e. for ALS: $U_s = 0.202$ m s⁻¹; for
44 CTAB, $U_s = 0.333$ m s⁻¹) which implies that the surface motion driven by unbalanced interfacial
45 tensions in the presence of cationic CTAB molecules exceeds that of ALS molecules. Taking the
46 initial droplet diameter, $2R$ (= 2 mm), as the characteristic length scale, an estimation of the
47 characteristic timescale for the oil-water interface to deform under the induced surfactant
48

1
2
3
4 408 concentration gradient can be obtained from $\tau_D = 2R/U_s$. Approximations of τ_D yield 10 ms for
5
6 409 ALS, and 6 ms for CTAB. These calculations for the characteristic timescales of interfacial
7
8 410 deformation under and induced surfactant concentration gradient provide additional evidence
9
10 411 that ALS molecules express a lower driving energy for solutal Marangoni-driven convection in
11
12 412 comparison to CTAB molecules. As the driving energy for solutal Marangoni convection is
13
14 413 lower for ALS, the overall motion of solutes attached to an oil-water interface when subjected to
15
16 414 a concentration gradient would be expected to be influenced less by gradients in surfactant
17
18 415 concentration because such gradients are short-lived.
19
20
21
22
23

24 416 The primary difference between the between measuring the interfacial spreading
25
26 417 properties that develop in a droplet-planar coalescence system as opposed to a droplet-droplet
27
28 418 system is the direction of the generated bulk flow between the aqueous droplet and planar water
29
30 419 reservoir upon coalescence. In the case of the droplet-planar interface arrangement, the capillary
31
32 420 pressure ratio, $\Delta P_2/\Delta P_1$ (where ΔP_1 and ΔP_2 are the capillary pressures for the surfactant-laden
33
34 421 droplet and planar water reservoir, respectively), would approach zero because of the
35
36 422 approximately infinite radius of curvature of the planar water reservoir. This would in turn
37
38 423 produce a driving energy for bulk fluid motion to propagate from the surfactant-laden droplet
39
40 424 into the surfactant-free, planar reservoir. This bulk fluid behavior stands in contrast to the bulk
41
42 425 flows observed and quantified in Section 3, where bulk fluid motion was driven from the
43
44 426 surfactant-free droplet into the surfactant-laden droplet due to the capillary pressure gradient.
45
46 427 However, Marangoni-induced interfacial flows always act in the direction of the interfacial
47
48 428 solute concentration gradient [19] and occur on a shorter timescale than bulk flows. Thus, the
49
50 429 measured values for the interfacial spreading velocities (i.e. the Marangoni-induced interfacial
51
52 430 flowrates) would presumably be minimally influenced by the experimental arrangement.
53
54
55
56
57
58
59
60
61
62
63
64
65

1
2
3
4 431 It is worth noting once again that this difference in interfacial spreading was observed for
5
6 432 two surfactants with distinct chemical architectures, which both reduced the interfacial tension of
7
8 433 the pure triglyceride oil-water interface to approximately 3 mN m^{-1} at a high bulk concentration.
9
10
11 434 The observed differences in interfacial spreading and jetting behavior during the coalescence of
12
13 435 binary droplets with nonuniform compositional properties must be explained by additional
14
15 436 interfacial relaxation mechanisms, which have not previously been studied in detail by the recent
16
17 437 literature.
18
19
20
21

22 438 **4. Summary and Conclusion**

23
24

25 439 Direct observation of the bulk flows generated during the coalescence of binary water-in-
26
27 440 oil droplets with non-uniform physical properties and characterization of the contributive
28
29 441 surfactant-induced interfacial phenomenon was performed. Mechanisms responsible for the
30
31 442 observed opposing interfacial and bulk flows between merging surfactant-laden and surfactant-
32
33 443 free droplets were also described. Fluid jets that developed during binary droplet coalescence
34
35 444 were a direct result of convection driven solutal Marangoni flows which generated a rapid
36
37 445 redistribution of low interfacial tension bulk fluid around the perimeter of the high interfacial
38
39 446 tension bulk fluid. The degree of interfacial spreading and bulk fluid redistribution was greater
40
41 447 for cationic CTAB molecules compared to ALS molecules due to stark differences in their
42
43 448 equilibrium adsorption values, kinetic re-adsorptive rates during droplet coalescence, and overall
44
45 449 tendency for expressing solutal Marangoni convection.
51
52

53 450 This work stands in contrast to work of previous researchers in that control over bulk
54
55 451 flows during the coalescence of binary water droplets was induced entirely through optimized
56
57 452 surfactant selection, with no need for modulation of the bulk viscosities of the outer or inner
58
59 453 liquid phases. Our experimental results provide additional experimental confirmation that the
60
61
62
63
64
65

1
2
3
4 454 governing power-law relationship for coalescing droplets in the inertial regime is obeyed in the
5 presence of an induced surfactant concentration gradient, but the prefactor in this relationship is
6
7 455 strongly dependent upon the interfacial properties of the added surfactant.
8
9 456
10
11
12 457 The analyses and relationships outlined in this work can be generalized for many
13 different surfactant types, including anionic or cationic surfactants with longer alkyl chains than
14 those investigated here, nonionic surfactants with various alkyl tail lengths, and zwitterionic
15 surfactants. The parameters which are expected to shorten the timescale of solutal Marangoni-
16 convection (while decreasing its driving energy) include the surfactant's diffusion coefficient
17 and bulk concentration, while equilibrium interfacial saturation adsorption is the primary
18 contributor in extending the timescale of solutal Marangoni convection. Thus, enhancing the
19 bulk mixing of binary drops with an induced concentration gradient can be done by selecting a
20 surfactant that packs densely at the immiscible fluid interface and adsorbs to the interface
21 strongly. Zwitterionic and polymeric surfactant would likely be ideal candidates for such
22 applications due to their relatively small diffusion coefficients and dense interfacial organization
23
24 464 capabilities. [47]
25
26
27
28
29
30
31
32
33
34
35
36
37
38
39
40
41
42 469 One of the most advantageous applications of using the controlled coalescence of
43
44 470 droplets with asymmetric properties is in the synthesis of functional nanoparticles. Recently,
45
46
47 471 Frenz et al. [27] demonstrated that magnetic iron oxide nanoparticles could be precipitated in a
48
49
50 472 highly reproducible reaction following the fusion of droplet pairs consisting of different reagents
51
52
53 473 in a hydrodynamically coupled, single-nozzle microfluidic device. Controlled pairwise mixing of
54
55
56 474 aqueous droplets in oil was produced by electrocoalescence [48] and the droplets were prevented
57
58
59 475 from fusing prematurely by using a uniformly distributed surfactant at the interfaces of both
60
61
62
63
64
65 476 droplets. The methodology developed by these researchers could be readily adapted to

1
2
3
4 477 incorporate the findings of the present manuscript by isolating the surfactant to one of the inlet
5
6 478 droplet flows, while leaving the other surfactant-free. Upon merging, Marangoni-induced flows
7
8 479 would produce pronounced bulk mixing between the drops, like those explored here. Moreover,
9
10 480 enhanced control over the degree of mixing obtained between the drops at different timescales
11
12 481 could be explored with the previously discussed surfactant selection criteria.
13
14
15
16

17 482 In this study, we proposed a simple, yet robust experimental methodology for directly
18
19 483 quantifying the solutal Marangoni timescales of surface active compounds at the oil-water
20
21 484 interface under an induced concentration gradient. With this method, the spreading efficiencies
22
23 485 and encouragement of bulk fluid mixing for potentially any surfactant type at the oil water
24
25 486 interface can be economically measured. The insights garnered from this work provide a
26
27 487 compelling alternative route for inducing bulk flows in microfluidic devices without the need for
28
29 488 modulating bulk phase viscosities.
30
31
32
33
34

35 489 Acknowledgements 36 37

38 490 Financial support for this work was provided by the National Science Foundation through
39
40 491 the East Asia and Pacific Summer Institutes (EAPSI) Fellowship Program (Award Number:
41
42 492 1713936). The authors would also like to thank the anonymous reviewer whose thorough
43
44 493 comments and suggestions led to a substantially improved manuscript.
45
46
47
48
49
50
51
52
53
54
55
56
57
58
59
60
61
62
63
64
65

1
2
3
4 494 **References**
5
6 495 [1] J.D. Paulsen, Approach and coalescence of liquid drops in air, *Phys. Rev. E - Stat.*
7 496 *Nonlinear, Soft Matter Phys.* 88 (2013) 1–13. doi:10.1103/PhysRevE.88.063010.
8
9 497 [2] J. Qian, C.K. Law, Regimes of coalescence and separation in droplet collision, *J. Fluid*
10 498 *Mech.* 331 (1997) 59–80.
11
12 499 [3] J.D. Paulsen, R. Carmignani, A. Kannan, J.C. Burton, S.R. Nagel, Coalescence of
13 500 bubbles and drops in an outer fluid, *Nat. Commun.* 5 (2014) 3182.
14 501 doi:10.1038/ncomms4182.
15
16 502 [4] J. Eggers, J.R. Lister, H.A. Stone, Coalescence of Liquid Drops, (1999) 1–37.
17 503 doi:10.1017/S002211209900662X.
18
19 504 [5] L. Duchemin, J. Eggers, C. Josserand, Inviscid coalescence of drops, *J. Fluid Mech.* 487
20 505 (2003) 167–178. doi:10.1017/S0022112003004646.
21
22 506 [6] D.T. Wasan, The Role of Coalescence Phenomena and Interfacial Rheological Properties
23 507 in Enhanced Oil Recovery: An Overview, *J. Rheol. (N. Y. N. Y.)* 23 (1979) 181.
24 508 doi:10.1122/1.549524.
25
26 509 [7] S. Tcholakova, N.D. Denkov, T. Banner, Role of surfactant type and concentration for the
27 510 mean drop size during emulsification in turbulent flow, *Langmuir*. 20 (2004) 7444–7458.
28 511 doi:10.1021/la049335a.
29
30 512 [8] A.M. Huebner, C. Abell, W.T.S. Huck, C.N. Baroud, F. Hollfelder, Monitoring a reaction
31 513 at submillisecond resolution in picoliter volumes, *Anal. Chem.* 83 (2011) 1462–1468.
32 514 doi:10.1021/ac103234a.
33
34 515 [9] J.H. Kim, T.Y. Jeon, T.M. Choi, T.S. Shim, S.H. Kim, S.M. Yang, Droplet microfluidics
35 516 for producing functional microparticles, *Langmuir*. 30 (2014) 1473–1488.
36 517 doi:10.1021/la403220p.
37
38 518 [10] A.B. Pawar, M. Caggioni, R. Ergun, R.W. Hartel, P.T. Spicer, Arrested coalescence in
39 519 Pickering emulsions, *Soft Matter*. 7 (2011) 7710. doi:10.1039/c1sm05457k.
40
41 520 [11] P. Dahiya, M. Caggioni, P.T. Spicer, Arrested coalescence of viscoelastic droplets:
42 521 Polydisperse doublets, *Philos. Trans. R. Soc. A Math. Phys. Eng. Sci.* 374 (2016) 1–13.
43 522 doi:10.1098/rsta.2015.0132.
44
45 523 [12] K. Ward, Z.H. Fan, Mixing in microfluidic devices and enhancement methods, *J.*
46 524 *Micromechanics Microengineering*. 25 (2015) 094001. doi:10.1088/0960-
47 525 1317/25/9/094001.
48
49 526 [13] T. Tofteberg, M. Skolimowski, E. Andreassen, O. Geschke, A novel passive micromixer:
50 527 Lamination in a planar channel system, *Microfluid. Nanofluidics*. 8 (2010) 209–215.
51 528 doi:10.1007/s10404-009-0456-z.
52
53 529 [14] T.J. Johnson, D. Ross, L.E. Locascio, Rapid microfluidic mixing, *Anal. Chem.* 74 (2002)
54 530 45–51. doi:10.1021/ac010895d.
55
56 531 [15] T. Krebs, C.G.P.H. Schroën, R.M. Boom, Coalescence kinetics of oil-in-water emulsions
57
58
59
60
61
62
63
64
65

1
2
3
4 532 studied with microfluidics, *Fuel.* 106 (2013) 327–334. doi:10.1016/j.fuel.2012.10.067.
5
6 533 [16] A. Arbor, G. Tryggvason, The Flow Induced by the Coalescence of Two Initially
7 534 Stationary Drops, *Nasa Tech. Memo.* (1994).
8
9 535 [17] E. Nowak, N.M. Kovalchuk, Z. Che, M.J.H. Simmons, Effect of surfactant concentration
10 536 and viscosity of outer phase during the coalescence of a surfactant-laden drop with a
11 537 surfactant-free drop, *Colloids Surfaces A Physicochem. Eng. Asp.* 505 (2016) 124–131.
12 538 doi:10.1016/j.colsurfa.2016.02.016.
13
14
15 539 [18] E. Nowak, Z. Xie, N.M. Kovalchuk, O.K. Matar, M.J.H. Simmons, Bulk advection and
16 540 interfacial flows in the binary coalescence of surfactant-laden and surfactant-free drops,
17 541 *Soft Matter.* 13 (2017) 4616–4628. doi:10.1039/C7SM00328E.
18
19 542 [19] C. V. Sternling, L.E. Scriven, Interfacial turbulence: Hydrodynamic instability and the
20 543 marangoni effect, *AIChE J.* 5 (1959) 514–523. doi:10.1002/aic.690050421.
21
22 544 [20] L.E. Scriven, C. V. Sternling, The Marangoni Effects, *Nature.* 187 (1960) 186–188.
23 545 doi:10.1038/187186a0.
24
25 546 [21] D.T. Wasan, Destabilization of Water-in-Oil Emulsions, in: *Emuls. - A Fundam. Pract.*
26 547 Approach, 1992: pp. 283–295.
27
28 548 [22] M. Saad Bhamla, C. Chai, M.A. Àlvarez-Valenzuela, J. Tajuelo, G.G. Fuller, Interfacial
29 549 mechanisms for stability of surfactant-laden films, *PLoS One.* 12 (2017) 1–14.
30 550 doi:10.1371/journal.pone.0175753.
31
32
33 551 [23] K. Szymczyk, B. Jańczuk, The adsorption at solution-air interface and volumetric
34 552 properties of mixtures of cationic and nonionic surfactants, *Colloids Surfaces A*
35 553 *Physicochem. Eng. Asp.* 293 (2007) 39–50. doi:10.1016/j.colsurfa.2006.07.006.
36
37 554 [24] B. Jańczuk, A. Zdziennicka, W. Wójcik, The properties of mixtures of two anionic
38 555 surfactants in water at the water | air interface, *Colloids Surfaces A Physicochem. Eng.*
39 556 *Asp.* 220 (2003) 61–68. doi:10.1016/S0927-7757(03)00060-8.
40
41 557 [25] S.D. Hudson, A.M. Jamieson, B.E. Burkhardt, The effect of surfactant on the efficiency of
42 558 shear-induced drop coalescence, *J. Colloid Interface Sci.* 265 (2003) 409–421.
43 559 doi:10.1016/S0021-9797(03)00396-5.
44
45
46 560 [26] W.H. Weheliye, T. Dong, P. Angeli, On the effect of surfactants on drop coalescence at
47 561 liquid/liquid interfaces, *Chem. Eng. Sci.* 161 (2017) 215–227.
48 562 doi:10.1016/j.ces.2016.12.009.
49
50 563 [27] L. Frenz, A. El Harrak, M. Pauly, S. Bégin-Colin, A.D. Griffiths, J.C. Baret, Droplet-
51 564 based microreactors for the synthesis of magnetic iron oxide nanoparticles, *Angew.*
52 565 *Chemie - Int. Ed.* 47 (2008) 6817–6820. doi:10.1002/anie.200801360.
53
54
55 566 [28] H. Diamant, D. Andelman, Kinetics of Surfactant Adsorption at Fluid-Fluid Interfaces, *J.*
56 567 *Phys. Chem.* 100 (1996) 13732–13742. doi:10.1021/jp960377k.
57
58 568 [29] K. Eliceiri, C.A. Schneider, W.S. Rasband, K.W. Eliceiri, NIH Image to ImageJ : 25 years
59 569 of image analysis, *Nat. Methods.* 9 (2012) 671–675. doi:10.1038/nmeth.2089.

1
2
3
4 570 [30] D.F. Evans, H. Wennerström, *The Colloidal Domain: Where Physics, Chemistry, Biology,*
5 571 and Technology Meet, 2nd ed., 1999.
6
7 572 [31] J.J. Nash, K.A. Erk, Stability and interfacial viscoelasticity of oil-water nanoemulsions
8 573 stabilized by soy lecithin and Tween 20 for the encapsulation of bioactive carvacrol,
9 574 *Colloids Surfaces A Physicochem. Eng. Asp.* 517 (2017) 1–11.
10 575 doi:10.1016/j.colsurfa.2016.12.056.
11
12
13 576 [32] J.D. Berry, M.J. Neeson, R.R. Dagastine, D.Y.C. Chan, R.F. Tabor, Measurement of
14 577 surface and interfacial tension using pendant drop tensiometry, *J. Colloid Interface Sci.*
15 578 454 (2015) 226–237. doi:10.1016/j.jcis.2015.05.012.
16
17 579 [33] G. Loglio, P. Pandolfini, R. Miller, A. V. Makievska, F. Ravera, M. Ferrari, L. Liggieri,
18 580 Drop and bubble shape analysis as a tool for dilational rheological studies of interfacial
19 581 layers, in: D. Möbius, R. Miller (Eds.), *Nov. Methods to Study Interfacial Layers*,
20 582 Elsevier, 2001: pp. 439–483. doi:10.1016/S1383-7303(01)80038-7.
21
22
23 583 [34] K.H. Kang, H.U. Kim, K.H. Lim, Effect of temperature on critical micelle concentration
24 584 and thermodynamic potentials of micellization of anionic ammonium dodecyl sulfate and
25 585 cationic octadecyl trimethyl ammonium chloride, *Colloids Surfaces A Physicochem. Eng.*
26 586 *Asp.* 189 (2001) 113–121. doi:10.1016/S0927-7757(01)00577-5.
27
28 587 [35] V. Mosquera, J.M. Del Río, D. Attwood, M. García, M.N. Jones, G. Prieto, M.J. Suarez,
29 588 F. Sarmiento, A study of the aggregation behavior of hexyltrimethylammonium bromide
30 589 in aqueous solution, *J. Colloid Interface Sci.* 206 (1998) 66–76.
31 590 doi:10.1006/jcis.1998.5708.
32
33
34 591 [36] T.G. Movchan, A.I. Rusanov, I. V Soboleva, N.R. Khlebunova, E. V Plotnikova, A.K.
35 592 Shchekin, *Diffusion Coefficients of Ionic Surfactants*, *Colloid J.* 77 (2015) 492–499.
36 593 doi:10.1134/S1061933X15040146.
37
38 594 [37] M.J. Rosen, *Surfactants and Interfacial Phenomena*, 3rd ed., John Wiley & Sons, Inc.,
39 595 2004.
40
41 596 [38] J. Eastoe, S. Nave, A. Downer, A. Paul, A. Rankin, J. Penfold, *Adsorption of Ionic*
42 597 *Surfactants at the Air - Solution Interface*, *Langmuir*. 16 (2000) 4511–4518.
43 598 doi:10.1021/la991564n.
44
45 599 [39] B.J. Park, J. Pantina, E.M. Furst, M. Oettel, S. Reynaert, *Direct Measurements of the*
46 600 *Effects of Salt and Surfactant on Interaction Forces between Colloidal Particles at Water-*
47 601 *Oil Interfaces*, *Langmuir*. 24 (2008) 1686–1694. doi:10.1021/la7008804.
48
49
50 602 [40] B.P. Binks, *Particles as surfactants - Similarities and differences*, *Curr. Opin. Colloid*
51 603 *Interface Sci.* 7 (2002) 21–41. doi:10.1016/S1359-0294(02)00008-0.
52
53 604 [41] M. Wu, T. Cubaud, C. Ho, *Scaling law in liquid drop coalescence driven by surface*
54 605 *tension*, *Phys. Fluids*. 16 (2004) 51–54. doi:10.1063/1.1756928.
55
56 606 [42] S.J. Rehfeld, *Adsorption of Sodium Dodecyl Sulfate at Various Hydrocarbon-Water*
57 607 *Interfaces*, *J. Phys. Chem.* 71 (1967) 738–745. doi:10.1021/j100862a039.
58
59 608 [43] V.B. Fainerman, E. V. Aksenenko, N. Mucic, A. Javadi, R. Miller, *Thermodynamics of*
60
61
62
63
64
65

1
2
3
4 609 adsorption of ionic surfactants at water/alkane interfaces, *Soft Matter*. 10 (2014) 6873–
5 610 6887. doi:10.1039/C4SM00463A.
6

7 611 [44] A. Prins, C. Arcuri, M. Van den Tempel, *Elasticity of Thin Liquid Films*, *J. Colloid*
8 612 *Interface Sci.* 24 (1967) 84–90. doi:10.1016/0021-9797(67)90281-0.
9
10 613 [45] A. Javadi, N. Mucic, D. Vollhardt, V.B. Fainerman, R. Miller, Effects of dodecanol on the
11 614 adsorption kinetics of SDS at the water–hexane interface, *J. Colloid Interface Sci.* 351
12 615 (2010) 537–541. doi:10.1016/j.jcis.2010.07.033.
13
14
15 616 [46] C. Stubenrauch, V.B. Fainerman, E. V Aksenenko, R. Miller, Adsorption behavior and
16 617 dilatational rheology of the cationic alkyl trimethylammonium bromides at the water/air
17 618 interface, *J. Phys. Chem. B*. 109 (2005) 1505–1509. doi:10.1021/jp0465251.
18
19 619 [47] V. Seredyuk, E. Alami, M. Nydén, K. Holmberg, A. V. Peresypkin, F.M. Menger,
20 620 Adsorption of zwitterionic gemini surfactants at the air-water and solid-water interfaces,
21 621 *Colloids Surfaces A Physicochem. Eng. Asp.* 203 (2002) 245–258. doi:10.1016/S0927-
22 622 7757(01)01106-2.
23
24
25 623 [48] K. Ahn, J. Agresti, H. Chong, M. Marquez, D.A. Weitz, Electrocoalescence of drops
26 624 synchronized by size-dependent flow in microfluidic channels, *Appl. Phys. Lett.* 88
27 625 (2006). doi:10.1063/1.2218058.
28
29 626
30
31
32
33
34
35
36
37
38
39
40
41
42
43
44
45
46
47
48
49
50
51
52
53
54
55
56
57
58
59
60
61
62
63
64
65

1 **Controllable internal mixing in coalescing droplets induced by the solutal Marangoni**
2 **convection of surfactants with distinct headgroup architectures**

3 Jerome J. Nash^a, Patrick T. Spicer^b, and Kendra A. Erk^{a*}

4 a. School of Materials Engineering, Purdue University, West Lafayette, IN 47907, USA;

5 b. School of Chemical Engineering, The University of New South Wales, Sydney 2052, Australia

6 *corresponding author, Email: erk@purdue.edu, Phone: (765) 494-4118

7 **Keywords:** Marangoni flow; convection; mixing; coalescence

8 **Abstract**

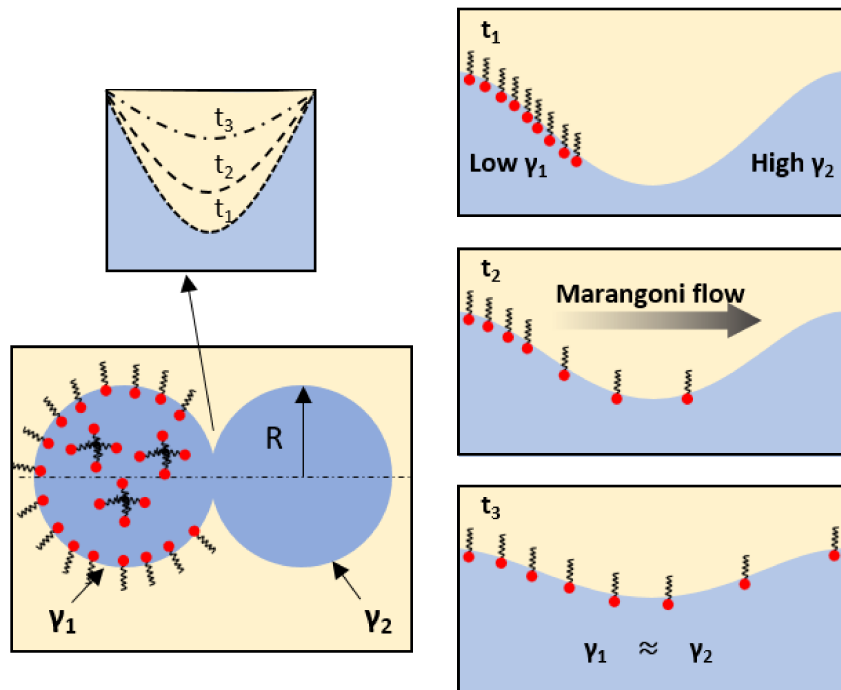
9 Through several complementary experiments, an investigation of the bulk and interfacial
10 flows that emerged during the coalescence of two water-in-oil droplets with asymmetric
11 compositional properties was performed. By adding surfactant to one of the coalescing droplets
12 and leaving the other surfactant-free, a strong interfacial tension gradient (i.e., solutal
13 Marangoni) driving energy between the merging droplets generated pronounced internal mixing.

14 The contributions of two distinct types of surfactant, anionic ammonium lauryl sulfate (ALS) and
15 cationic cetyltrimethylammonium bromide (CTAB) on the rate of coalescence bridge expansion
16 and on the generation of opposing flows during coalescence were investigated. All coalescence
17 experiments supported the power law relation between the radius of the expanding connective
18 liquid bridge and time, $r_b \propto t^{1/2}$. However, the presence of surfactant decreased the magnitude of
19 the prefactor in this relationship due to induced interfacial solutal Marangoni convection.

20 Experiments showed that packing efficiency, diffusivity, and bulk concentration of the selected
21 surfactant are vital in solutal Marangoni convection and thus the degree and timescale of internal
22 mixing between merging droplets, which has yet to be adequately discussed within the literature.

23 Denser interfacial packing efficiency and lower diffusivity of CTAB produced stronger opposing

1
2
3
4 24 bulk and interfacial flow as well as greater bulk mixing. A discussion of how optimized
5 surfactant selection and solutal Marangoni convection can be used for passively inducing
6
7 25 convective mixing between coalescing drops in microfluidic channels when viscosity modulation
8
9 26 is not feasible is provided.
10
11
12



39 28 **Graphical Abstract**
40
41

42 29 **1. Introduction**
43
44

45 30 The coalescence of two identical droplets, and the corresponding bulk fluid flows that
46
47 31 emerge, has been studied at length in the literature. [1–5] However, far less attention has been
48
49 32 given to the coalescence of binary droplets with asymmetric physical properties, despite its
50
51 33 importance to many industrial and research applications including enhanced oil recovery [6],
52
53 34 emulsification [7], microfluidic reactors [8], and functional microparticle fabrication. [9–11]
54
55
56
57
58
59
60
61
62
63
64
65

1
2
3
4 35 Many additional examples can be found in the literature of microfluidic applications that
5
6 36 utilize the coalescence of droplets as a vital processing step in material fabrication. However,
7
8 37 mixing immiscible phases in microfluidic devices often proves difficult because of the low
9
10 38 Reynolds number flows encountered within microchannels. Several researchers have shown that
11
12 39 the combination of immiscible fluids in microchannels can be improved with modified channel
13
14 40 designs [12–14] or, quite often, by modulating the viscosity of one or both of the coalescing
15
16 41 fluids to achieve desired bulk convective mixing. [15,16] While several detailed coalescence
17
18 42 studies have investigated the effects of variable external oil phase viscosity on the generation of
19
20 43 bulk flows in coalescing water droplets [17,18], little attention was given to the potential
21
22 44 influence of polar surfactant headgroup architecture in the generation of the observed opposing
23
24 45 interfacial and bulk flows. Moreover, altering the viscosities of the bulk fluids is not always a
25
26 46 viable option in microfluidic applications (for example, when high throughput is a processing
27
28 47 requirement, or when a system is restricted to fluids with predetermined viscosities). Thus,
29
30 48 additional routes for inducing a similar degree of internal mixing under these restrictions are
31
32 49 necessary, and currently, no experimental studies in the literature have sought to provide insight
33
34 50 into how appropriate surfactant selection can influence this phenomenon.

43
44 51 Utilizing solutal Marangoni convection, also known as the Gibbs-Marangoni effect,
45
46 52 [19,20] provides a compelling avenue for inducing desired bulk flows in coalescing binary fluid
47
48 53 systems, without the need for modulating bulk fluid viscosity. The Gibbs-Marangoni effect can
49
50 54 be induced simply by adding a dilute concentration of a highly surface-active solute to one of the
51
52 55 fluid droplets, while keeping the second drop initially free of any surfactant, then bringing the
53
54 56 droplets into contact. When the two fluid droplets coalesce, a highly curved connective liquid
55
56 57 bridge forms between them and expands rapidly due to interfacial stresses. In the inertial regime,

1
2
3
4 58 a scaling relation derived from a simple physical argument can be used to describe the expansion
5
6 59 of the coalescence bridge. [4] This scaling law predicts linear proportionality between the radius
7
8 60 of the connective liquid bridge, r_b ($= D_b/2$), and the square root of the coalescence time, $t^{1/2}$,
9
10 61 given by the equation, $D_b/2 \propto (R\gamma/\rho_{out})^{1/4}t^{1/2}$, where R is the initial drop radius, γ is the
11
12 62 interfacial tension, and ρ_{out} is the density of the outer fluid.
13
14
15

16
17 63 As bridge expansion proceeds, the resulting fluid motion acts to pull the droplets together
18
19 64 to form a single, larger drop. However, in the presence of an induced surface tension (i.e.,
20
21 65 surfactant concentration) gradient between the droplets, opposing interfacial and bulk flows can
22
23 66 emerge. This is because surfactant molecules become nonuniformly distributed at the interface
24
25 67 along the highly curved, connective liquid bridge separating the surfactant-laden and surfactant-
26
27 68 free drops. [21] Relaxation to a homogenous surfactant coverage does not proceed primarily by
28
29 69 diffusion, but by a far more rapid process (i.e., the Gibbs-Marangoni effect) where the surfactant
30
31 70 molecules at the interface swiftly migrate toward regions of highest local interfacial tension. This
32
33 71 in turn generates interfacial motion in the direction of the surfactant concentration gradient that
34
35 72 acts tangentially to the merging droplets, which is accompanied by bulk motion in the adjacent
36
37 73 fluid layers. Consequently, bulk flows which drive the droplets together under the influence of a
38
39 74 favorable reduction in capillary pressure, $\Delta P = 2\gamma/R$, become unbalanced with interfacial flows.
40
41 75 This ultimately results in opposing interfacial and bulk convective motion and can lead to
42
43 76 pronounced bulk fluid mixing.
44
45
46
47
48
49
50
51

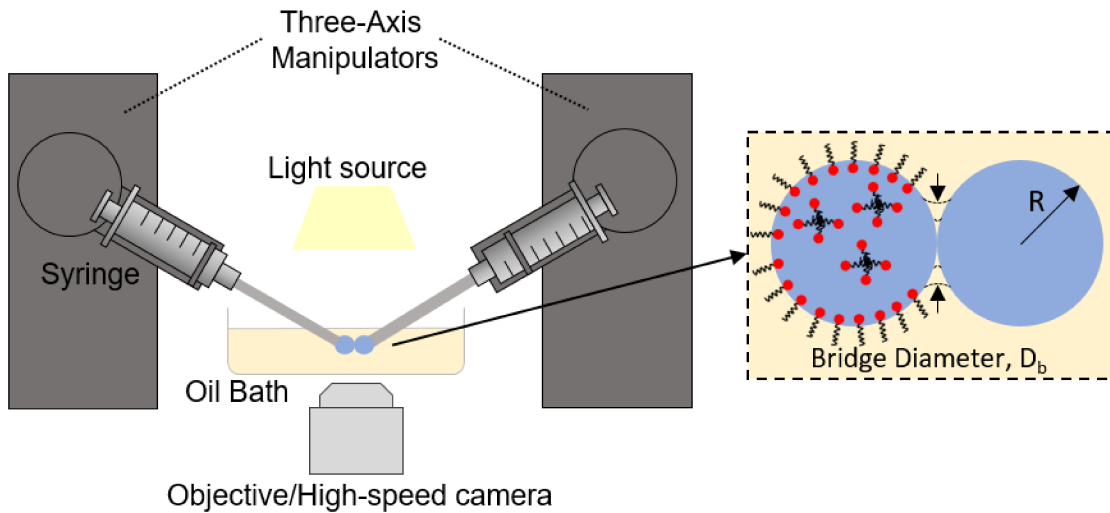
52 77 It has been shown that the mobility [22], as well as the degree of equilibrium interfacial
53
54 78 adsorption of low molecular weight surfactants [23,24], can vary substantially depending on the
55
56 79 nature of the surfactant's polar headgroup in a polar solvent such as water (i.e., whether it is
57
58 80 anionic, cationic, nonionic, or zwitterionic). These interfacial characteristics are also well-known
59
60
61
62
63
64
65

1
2
3
4 81 to have demonstrated importance in the occurrence of film rupture and coalescence for
5 surfactant-laden fluid interfaces. [25,26] Therefore, it would stand to reason that strategically
6 82 modulating the interfacial mobility, equilibrium saturation adsorption, and adsorption-desorption
7 kinetics of the added surfactant would enable interested parties to control coalescence related
8 83 phenomena, such as passively-induced internal mixing between emulsion droplets in the
9 presence of a surfactant concentration gradient. Optimized design of such small-scale processes
10 84 will require the ability to identify appropriate surfactants based on their physicochemical
11 properties and performance in applications like diagnostic chips and other microfluidics systems.
12 85 Thus, this work seeks to demonstrate several key mechanisms relating the adsorption of two
13 oppositely charged ionic surfactants and the manifested solutal Marangoni flows that drive bulk
14 mixing between coalescing aqueous droplets in a viscous surrounding oil. Generalized
15 86 relationships between the interfacial properties of low molecular weight surfactant and their
16 potential influence on bulk coalescing phenomena are also provided.
17
18
19
20
21
22
23
24
25
26
27
28
29
30
31
32
33
34
35
36
37
38
39
40
41
42
43
44
45
46
47
48
49
50
51
52
53
54
55
56
57
58
59
60
61
62
63
64
65

94 Many detailed experimental and theoretical analyses have been performed which
95 elucidate early-stage coalescence phenomena of uniform liquid droplets both in air and an
96 external liquid. [1–5] However, fully developed mixing behaviors in the later stages of
97 coalescence (i.e., several milliseconds following the onset of coalescence) are often a primary
98 concern in microfluidic reactor applications. [8,27] Therefore, to aid in the design of such
99 systems, the specific aims of this work were to (1) investigate the late-stage coalescence
100 behavior of binary liquid droplets with an induced surfactant concentration gradient along the
101 connective liquid bridge, and (2) illustrate how controlling equilibrium adsorption and solutal
102 Marangoni motion through appropriate surfactant selection can encourage varying degrees of
103 bulk fluid mixing. Through several complementary experiments, including equilibrium

1
2
3
4 104 surfactant adsorption measurements, high-speed image processing, and concentration gradient-
5
6 105 induced interfacial velocity measurements via particle tracking, we provide new insights into the
7
8 106 fundamental relationships between optimized surfactant selection and bulk fluid mixing.
9
10 107 Considering that the adsorption and interfacial spreading behavior of surfactants can vary
11
12 108 dramatically depending on the electrostatic interactions of the surfactant present at the fluid
13
14 109 interface in the bulk aqueous solution [28], detailed investigations which further elucidate the
15
16 110 role of surfactant selection in the development of varying degrees of opposing flows within
17
18 111 coalescing binary droplets are essential.
19
20
21
22
23
24 112 **2. Materials and Experimental Methods**
25
26
27
28 113 *2.1. Materials*
29
30
31 114 The external liquid phase used during drop coalescence measurements was a triglyceride
32
33 115 oil (Stepan Company, CAS # 73398-61-5) with a manufacturer reported viscosity of 25 mPa·s
34
35 116 and density of 0.95 g cm⁻³, both at 25 °C. The oil was double-filtered through a chromatography
36
37 117 column containing alumina (Fisher, CAS # 1344-28-1) to remove trace surface-active impurities
38
39 118 prior to use. The droplets consisted of aqueous solutions prepared with water passed through a
40
41 119 Filmtec™ reverse osmosis membrane (total dissolved solids ≤ 15 ppm, Dow Chemical
42
43 120 Company). The two commercially available surfactants used in this study, ammonium lauryl
44
45 121 sulfate, ALS (anionic surfactant, 30% in water, CAS # 2235-54-3) and cetyltrimethylammonium
46
47 122 bromide, CTAB (cationic surfactant, ≥ 99%, CAS # 57-09-0), were obtained from Sigma-
48
49 123 Aldrich and used without further purification. The blue dye added to the surfactant-free droplet
50
51 124 in each binary droplet coalescence measurement as an aid for visualizing bulk motion was
52
53 125 purchased from Queen Fine Foods Pty Ltd. The flat metal capillaries (18-gauge x 1.0" blunt tip
54
55 126 dispensing needles) used in droplet coalescence experiments were obtained from CML Supply.
56
57
58
59
60
61
62
63
64
65

1
2
3
4 127 2.2. Visualizing rapid binary drop coalescence
5
6
7
8
9
10
11
12
13
14
15
16
17
18
19
20
21
22
23
24



25 **Figure 1.** An illustration of the experimental setup used to study coalescence phenomena between binary aqueous
26 droplets in a surrounding oil. The leftmost aqueous droplet was laden with surfactant and the rightmost droplet was
27 surfactant-free, yet contained a small concentration of dye to aid in flow visualization.

28 128 A schematic of the experimental setup used for visualizing binary liquid droplet
29 129 coalescence is shown in Figure 1. Experiments were performed using a pair of three-axis
30 130 micromanipulators (Sensapex) secured to z-axis translational stages (THORLABS) flanking an
31 131 inverted optical microscope (AE31, Motic Microscopes). Two water droplets with asymmetric
32 132 compositional properties, each having an initial diameter of 2 mm (unless otherwise specified)
33 133 were formed at the tips of 18-gauge metal capillaries and were made to contact at negligible
34 134 approach velocities ($\sim 0.01 \text{ mm s}^{-1}$) in a clear petri dish containing the low viscosity triglyceride
35 135 oil (5 mL working volume). Coalescence of the binary droplets was captured with a high-speed
36 136 camera (Phantom v7.3) at 11000 frames per second. Measurements of the bridge expansion
37 137 kinetics were performed via image processing using open-source ImageJ software. [29]

38 138 A concentration gradient along the connective liquid between the two merging water

39 139 drops was generated by adding the surfactant of interest to the leftmost coalescing droplet
40 140 (Figure 1), while keeping the rightmost droplet surfactant-free. The surfactant-loaded droplet in

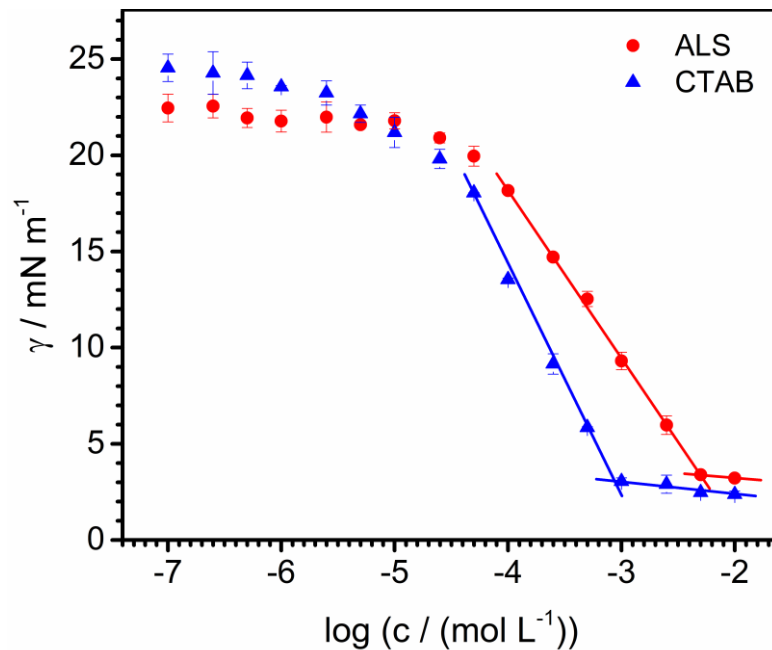
41
42
43
44
45
46
47
48
49
50
51
52
53
54
55
56
57
58
59
60
61
62
63
64
65

1
2
3
4 141 each experiment contained either ALS or CTAB at a concentration of 2.5×10^{-3} mol L⁻¹, which
5
6 142 was near the experimentally determined critical micelle concentration (CMC) for each surfactant
7
8 143 type. The relevant data used in determining the CMC for each surfactant is provided in Section
9
10 144 2.3. This initial bulk surfactant concentration was chosen because near and above the CMC, the
11
12 145 chemical potential of the surfactant negligibly changes and as a result conditions at the interface
13
14 146 do not change. [30] Thus, the surfactant-laden droplet interface in this experimental setup
15
16 147 represents an interfacial monolayer near saturation equilibrium. At the chosen bulk
17
18 148 concentration, the equilibrium interfacial tension of the oil-water interface was 3.40 ± 0.48 mN
19
20 149 m⁻¹ for ALS and 3.01 ± 0.41 mN m⁻¹ for CTAB, as determined by the drop shape analysis
21
22 150 technique (Section 2.3).
23
24
25
26
27
28

29 151 To help visualize the emergent bulk fluid motion during droplet coalescence, dye was
30
31 152 added to the surfactant-free droplet at a concentration of 0.1 g L⁻¹. The addition of dye did not
32
33 153 substantially affect the oil-water interfacial tension (surfactant-free, pure droplet: $\gamma = 23.67 \pm$
34
35 154 0.13 mN m⁻¹; surfactant-free, dyed droplet: $\gamma = 21.42 \pm 0.27$ mN m⁻¹), and thus its contribution to
36
37 155 the emergent coalescence flows was presumed to be negligible in comparison to the presence of
38
39 156 the highly surface-active molecules, ALS and CTAB.
40
41
42
43
44
45 157 *2.3. Determination of interfacial adsorptive properties at the oil-water interface*
46
47

48 158 Interpreting the relationship between the induced bulk flows and the contributing
49
50 159 interfacial Marangoni stresses of coalescing binary droplets requires knowledge of the
51
52 160 equilibrated interfacial adsorption for each surfactant-laden droplet prior to merging. The
53
54 161 effective interfacial tension values for pure and surfactant-laden oil-water interfaces were
55
56 162 obtained using axisymmetric drop shape analysis with a contact angle goniometer/tensiometer
57
58 163 (Ramé-Hart) following experimental procedures established in previous work by Nash and Erk.
59
60
61
62
63
64
65

1
 2
 3
 4 164 [31] The theory underpinning this technique and its corresponding application to study the
 5 effective interfacial tensions for air-liquid and liquid-liquid monolayers have been previously
 6 discussed in the literature. [32,33] In brief, the interfacial tension of each oil-water interface was
 7 determined by fitting the shape profile of an aqueous pendant drop suspended from the tip of a
 8 flat 12-gauge PTFE capillary immersed in oil to the theoretical profile prescribed by the Young-
 9 Laplace equation, $\Delta P = \gamma \left(\frac{1}{R_1} + \frac{1}{R_2} \right)$. This force balance relates the differential in pressure, ΔP ,
 10 across a curved interface to its principle radii of curvature R_1 and R_2 , and interfacial tension, γ .
 11
 12 171 As surface active solutes become adsorbed to the interface, there is a demonstrable reduction in
 13 the capillary pressure. For a known pressure and interfacial curvature, the effective interfacial
 14 tension of the surfactant-laden interface can be directly measured.
 15
 16
 17
 18
 19
 20
 21
 22
 23
 24
 25
 26
 27
 28
 29
 30 174 The equilibrium interfacial adsorption isotherms for dilute aqueous solutions of ALS or
 31
 32 175 CTAB in contact with triglyceride oil are provided in Figure 2. In each adsorption experiment,
 33
 34 176 the interfacial tension was measured over time for at least 45 minutes, or until a constant
 35
 36
 37
 38



61
 62
 63
 64
 65 **Figure 2.** Interfacial tension, γ , versus log of surfactant concentration, c , in aqueous solution at 23 °C at the
 triglyceride oil-water interface measured by the drop shape analysis technique. Lines represent best-fitting straight
 lines of the data in the low and high surfactant concentration regimes for each surfactant. The slope value of the
 best-fitting line in the low surfactant concentration regime was used in the determination of the surface excess
 concentration, Γ_m , for ALS and CTAB.

1
2
3
4 177 interfacial tension value was reached. The critical micelle concentration (CMC's) for each
5 surfactant was determined graphically from Figure 2 as the intersection of the linear fits to the
6
7 178 low and high concentration regimes for each surfactant. Experimental CMC values for ALS and
8
9 179 CTAB at 23 °C were ca. 5.5×10^{-3} mol L⁻¹ and 0.95×10^{-3} mol L⁻¹, respectively. The CMC value
10
11 180 obtained here for ALS closely corresponded to the value found in the literature, 6.25×10^{-3} mol L⁻¹
12
13 181¹. [34] Likewise, the CMC value obtained here for CTAB agreed well with previous observations
14
15 182 in the literature of 0.9×10^{-3} mol L⁻¹ [35] and 1×10^{-3} mol L⁻¹ [36].
16
17
18
19
20
21

22 184 The surface excess concentration, Γ_m , corresponds to the maximum concentration of
23 surfactant adsorbed to the oil-water interface of the surfactant-laden droplet at equilibrium and
24
25 185 was approximated for each surfactant using the Gibbs adsorption equation,
26
27 186
$$\Gamma_m = -\frac{1}{mRT} \left(\frac{dy}{d \log c} \right)_{T,P}$$
, where γ is the interfacial tension (mN m⁻¹), c is the bulk surfactant
28
29 187 concentration (mol L⁻¹), R is the gas constant, T is the temperature (K), and the integer, m ,
30
31 188 accounts for the charge interactions within the polar head group of the surfactant. For dilute
32
33 189 aqueous solutions containing a single, 1:1 ionic surfactant in the absence of excess salt, $m =$
34
35 190 4.606, which was taken for both anionic ALS and cationic CTAB. [37,38] Substituting the slope
36
37 191 value of the best-fitting straight line in the low surfactant concentration regime from the
38
39 192 interfacial tension versus log of surfactant concentration curve for $\frac{dy}{d \log c}$ in the Gibbs adsorption
40
41 193 equation, Γ_m was calculated for ALS and CTAB at the triglyceride oil-water interface. The
42
43
44
45
46
47
48
49
50
51
52
53
54
55
56
57
58
59
60
61
62
63
64
65

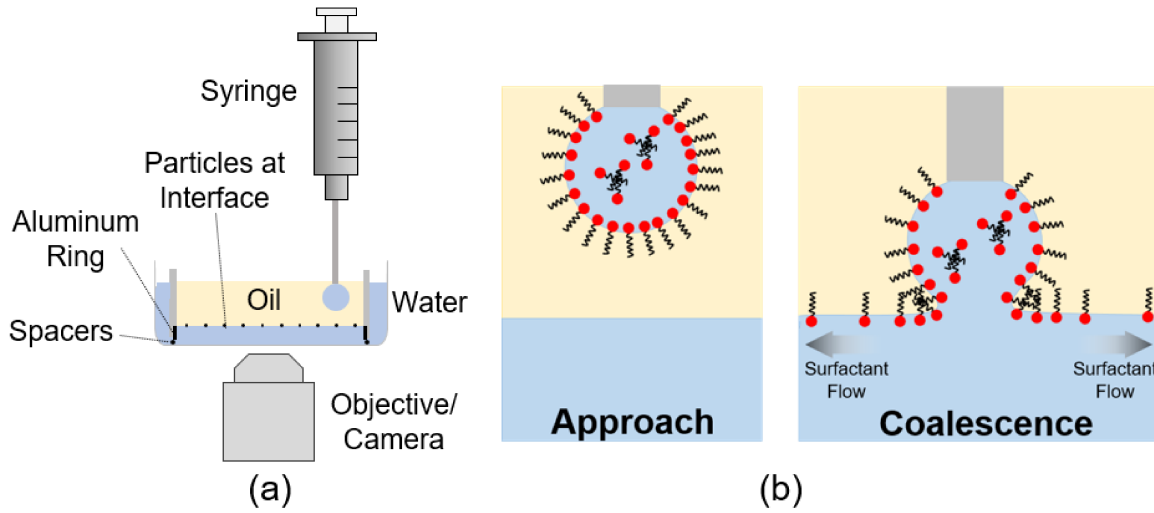
Table 1. Surface excess concentrations and minimum molecular areas calculated for ALS and CTAB at 23 °C at the triglyceride oil-water interface.

Surfactant	Surface Excess Concentration, $\Gamma_m/(10^{-6}$ mol m ⁻²)	Minimum Molecular Area, $A_{min}/(\text{\AA}^2 \text{ molecule}^{-1})$
Ammonium Lauryl Sulfate (ALS)	0.76	218
Cetyltrimethylammonium bromide (CTAB)	1.07	156

1
2
3
4 195 minimum molecular area, A_{\min} (\AA^2 molecule $^{-1}$), was then determined from the equation, $A_{\min} =$
5
6
7 196 $\frac{1 \times 10^{20}}{\Gamma_m N_A}$, where N_A is Avogadro's number. (Table 1).
8
9
10
11
12
13
14
15
16
17
18
19
20
21
22
23
24
25
26
27
28
29
30
31
32
33
34
35
36
37
38
39
40
41
42
43
44
45
46
47
48
49
50
51
52
53
54
55
56
57
58
59
60
61
62
63
64
65

1
2
3
4 197 2.4. Determination of surfactant-induced interfacial spreading velocity, U_s
5
6

7 198 The experimental setup used to study the interfacial spreading velocity, U_s , of each
8 surfactant when introduced into the pure triacylglyceride oil-water interface is shown in Figure 3.
9
10 199 The displacement of tracer particles (hollow glass spheres, 9-13 μm diameter, Sigma-Aldrich,
11
12 200 CAS # 65997-17-3) seeded at the pure oil-water interface initiated by the introduction of a
13
14 201 surfactant-loaded water droplet to the pure oil-water interface and driven by solutal Marangoni
15
16 202 surfactant-loaded water droplet to the pure oil-water interface and driven by solutal Marangoni
17
18
19
20



39 505 **Figure 3.** Schematic representation of the experimental setup used to quantify interfacial spreading velocities, U_s ,
40 506 under an induced interfacial tension gradient at the triglyceride oil-water interface. A side view depicting the
41 507 introduction of a surfactant loaded water droplet at the surfactant-free, oil-water interface (containing tracer
42 508 particles) is shown in (a) and an illustration of the surfactant diffusion mechanism, quantified by measuring the rate
43 509 of displacement for tracer particles attached to the interface, is shown in (b).

44 203 flow was measured.
45
46

47 204 The motion of tracer particles was measured at a planar oil-water interface because this
48 205 experimental scheme specifically enabled the measurement of Marangoni-induced flow rates
49 206 under the effect of a surfactant concentration gradient at the oil-water interface. Ensuring that the
50 207 measured flow rates were obtained for tracer particles located specifically at the oil-water
51 208 interface and not within one of the subphases was most directly accomplished with a droplet
52 209 coalescing with a planar oil-water interface.
53
54
55
56
57
58
59
60
61
62
63
64
65

1
2
3
4 210 Preparation of a planar triglyceride oil-water interface containing the seeded glass
5
6
7 211 spheres was performed using a modified optical microscopy cell and methodology adapted from
8
9 212 the work of Park et al. [39] The cell used here consisted of a polystyrene petri dish (height 1 cm,
10
11 213 outer diameter of 40 mm) and a concentric polystyrene cylinder (height 1 cm, outer diameters of
12
13 214 30 mm). An aluminum ring was inserted into the bottom of the inner polystyrene cylinder to pin
14
15 215 the contact line of the oil-water interface. The inner cylinder was secured to the polystyrene petri
16
17 216 dish using a fast curing epoxy and 0.1 mm glass spacers. This allowed for the oil-water system to
18
19 217 achieve hydrostatic equilibrium, ensuring that a planar oil-water interface could be attained via
20
21 218 the addition or removal of water from the outer portion of the sample cell.

22
23
24 219 After forming a planar oil-water interface free of any solutes, an oil droplet containing
25
26
27 220 tracer particles was directly added to the upper oil phase of the sample cell. This yielded a seeded
28
29 221 tracer concentration of $\sim 4 \times 10^6$ particles-cm⁻² at the interface, a concentration which was
30
31 222 necessary for accurate particle tracking measurements and quantifying the interfacial spreading
32
33 223 velocities resulting from the introduction of surfactant. It should be noted that at this
34
35 224 concentration, seeded tracer particles displayed slight aggregation. Very large aggregates would
36
37 225 be expected to display lower interfacial spreading velocities in comparison to unaggregated
38
39 226 primary particles due to their larger mass and could therefore introduce some degree of
40
41 227 uncertainty into the measured interfacial spreading velocities in this experimental setup.

42
43
44 228 However, the largest aggregates observed in this study consisted of 2-3 primary particles, and
45
46 229 measurements of the steady-state, fully developed displacement rates for these aggregates were
47
48 230 indistinguishable from the measured displacement rates of unaggregated, interfacially adsorbed
49
50 231 primary particles.

1
2
3
4 232 Following the seeding of tracer particles, the experimental cell was stabilized for 15
5 minutes, then a 10 μL droplet of either surfactant solution was formed at the tip of a metal
6 capillary within the oil layer. The droplet was equilibrated for an additional 30 minutes within
7 the upper oil layer prior to contact with the planar oil-water interface to allow for saturated
8 interfacial adsorption of the surfactant. Finally, the droplet was lowered slowly ($\sim 0.01 \text{ mm s}^{-1}$) to
9 contact the planar oil-water interface and the resulting isotropic tracer particle motion was
10 captured using an inverted microscope and high-speed camera (Photron Mini UX) at 2000
11 frames per second. Due to the remarkably high energy of attachment for micrometer-scale
12 particles at the oil-water interface, [40] particle motion was presumed to be approximately two-
13 dimensional for the duration of particle spreading. Care was taken to quantify the displacement
14 of at least five tracer particles from two separate experiments for each oil-water-surfactant
15 system, measured manually using ImageJ software.
16
17
18
19
20
21
22
23
24
25
26
27
28
29
30
31
32
33
34 244 **3. Results and Discussion**
35
36
37 245 *3.1. Effect of surfactant type on bridge expansion and bulk mixing during the coalescence of*
38
39 246 *equally sized drops*
40
41
42
43 247 Our investigation of surfactant contributions in the generation of opposing flows within
44
45 248 coalescing binary droplets begins with the consideration of two surfactant-free droplets sharing
46
47 249 an equivalent initial diameter, $2R$ ($= 2 \text{ mm}$), and approximately equal oil-water interfacial
48
49 250 tensions (surfactant-free, undyed droplet: $\gamma_1 = 23.67 \pm 0.13 \text{ mN m}^{-1}$; surfactant-free, dyed
50
51 251 droplet: $\gamma_2 = 21.42 \pm 0.27 \text{ mN m}^{-1}$). Analysis of bridge expansion for the two, equally sized
52
53 252 coalescing droplets with no added surfactant revealed that this system closely obeyed the
54
55 253 $D_b/2 \propto (R\gamma/\rho_{\text{out}})^{1/4}t^{1/2}$ scaling relation over the entire duration of droplet merging (Figure
56
57 254 4), agreeing well with the experimental observations of previous researchers. [17,18]

1
2
3
4
5
6
7
8
9
10
11
12
13
14
15
16
17
18
19
20
21
22
23
24
25
26
27
28
29
30
31
32
33
34
35
36
37
38
39
40
41
42
43
44
45
46
47
48
49
50
51
52
53
54
55
56
57
58
59
60
61
62
63
64
65

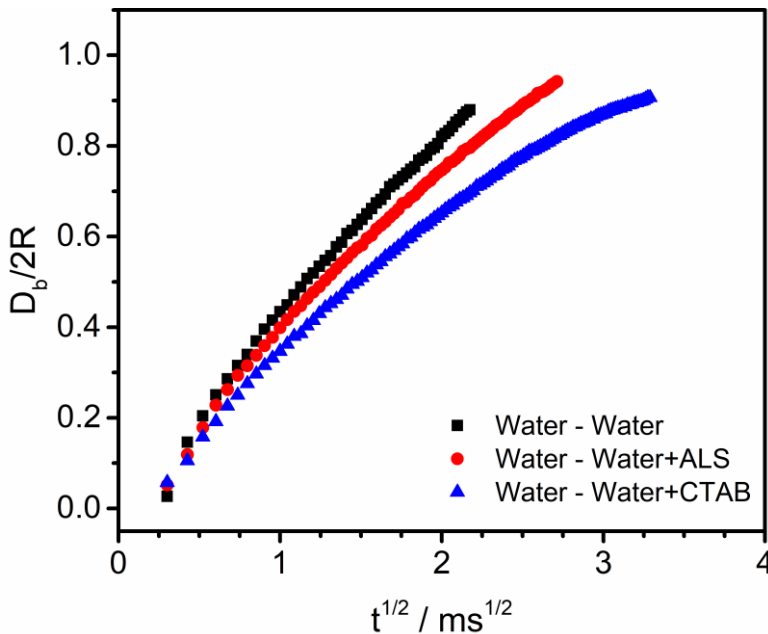
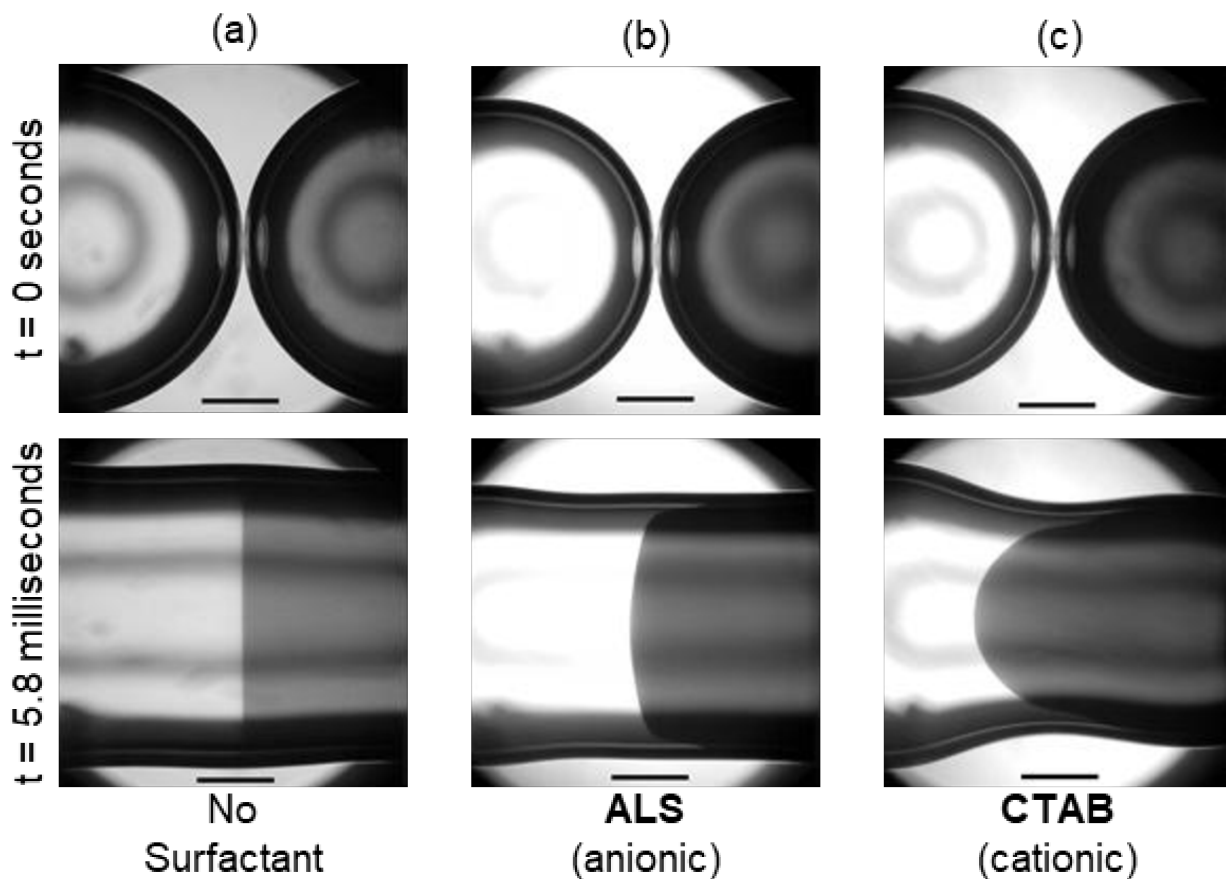


Figure 4. Kinetics of expansion for the connective bridge separating spherical droplets with an equivalent initial diameter, $2R$ ($= 2$ mm). The data represent the increase in the connective bridge diameter, D_b , relative to $2R$, as a function of the square-root-of-time, $t^{1/2}$, succeeding the onset of droplet coalescence.

For equally sized coalescing droplets, where one of the drops contained 2.5×10^{-3} mol L⁻¹

ALS, the $D_b/2 \propto t^{1/2}$ scaling relation was also closely obeyed, but a slightly reduced slope in the experimental data was observed. This indicates that the value of the prefactor, $(R\gamma/\rho_{out})^{1/4}$, in the coalescence scaling relation was influenced by the presence of ALS. Likewise, an even more pronounced decrease in the slope of this scaling relationship became apparent at longer times for systems containing 2.5×10^{-3} mol L⁻¹ CTAB. This further suggests that the gradient in interfacial tension and timescale of solutal Marangoni flow of the chosen surfactant along the interface of expanding liquid bridge has a demonstrable influence on the value of the prefactor in the scaling relation, which was not explicitly accounted for or discussed in the derivation of this scaling relation.

1
 2
 3
 4 265 The characteristic time scale for coalescence of two equally sized drops with equal
 5
 6 interfacial tensions in inviscid flow is set by $\tau_C = \sqrt{(\rho R^3)/\gamma}$. [41] For the merging of two 0.75-
 7 mm radius water drops in the inertial regime, with $\gamma = 23 \text{ mN m}^{-1}$, τ_C is $\sim 4.2 \text{ ms}$. This
 8
 9 267 characteristic relaxation time closely approximates the experimentally measured time required
 10
 11 268 for the expanding bridge between the surfactant-free water droplets to become equal to the initial
 12
 13 269 drop diameter for the system shown in Figure 5a. This approximation is less representative in the
 14
 15 270 presence of a surfactant concentration gradient, which can be seen from the data in Figure 5b and
 16
 17 271 5c, for ALS and CTAB, respectively. Each of these systems require a longer duration for the
 18
 19 272 diameter of the expanding bridge to be equal to the initial diameter of the drops. The observed
 20
 21 273
 22
 23
 24
 25
 26
 27



57 **Figure 5.** Temporal shape profiles of equally sized water droplets coalescing in triglyceride oil. The leftmost droplet
 58 in each image contained either (a) no surfactant, (b) $2.5 \times 10^{-3} \text{ mol L}^{-1}$ ALS, or (c) $2.5 \times 10^{-3} \text{ mol L}^{-1}$ CTAB, while the
 59 rightmost droplet in each image was surfactant-free, with dye added for flow visualization. The absence or presence
 60 of opposing flows at the interface and within the bulk of the merging droplets illustrate the effect of interfacially
 61 adsorbed surfactant molecules. Differences in the curvature of the jetted fluid following coalescence in (b) and (c)
 62 demonstrate the influence of surfactant headgroup architecture on the relative magnitude of these induced flows.
 63 The scale bars in each image are 0.5 mm in length.

1
2
3
4 274 increase in τ_C for systems containing ALS or CTAB, as well as the clear difference between their
5 corresponding τ_C values, suggests that interfacial adsorptive and convective properties of the
6 surfactant contribute to the decrease in the value of the prefactor in the coalescence scaling
7 relation. This observation is discussed in greater detail in Section 3.3.
8
9
10
11
12
13
14

15 278 Figure 5a illustrates that negligible internal mixing occurred during the merging of
16 surfactant-free droplets due to the generation of two balanced, plug-flow water jets which
17 converged at the propagating coalescence neck. In this instance, the interfacial tensions of the
18 converging droplets are balanced and thus no tangential stress was competing with the bulk fluid
19 motion of the merging drops. This behavior agreed well with experimental observations of
20 previous researchers. [17,18] Contrarily, coalescence of binary droplets with non-uniform
21 compositions of a surface-active species displayed pronounced internal convective mixing during
22 the coalescence process, the degrees of which strongly depended on the surfactant present at the
23 oil-water interface of the surfactant-laden droplet.
24
25
26
27
28
29
30
31
32
33
34
35
36
37
38
39
40
41
42
43
44
45
46
47
48
49
50
51
52
53
54
55
56
57
58
59
60
61
62
63
64
65

287 Distinct bulk fluid motion was observed in the presence of either anionic ALS or cationic
288 surfactant CTAB for equally sized droplet with a capillary pressure ratio of $\Delta P_2/\Delta P_1 \approx 5$ (where
289 ΔP_1 and ΔP_2 are the capillary pressures of the leftmost droplet and the rightmost droplet,
290 respectively) and are shown in Figures 5b and 5c. The presence of surfactant in the undyed,
291 leftmost drop led to the formation of a fluid jet which propagated from the bulk of dyed,
292 surfactant-free drop as direct result of this droplet's higher capillary pressure. For the binary
293 droplets system containing 2.5×10^{-3} mol L⁻¹ ALS, the motion of the jetted fluid appeared to
294 occur under near plug flow conditions, with some discernable curvature of the jetting dyed fluid
295 at later times. However, the internal mixing for the binary systems containing 2.5×10^{-3} mol L⁻¹

1
2
3
4 296 CTAB was demonstrably more pronounced, displaying a much higher curvature of the jetted
5
6
7 297 fluid at later stages of coalescence (i.e., after 5.8 milliseconds).
8
9
10 298 *3.2. Influence of surfactant type on the development of bulk fluid jetting*
11
12
13 299 To further aid in illustrating the marked influence of surfactant in the jetting behavior
14
15 300 observed for binary droplet systems, the initial diameters of the two merging droplets were
16
17 301 modulated by increasing the initial diameter of the leftmost droplet to 2.2 mm and decreasing the
18
19 302 initial diameter of the rightmost droplet to 1.0 mm. Figure 6a shows that for asymmetrically
20
21 303 sized droplets, both free of any added surfactant and of approximately equal interfacial tension,
22
23 304 droplet merging led to only slight jetting of the fluid within the smaller diameter, surfactant-free
24
25 305 droplet into the larger droplet as a direct result of the relatively small capillary pressure gradient
26
27 306 ($\Delta P_2/\Delta P_1 \approx 2$) originating from the difference in initial droplet sizes. However, the magnitude of
28
29 307 the capillary pressure gradient was insufficient to induce a great deal of internal mixing.
30
31
32
33
34
35
36
37
38
39
40
41
42
43
44
45
46
47
48
49
50
51
52
53
54
55
56
57
58
59
60
61
62
63
64
65

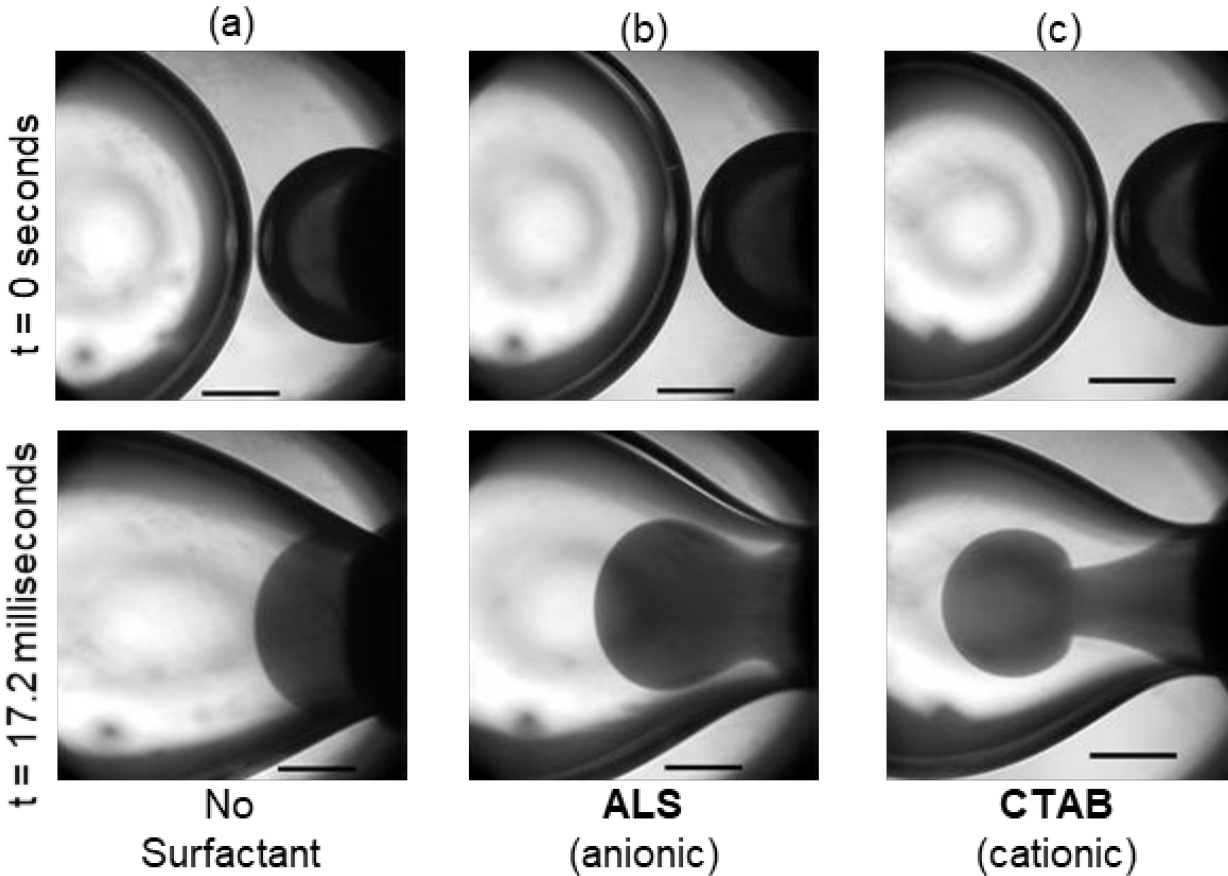


Figure 6. Flow profiles depicting the formation of fluid jets of different sizes for asymmetrically sized water droplets coalescing in triglyceride oil. The leftmost droplet in each image contained either (a) no surfactant, (b) 2.5×10^{-3} mol L⁻¹ ALS, or (c) 2.5×10^{-3} mol L⁻¹ CTAB, while the rightmost droplet in each image was surfactant-free, with dye added for flow visualization. The scale bars in each image are 0.5 mm in length.

308 In the case of binary droplet systems that contained a concentration gradient of either

409 ALS or CTAB, the difference in diameter and interfacial tension between the binary droplets

440 provided a much larger capillary pressure ratio ($\Delta P_2/\Delta P_1 \approx 11.5$) and thus a greater driving

471 energy for jetting of the fluid from the smaller droplet into the larger droplet containing

492 surfactant during coalescence. The late-stage flows that emerged under these experimental

513 conditions are shown in Figure 6b and 6c, respectively. For the binary droplet system with

544 2.5×10^{-3} mol L⁻¹ ALS present in the surfactant-laden droplet, the profile of the fluid jetted from

565 the smaller, surfactant-free droplet took the shape of a bulb-like plume with a relatively large

596 diameter forming near the apex of the jetted fluid and slightly narrower base. Similarly, for the

1
2
3
4 317 binary droplet system containing 2.5×10^{-3} mol L⁻¹ CTAB, the late-stage internal flow also
5
6 318 resulted in the formation of a fluid jet with a large bulb and narrow base. However, the jetting
7
8 319 that occurred in this case was demonstrably stronger, with the formation of a mushroom-shaped
9
10 320 plume of dyed water and a far narrower base.
11
12
13
14
15 321 The difference in the shape of the jetted fluid that emerged in systems containing ALS or
16
17 322 CTAB stemmed from the magnitudes of the convective mixing generated by the opposing bulk
18
19 323 and Marangoni interfacial flows upon droplet coalescence. As the fluid from the dyed droplet
20
21 324 flowed through the propagating coalescence neck, an interfacial diffusional flux developed in the
22
23 325 opposite direction, as interfacially adsorbed surfactant molecules in the surfactant-laden droplet
24
25 326 migrated from regions of high concentration to low concentration. This in turn generated eddy
26
27 327 currents within the bulk of the merging droplets, just beneath the interface. In the case of CTAB,
28
29 328 the driving energy for interfacial flux appeared to be sustained for a longer time than in the case
30
31 329 of ALS, which led to more pronounced eddy currents and thus the observed jetting behavior.
32
33
34
35
36
37 330 Furthermore, assessment of the displacement of the jetted fluid apex as a function of time
38
39
40
41
42
43
44
45
46
47
48
49
50
51
52
53
54
55
56
57
58
59
60
61
62
63
64
65

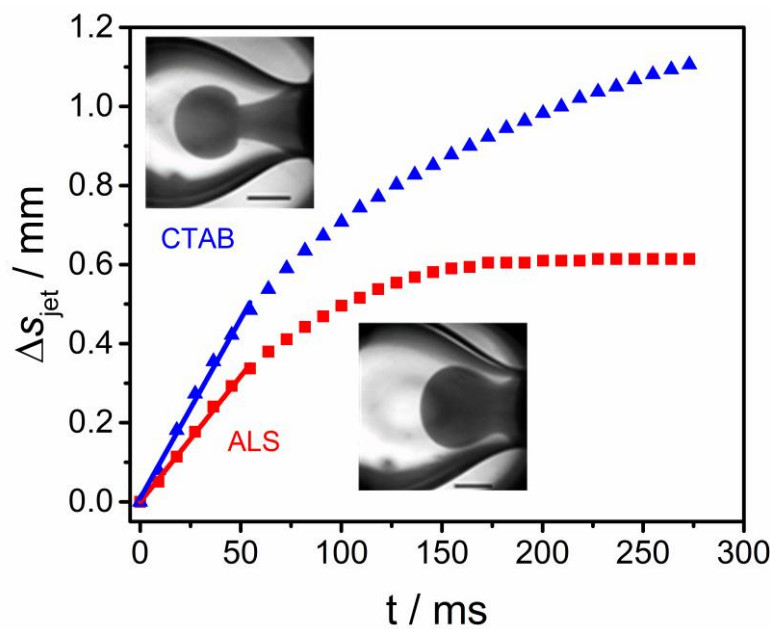


Figure 7. Displacement of the jetted fluid apex, Δs_{jet} , apex originating from the surfactant-free droplet into the surfactant-laden droplet as a function of time, t , succeeding droplet contact for asymmetrically sized droplet systems. Micrograph insets depict the position of the fluid jets 17.2 ms after the onset of coalescence. The scale bars in each image are 0.5 mm in length.

1
2
3
4 331 for asymmetrically sized binary droplet systems, containing either ALS or CTAB (Figure 7),
5
6 332 indicates a clear difference in the induced fluid motion. The rate of fluid jetting during the initial
7
8 333 stages of coalescence was roughly 30% faster for the droplet system containing cationic CTAB
9
10 334 compared to the analogous system containing anionic ALS (9.08 mm s^{-1} and 6.37 mm s^{-1} ,
11
12 335 respectively, from a linear regression fit to the initial data in Figure 7). In the following sections,
13
14 336 we discuss in detail our experimental basis for attributing differences in the emerged jetting
15
16 337 phenomena to differences in the magnitudes of the induced interfacial Marangoni flows
17
18 338 accompanying each surfactant. The jetting phenomena observed between merging drops with an
19
20 339 induced surfactant concentration gradient can also be explained by the induction of Marangoni
21
22 340 convection, where low interfacial tension liquid along the oil-water interface of the coalescing
23
24 341 neck is carried toward the higher interfacial tension regions in the surfactant-free droplet and
25
26 342 accumulates. A localized increase in the hydrostatic pressure of this region follows and the
27
28 343 development of a bulk flow of liquid from the surfactant-free droplet in the opposite direction of
29
30 344 the Marangoni flow.
31
32
33
34
35
36
37
38
39 345 *3.3. Comparison of adsorptive properties of ALS and CTAB at the triglyceride oil – water*
40
41 346 *interface*
42
43
44
45 347 Values for the surface excess concentration, Γ_m , in Table 1 indicate that CTAB molecules
46
47 348 pack more densely at the triglyceride oil-water interface than ALS molecules, which is in line
48
49 349 with previous experimental observations for the same or similar ionic surfactants at the oil-water
50
51 350 interface. [42,43] The negatively charged moiety of 1:1 anionic surfactants leads these molecules
52
53 351 to have a relatively large hydrodynamic diameter in comparison to cationic surfactants, which
54
55 352 have a comparably small hydrodynamic diameter surrounding their positively charged
56
57 353 headgroups. [44] These differences in the hydrodynamic volume surrounding the hydrophilic
58
59
60
61
62
63
64
65

347 Values for the surface excess concentration, Γ_m , in Table 1 indicate that CTAB molecules
348 pack more densely at the triglyceride oil-water interface than ALS molecules, which is in line
349 with previous experimental observations for the same or similar ionic surfactants at the oil-water
350 interface. [42,43] The negatively charged moiety of 1:1 anionic surfactants leads these molecules
351 to have a relatively large hydrodynamic diameter in comparison to cationic surfactants, which
352 have a comparably small hydrodynamic diameter surrounding their positively charged
353 headgroups. [44] These differences in the hydrodynamic volume surrounding the hydrophilic

1
2
3
4 354 portions of each surfactant molecule lead to differences in their corresponding equilibrium
5
6
7 355 adsorptive capabilities at immiscible fluid interfaces. As a direct result, anionic surfactants tend
8
9 356 to pack less efficiently at fluid interfaces than their cationic counterparts.
10
11

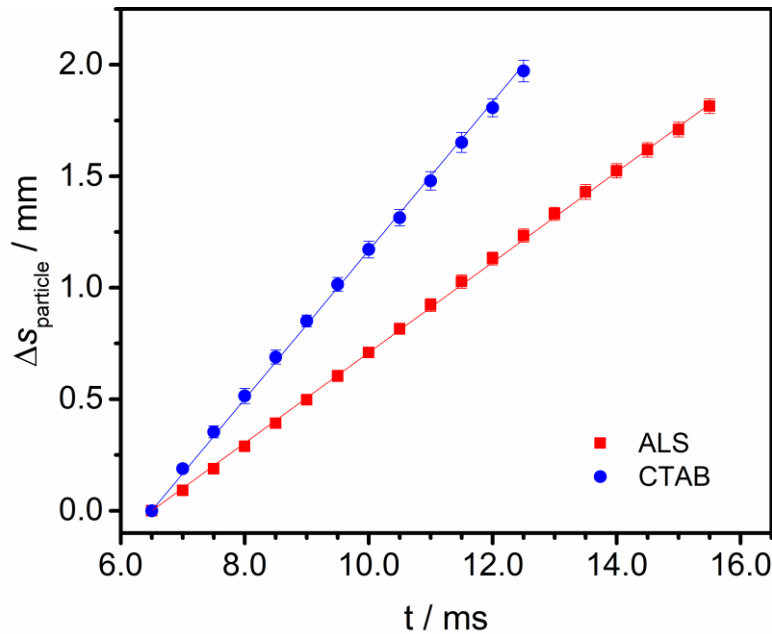
12 357 Each of the experimental observations of the differences in the magnitudes of solutal
13
14 358 Marangoni convection for ALS and CTAB would also suggest that Γ_m has a pivotal role in the
15
16 359 timescale of Marangoni interfacial flow. A more densely packed interfacial layer laden with
17
18 360 surfactant would be expected to behave more rigidly in response to interfacial tension and
19
20 361 surfactant concentration perturbations. This rigidity restricts lateral surface movements and
21
22 362 solutal Marangoni convention. Thus, the timescale for solutal Marangoni flow would increase, as
23
24 363 the interface overall would take longer to relax to a homogenous state (i.e., regions of high
25
26 364 interfacial tension and regions of low interfacial tension would exist longer for more densely
27
28 365 packed interfaces). Under these conditions, the high interfacial tension regions would apply a
29
30 366 high tangential surface stress over a longer duration.
31
32
33
34
35
36

37 367 Likewise, considering that both ALS and CTAB are soluble in the aqueous phase, and
38
39 368 can therefore adsorb and desorb from the bulk aqueous phase during droplet coalescence, both
40
41 369 the surfactant's diffusion coefficient, D , and bulk surfactant concentration, c , would be expected
42
43 370 to decrease the timescale of solutal Marangoni flow. A surfactant that can diffuse swiftly to the
44
45 371 interface from the bulk would be expected to decrease the lifetime of interfacial tension gradient,
46
47 372 (i.e., higher diffusion coefficients will favor a small concentration difference). Similarly, high
48
49 373 concentrations of surfactant in the bulk would be expected to increase the overall adsorption rate
50
51 374 of molecules near the interface, thus favoring small concentration gradients and reducing the
52
53 375 timescale of solutal Marangoni convection.
54
55
56
57
58
59
60
61
62
63
64
65

1
2
3
4 376 The timescale of solutal Marangoni convection, τ_M , was approximated using these
5
6
7 377 parameters in the equation, $\tau_M = \frac{\Gamma_m^2}{Dc^2}$. Incorporating the experimentally determined saturation
8
9
10 378 adsorption values from Table 1, a bulk surfactant concentration of 2.5×10^{-3} mol L⁻¹, and
11
12 379 diffusion coefficients of 5×10^{-10} m² s⁻¹ for ALS, [45] and 1×10^{-10} m² s⁻¹ [46] for CTAB, the
13
14 380 characteristic timescale of solutal Marangoni becomes ~ 0.2 ms for ALS and ~ 2 ms for CTAB.
15
16
17 381 The order of magnitude difference in τ_M implies that the time required for interfacially adsorbed
18
19 382 ALS molecules to respond and dampen interfacial tension fluctuation is far faster than that of
20
21
22 383 CTAB molecules.
23
24

25 384 Regarding the flows observed in the coalescence of binary droplets with asymmetric
26
27 385 compositions, the differences in interfacial motion between surfactants can be directly attributed
28
29
30 386 to the magnitudes of the surfactant molecule's corresponding τ_M values. The timescale of solutal
31
32 387 Marangoni convection is shorter than the characteristic coalescence timescale for two water
33
34 388 droplets of equal diameters and interfacial tensions in the inertial regime for ALS (i.e., $\tau_M < \tau_C$).
35
36
37 389 The driving energy for solutal Marangoni-driven convection is therefore relatively low because
38
39 390 interfacial relaxation toward a homogenous interfacial tension along the coalescing bridge occurs
40
41 391 faster than the time required for droplets to completely merge. In contrast, these timescales are
42
43 392 very close in magnitude for systems containing CTAB (i.e., $\tau_M \approx \tau_C$). Thus, for CTAB molecules,
44
45 393 relaxation toward homogenous interfacial tension takes much longer and is on the order of the
46
47 394 time required for droplets to merge, which leads to the development of strong Marangoni-driven
48
49 395 convection and competing bulk and interfacial flows.
50
51
52
53
54
55 396 *3.3. Surfactant interfacial spreading properties under an induced concentration gradient*
56
57
58
59
60
61
62
63
64
65

1
2
3
4 397 Figure 8 shows the distance tracer particles travel as a function of time at the (initially)
5
6 398 pure triglyceride oil-water interface following the introduction of a 2.5×10^{-3} mol L⁻¹ aqueous
7
8 399 droplet solution of either anionic ALS or cationic CTAB. These data represent the fully-
9
10 400 developed motion of the particles, starting 6.5 ms after the introduction of surfactant into the
11
12
13
14
15



37
38
39
40
41
42
43
44
45
46
47
48
49
50
51
52
53
54
55
56
57
58
59
60
61
62
63
64
65 **Figure 8.** Seeded tracer particle displacement, $\Delta s_{\text{particle}}$, versus time, t , following the introduction of a 2.5×10^{-3} mol L⁻¹ aqueous droplet solution of anionic ALS or cationic CTAB surfactant at a planar triglyceride oil-water interface. Motion of the interfacially seeded tracer particles resulted directly from the induced surfactant concentration gradient of either ALS or CTAB. Data are shown for fully developed particle displacement rates, 6.5 milliseconds after initial contact between the surfactant-laden drop and the planar oil water interface.

401 pure oil-water interface.

402 These data show a clear difference in the steady-state spreading velocities, U_s , of seeded
403 glass spheres under the induced concentration gradient (i.e. for ALS: $U_s = 0.202$ m s⁻¹; for
404 CTAB, $U_s = 0.333$ m s⁻¹) which implies that the surface motion driven by unbalanced interfacial
405 tensions in the presence of cationic CTAB molecules exceeds that of ALS molecules. Taking the
406 initial droplet diameter, $2R$ (= 2 mm), as the characteristic length scale, an estimation of the
407 characteristic timescale for the oil-water interface to deform under the induced surfactant

1
2
3
4 408 concentration gradient can be obtained from $\tau_D = 2R/U_s$. Approximations of τ_D yield 10 ms for
5
6 409 ALS, and 6 ms for CTAB. These calculations for the characteristic timescales of interfacial
7
8 410 deformation under and induced surfactant concentration gradient provide additional evidence
9
10 411 that ALS molecules express a lower driving energy for solutal Marangoni-driven convection in
11
12 412 comparison to CTAB molecules. As the driving energy for solutal Marangoni convection is
13
14 413 lower for ALS, the overall motion of solutes attached to an oil-water interface when subjected to
15
16 414 a concentration gradient would be expected to be influenced less by gradients in surfactant
17
18 415 concentration because such gradients are short-lived.
19
20
21
22
23
24 416 The primary difference between the between measuring the interfacial spreading
25
26 417 properties that develop in a droplet-planar coalescence system as opposed to a droplet-droplet
27
28 418 system is the direction of the generated bulk flow between the aqueous droplet and planar water
29
30 419 reservoir upon coalescence. In the case of the droplet-planar interface arrangement, the capillary
31
32 420 pressure ratio, $\Delta P_2/\Delta P_1$ (where ΔP_1 and ΔP_2 are the capillary pressures for the surfactant-laden
33
34 421 droplet and planar water reservoir, respectively), would approach zero because of the
35
36 422 approximately infinite radius of curvature of the planar water reservoir. This would in turn
37
38 423 produce a driving energy for bulk fluid motion to propagate from the surfactant-laden droplet
39
40 424 into the surfactant-free, planar reservoir. This bulk fluid behavior stands in contrast to the bulk
41
42 425 flows observed and quantified in Section 3, where bulk fluid motion was driven from the
43
44 426 surfactant-free droplet into the surfactant-laden droplet due to the capillary pressure gradient.
45
46 427 However, Marangoni-induced interfacial flows always act in the direction of the interfacial
47
48 428 solute concentration gradient [19] and occur on a shorter timescale than bulk flows. Thus, the
49
50 429 measured values for the interfacial spreading velocities (i.e. the Marangoni-induced interfacial
51
52 430 flowrates) would presumably be minimally influenced by the experimental arrangement.
53
54
55
56
57
58
59
60
61
62
63
64
65

1
2
3
4 431 It is worth noting once again that this difference in interfacial spreading was observed for
5
6 432 two surfactants with distinct chemical architectures, which both reduced the interfacial tension of
7
8 433 the pure triglyceride oil-water interface to approximately 3 mN m^{-1} at a high bulk concentration.
9
10
11 434 The observed differences in interfacial spreading and jetting behavior during the coalescence of
12
13 435 binary droplets with nonuniform compositional properties must be explained by additional
14
15 436 interfacial relaxation mechanisms, which have not previously been studied in detail by the recent
16
17 437 literature.
18
19
20
21

22 438 **4. Summary and Conclusion**

23
24

25 439 Direct observation of the bulk flows generated during the coalescence of binary water-in-
26
27 440 oil droplets with non-uniform physical properties and characterization of the contributive
28
29 441 surfactant-induced interfacial phenomenon was performed. Mechanisms responsible for the
30
31 442 observed opposing interfacial and bulk flows between merging surfactant-laden and surfactant-
32
33 443 free droplets were also described. Fluid jets that developed during binary droplet coalescence
34
35 444 were a direct result of convection driven solutal Marangoni flows which generated a rapid
36
37 445 redistribution of low interfacial tension bulk fluid around the perimeter of the high interfacial
38
39 446 tension bulk fluid. The degree of interfacial spreading and bulk fluid redistribution was greater
40
41 447 for cationic CTAB molecules compared to ALS molecules due to stark differences in their
42
43 448 equilibrium adsorption values, kinetic re-adsorptive rates during droplet coalescence, and overall
44
45 449 tendency for expressing solutal Marangoni convection.
46
47
48
49
50

51
52 450 This work stands in contrast to work of previous researchers in that control over bulk
53
54 451 flows during the coalescence of binary water droplets was induced entirely through optimized
55
56 452 surfactant selection, with no need for modulation of the bulk viscosities of the outer or inner
57
58 453 liquid phases. Our experimental results provide additional experimental confirmation that the
59
60
61
62
63
64
65

1
2
3
4 454 governing power-law relationship for coalescing droplets in the inertial regime is obeyed in the
5
6 455 presence of an induced surfactant concentration gradient, but the prefactor in this relationship is
7
8 456 strongly dependent upon the interfacial properties of the added surfactant.
9
10
11

12 457 The analyses and relationships outlined in this work can be generalized for many
13
14 458 different surfactant types, including anionic or cationic surfactants with longer alkyl chains than
15
16 459 those investigated here, nonionic surfactants with various alkyl tail lengths, and zwitterionic
17
18 460 surfactants. The parameters which are expected to shorten the timescale of solutal Marangoni-
19
20 461 convection (while decreasing its driving energy) include the surfactant's diffusion coefficient
21
22 462 and bulk concentration, while equilibrium interfacial saturation adsorption is the primary
23
24 463 contributor in extending the timescale of solutal Marangoni convection. Thus, enhancing the
25
26 464 bulk mixing of binary drops with an induced concentration gradient can be done by selecting a
27
28 465 surfactant that packs densely at the immiscible fluid interface and adsorbs to the interface
29
30 466 strongly. Zwitterionic and polymeric surfactant would likely be ideal candidates for such
31
32 467 applications due to their relatively small diffusion coefficients and dense interfacial organization
33
34 468 capabilities. [47]
35
36
37
38
39
40
41

42 469 One of the most advantageous applications of using the controlled coalescence of
43
44 470 droplets with asymmetric properties is in the synthesis of functional nanoparticles. Recently,
45
46 471 Frenz et al. [27] demonstrated that magnetic iron oxide nanoparticles could be precipitated in a
47
48 472 highly reproducible reaction following the fusion of droplet pairs consisting of different reagents
49
50 473 in a hydrodynamically coupled, single-nozzle microfluidic device. Controlled pairwise mixing of
51
52 474 aqueous droplets in oil was produced by electrocoalescence [48] and the droplets were prevented
53
54 475 from fusing prematurely by using a uniformly distributed surfactant at the interfaces of both
55
56 476 droplets. The methodology developed by these researchers could be readily adapted to
57
58
59
60
61
62
63
64
65

1
2
3
4 477 incorporate the findings of the present manuscript by isolating the surfactant to one of the inlet
5
6 478 droplet flows, while leaving the other surfactant-free. Upon merging, Marangoni-induced flows
7
8 479 would produce pronounced bulk mixing between the drops, like those explored here. Moreover,
9
10 480 enhanced control over the degree of mixing obtained between the drops at different timescales
11
12 481 could be explored with the previously discussed surfactant selection criteria.
13
14
15
16

17 482 In this study, we proposed a simple, yet robust experimental methodology for directly
18
19 483 quantifying the solutal Marangoni timescales of surface active compounds at the oil-water
20
21 484 interface under an induced concentration gradient. With this method, the spreading efficiencies
22
23 485 and encouragement of bulk fluid mixing for potentially any surfactant type at the oil water
24
25 486 interface can be economically measured. The insights garnered from this work provide a
26
27 487 compelling alternative route for inducing bulk flows in microfluidic devices without the need for
28
29 488 modulating bulk phase viscosities.
30
31
32
33
34

35 489 **Acknowledgements**
36
37

38 490 Financial support for this work was provided by the National Science Foundation through
39
40 491 the East Asia and Pacific Summer Institutes (EAPSI) Fellowship Program (Award Number:
41
42 492 1713936). The authors would also like to thank the anonymous reviewer whose thorough
43
44 493 comments and suggestions led to a substantially improved manuscript.
45
46
47
48
49
50
51
52
53
54
55
56
57
58
59
60
61
62
63
64
65

1
2
3
4 494 **References**
5
6 495 [1] J.D. Paulsen, Approach and coalescence of liquid drops in air, *Phys. Rev. E - Stat.*
7 496 *Nonlinear, Soft Matter Phys.* 88 (2013) 1–13. doi:10.1103/PhysRevE.88.063010.
8
9 497 [2] J. Qian, C.K. Law, Regimes of coalescence and separation in droplet collision, *J. Fluid*
10 498 *Mech.* 331 (1997) 59–80.
11
12 499 [3] J.D. Paulsen, R. Carmignani, A. Kannan, J.C. Burton, S.R. Nagel, Coalescence of
13 500 bubbles and drops in an outer fluid, *Nat. Commun.* 5 (2014) 3182.
14 501 doi:10.1038/ncomms4182.
15
16 502 [4] J. Eggers, J.R. Lister, H.A. Stone, Coalescence of Liquid Drops, (1999) 1–37.
17 503 doi:10.1017/S002211209900662X.
18
19 504 [5] L. Duchemin, J. Eggers, C. Josserand, Inviscid coalescence of drops, *J. Fluid Mech.* 487
20 505 (2003) 167–178. doi:10.1017/S0022112003004646.
21
22 506 [6] D.T. Wasan, The Role of Coalescence Phenomena and Interfacial Rheological Properties
23 507 in Enhanced Oil Recovery: An Overview, *J. Rheol. (N. Y. N. Y.)* 23 (1979) 181.
24 508 doi:10.1122/1.549524.
25
26 509 [7] S. Tcholakova, N.D. Denkov, T. Banner, Role of surfactant type and concentration for the
27 510 mean drop size during emulsification in turbulent flow, *Langmuir*. 20 (2004) 7444–7458.
28 511 doi:10.1021/la049335a.
29
30 512 [8] A.M. Huebner, C. Abell, W.T.S. Huck, C.N. Baroud, F. Hollfelder, Monitoring a reaction
31 513 at submillisecond resolution in picoliter volumes, *Anal. Chem.* 83 (2011) 1462–1468.
32 514 doi:10.1021/ac103234a.
33
34 515 [9] J.H. Kim, T.Y. Jeon, T.M. Choi, T.S. Shim, S.H. Kim, S.M. Yang, Droplet microfluidics
35 516 for producing functional microparticles, *Langmuir*. 30 (2014) 1473–1488.
36 517 doi:10.1021/la403220p.
37
38 518 [10] A.B. Pawar, M. Caggioni, R. Ergun, R.W. Hartel, P.T. Spicer, Arrested coalescence in
39 519 Pickering emulsions, *Soft Matter*. 7 (2011) 7710. doi:10.1039/c1sm05457k.
40
41 520 [11] P. Dahiya, M. Caggioni, P.T. Spicer, Arrested coalescence of viscoelastic droplets:
42 521 Polydisperse doublets, *Philos. Trans. R. Soc. A Math. Phys. Eng. Sci.* 374 (2016) 1–13.
43 522 doi:10.1098/rsta.2015.0132.
44
45 523 [12] K. Ward, Z.H. Fan, Mixing in microfluidic devices and enhancement methods, *J.*
46 524 *Micromechanics Microengineering*. 25 (2015) 094001. doi:10.1088/0960-
47 525 1317/25/9/094001.
48
49 526 [13] T. Tofteberg, M. Skolimowski, E. Andreassen, O. Geschke, A novel passive micromixer:
50 527 Lamination in a planar channel system, *Microfluid. Nanofluidics*. 8 (2010) 209–215.
51 528 doi:10.1007/s10404-009-0456-z.
52
53 529 [14] T.J. Johnson, D. Ross, L.E. Locascio, Rapid microfluidic mixing, *Anal. Chem.* 74 (2002)
54 530 45–51. doi:10.1021/ac010895d.
55
56 531 [15] T. Krebs, C.G.P.H. Schroën, R.M. Boom, Coalescence kinetics of oil-in-water emulsions
57
58
59
60
61
62
63
64
65

1
2
3
4 532 studied with microfluidics, *Fuel.* 106 (2013) 327–334. doi:10.1016/j.fuel.2012.10.067.
5
6 533 [16] A. Arbor, G. Tryggvason, The Flow Induced by the Coalescence of Two Initially
7 534 Stationary Drops, *Nasa Tech. Memo.* (1994).
8
9 535 [17] E. Nowak, N.M. Kovalchuk, Z. Che, M.J.H. Simmons, Effect of surfactant concentration
10 536 and viscosity of outer phase during the coalescence of a surfactant-laden drop with a
11 537 surfactant-free drop, *Colloids Surfaces A Physicochem. Eng. Asp.* 505 (2016) 124–131.
12 538 doi:10.1016/j.colsurfa.2016.02.016.
13
14
15 539 [18] E. Nowak, Z. Xie, N.M. Kovalchuk, O.K. Matar, M.J.H. Simmons, Bulk advection and
16 540 interfacial flows in the binary coalescence of surfactant-laden and surfactant-free drops,
17 541 *Soft Matter.* 13 (2017) 4616–4628. doi:10.1039/C7SM00328E.
18
19 542 [19] C. V. Sternling, L.E. Scriven, Interfacial turbulence: Hydrodynamic instability and the
20 543 marangoni effect, *AIChE J.* 5 (1959) 514–523. doi:10.1002/aic.690050421.
21
22 544 [20] L.E. Scriven, C. V. Sternling, The Marangoni Effects, *Nature.* 187 (1960) 186–188.
23 545 doi:10.1038/187186a0.
24
25 546 [21] D.T. Wasan, Destabilization of Water-in-Oil Emulsions, in: *Emuls. - A Fundam. Pract.*
26 547 Approach, 1992: pp. 283–295.
27
28 548 [22] M. Saad Bhamla, C. Chai, M.A. Àlvarez-Valenzuela, J. Tajuelo, G.G. Fuller, Interfacial
29 549 mechanisms for stability of surfactant-laden films, *PLoS One.* 12 (2017) 1–14.
30 550 doi:10.1371/journal.pone.0175753.
31
32
33 551 [23] K. Szymczyk, B. Jańczuk, The adsorption at solution-air interface and volumetric
34 552 properties of mixtures of cationic and nonionic surfactants, *Colloids Surfaces A*
35 553 *Physicochem. Eng. Asp.* 293 (2007) 39–50. doi:10.1016/j.colsurfa.2006.07.006.
36
37 554 [24] B. Jańczuk, A. Zdziennicka, W. Wójcik, The properties of mixtures of two anionic
38 555 surfactants in water at the water | air interface, *Colloids Surfaces A Physicochem. Eng.*
39 556 *Asp.* 220 (2003) 61–68. doi:10.1016/S0927-7757(03)00060-8.
40
41 557 [25] S.D. Hudson, A.M. Jamieson, B.E. Burkhardt, The effect of surfactant on the efficiency of
42 558 shear-induced drop coalescence, *J. Colloid Interface Sci.* 265 (2003) 409–421.
43 559 doi:10.1016/S0021-9797(03)00396-5.
44
45
46 560 [26] W.H. Weheliye, T. Dong, P. Angeli, On the effect of surfactants on drop coalescence at
47 561 liquid/liquid interfaces, *Chem. Eng. Sci.* 161 (2017) 215–227.
48 562 doi:10.1016/j.ces.2016.12.009.
49
50 563 [27] L. Frenz, A. El Harrak, M. Pauly, S. Bégin-Colin, A.D. Griffiths, J.C. Baret, Droplet-
51 564 based microreactors for the synthesis of magnetic iron oxide nanoparticles, *Angew.*
52 565 *Chemie - Int. Ed.* 47 (2008) 6817–6820. doi:10.1002/anie.200801360.
53
54
55 566 [28] H. Diamant, D. Andelman, Kinetics of Surfactant Adsorption at Fluid-Fluid Interfaces, *J.*
56 567 *Phys. Chem.* 100 (1996) 13732–13742. doi:10.1021/jp960377k.
57
58 568 [29] K. Eliceiri, C.A. Schneider, W.S. Rasband, K.W. Eliceiri, NIH Image to ImageJ : 25 years
59 569 of image analysis, *Nat. Methods.* 9 (2012) 671–675. doi:10.1038/nmeth.2089.

1
2
3
4 570 [30] D.F. Evans, H. Wennerström, *The Colloidal Domain: Where Physics, Chemistry, Biology,*
5 571 and Technology Meet, 2nd ed., 1999.
6
7 572 [31] J.J. Nash, K.A. Erk, Stability and interfacial viscoelasticity of oil-water nanoemulsions
8 573 stabilized by soy lecithin and Tween 20 for the encapsulation of bioactive carvacrol,
9 574 *Colloids Surfaces A Physicochem. Eng. Asp.* 517 (2017) 1–11.
10 575 doi:10.1016/j.colsurfa.2016.12.056.
11
12
13 576 [32] J.D. Berry, M.J. Neeson, R.R. Dagastine, D.Y.C. Chan, R.F. Tabor, Measurement of
14 577 surface and interfacial tension using pendant drop tensiometry, *J. Colloid Interface Sci.*
15 578 454 (2015) 226–237. doi:10.1016/j.jcis.2015.05.012.
16
17 579 [33] G. Loglio, P. Pandolfini, R. Miller, A. V. Makievska, F. Ravera, M. Ferrari, L. Liggieri,
18 580 Drop and bubble shape analysis as a tool for dilational rheological studies of interfacial
19 581 layers, in: D. Möbius, R. Miller (Eds.), *Nov. Methods to Study Interfacial Layers*,
20 582 Elsevier, 2001: pp. 439–483. doi:10.1016/S1383-7303(01)80038-7.
21
22
23 583 [34] K.H. Kang, H.U. Kim, K.H. Lim, Effect of temperature on critical micelle concentration
24 584 and thermodynamic potentials of micellization of anionic ammonium dodecyl sulfate and
25 585 cationic octadecyl trimethyl ammonium chloride, *Colloids Surfaces A Physicochem. Eng.*
26 586 *Asp.* 189 (2001) 113–121. doi:10.1016/S0927-7757(01)00577-5.
27
28 587 [35] V. Mosquera, J.M. Del Río, D. Attwood, M. García, M.N. Jones, G. Prieto, M.J. Suarez,
29 588 F. Sarmiento, A study of the aggregation behavior of hexyltrimethylammonium bromide
30 589 in aqueous solution, *J. Colloid Interface Sci.* 206 (1998) 66–76.
31 590 doi:10.1006/jcis.1998.5708.
32
33
34 591 [36] T.G. Movchan, A.I. Rusanov, I. V Soboleva, N.R. Khlebunova, E. V Plotnikova, A.K.
35 592 Shchekin, *Diffusion Coefficients of Ionic Surfactants*, *Colloid J.* 77 (2015) 492–499.
36 593 doi:10.1134/S1061933X15040146.
37
38 594 [37] M.J. Rosen, *Surfactants and Interfacial Phenomena*, 3rd ed., John Wiley & Sons, Inc.,
39 595 2004.
40
41 596 [38] J. Eastoe, S. Nave, A. Downer, A. Paul, A. Rankin, J. Penfold, *Adsorption of Ionic*
42 597 *Surfactants at the Air - Solution Interface*, *Langmuir*. 16 (2000) 4511–4518.
43 598 doi:10.1021/la991564n.
44
45 599 [39] B.J. Park, J. Pantina, E.M. Furst, M. Oettel, S. Reynaert, *Direct Measurements of the*
46 600 *Effects of Salt and Surfactant on Interaction Forces between Colloidal Particles at Water-*
47 601 *Oil Interfaces*, *Langmuir*. 24 (2008) 1686–1694. doi:10.1021/la7008804.
48
49
50 602 [40] B.P. Binks, *Particles as surfactants - Similarities and differences*, *Curr. Opin. Colloid*
51 603 *Interface Sci.* 7 (2002) 21–41. doi:10.1016/S1359-0294(02)00008-0.
52
53 604 [41] M. Wu, T. Cubaud, C. Ho, *Scaling law in liquid drop coalescence driven by surface*
54 605 *tension*, *Phys. Fluids*. 16 (2004) 51–54. doi:10.1063/1.1756928.
55
56 606 [42] S.J. Rehfeld, *Adsorption of Sodium Dodecyl Sulfate at Various Hydrocarbon-Water*
57 607 *Interfaces*, *J. Phys. Chem.* 71 (1967) 738–745. doi:10.1021/j100862a039.
58
59 608 [43] V.B. Fainerman, E. V. Aksenenko, N. Mucic, A. Javadi, R. Miller, *Thermodynamics of*
60
61
62
63
64
65

1
2
3
4 609 adsorption of ionic surfactants at water/alkane interfaces, *Soft Matter*. 10 (2014) 6873–
5 610 6887. doi:10.1039/C4SM00463A.
6

7 611 [44] A. Prins, C. Arcuri, M. Van den Tempel, *Elasticity of Thin Liquid Films*, *J. Colloid*
8 612 *Interface Sci.* 24 (1967) 84–90. doi:10.1016/0021-9797(67)90281-0.
9

10 613 [45] A. Javadi, N. Mucic, D. Vollhardt, V.B. Fainerman, R. Miller, Effects of dodecanol on the
11 614 adsorption kinetics of SDS at the water–hexane interface, *J. Colloid Interface Sci.* 351
12 615 (2010) 537–541. doi:10.1016/j.jcis.2010.07.033.
13

14 616 [46] C. Stubenrauch, V.B. Fainerman, E. V Aksenenko, R. Miller, Adsorption behavior and
15 617 dilatational rheology of the cationic alkyl trimethylammonium bromides at the water/air
16 618 interface, *J. Phys. Chem. B*. 109 (2005) 1505–1509. doi:10.1021/jp0465251.
17

18 619 [47] V. Seredyuk, E. Alami, M. Nydén, K. Holmberg, A. V. Peresypkin, F.M. Menger,
19 620 Adsorption of zwitterionic gemini surfactants at the air-water and solid-water interfaces,
20 621 *Colloids Surfaces A Physicochem. Eng. Asp.* 203 (2002) 245–258. doi:10.1016/S0927-
21 622 7757(01)01106-2.
22

23 623 [48] K. Ahn, J. Agresti, H. Chong, M. Marquez, D.A. Weitz, Electrocoalescence of drops
24 624 synchronized by size-dependent flow in microfluidic channels, *Appl. Phys. Lett.* 88
25 625 (2006). doi:10.1063/1.2218058.
26

27 626
28
29
30

31

32

33

34

35

36

37

38

39

40

41

42

43

44

45

46

47

48

49

50

51

52

53

54

55

56

57

58

59

60

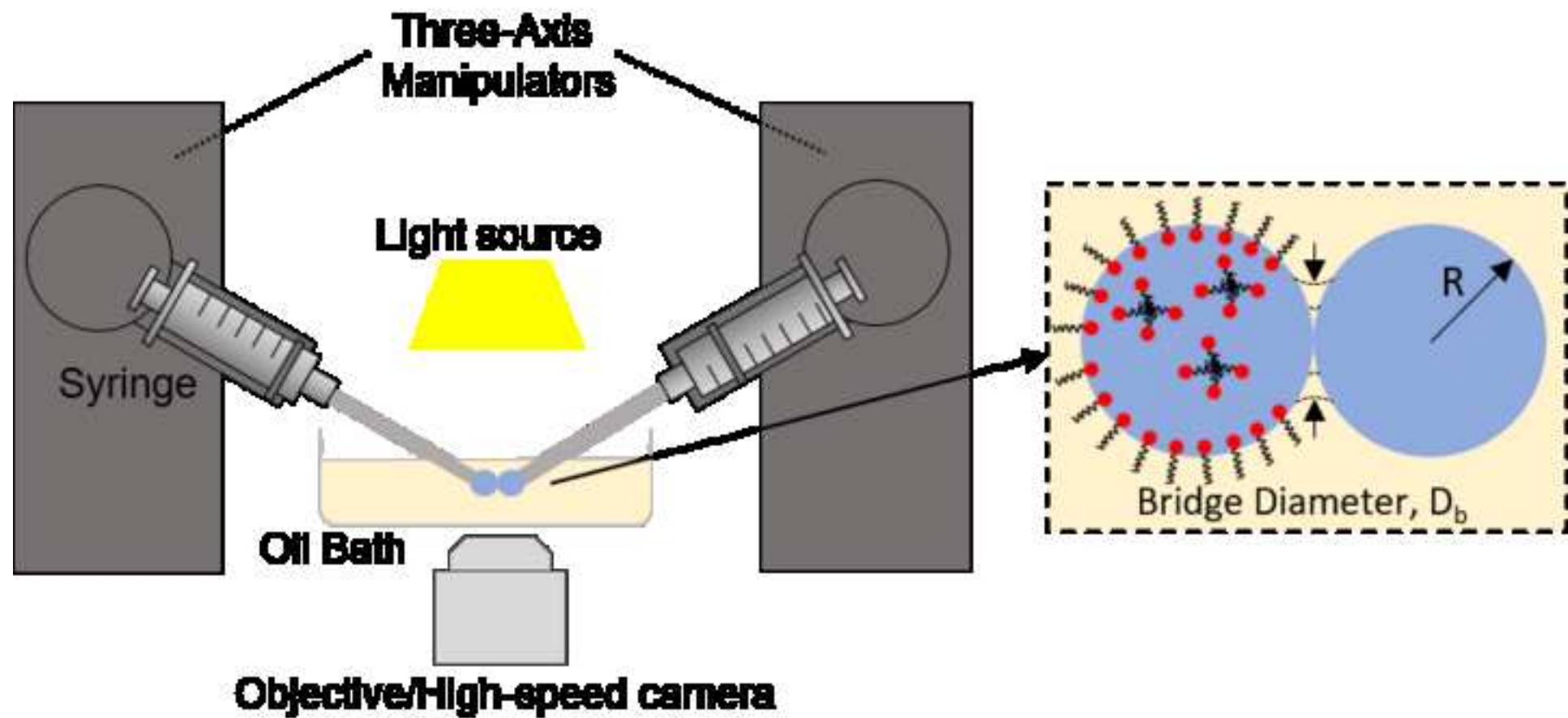
61

62

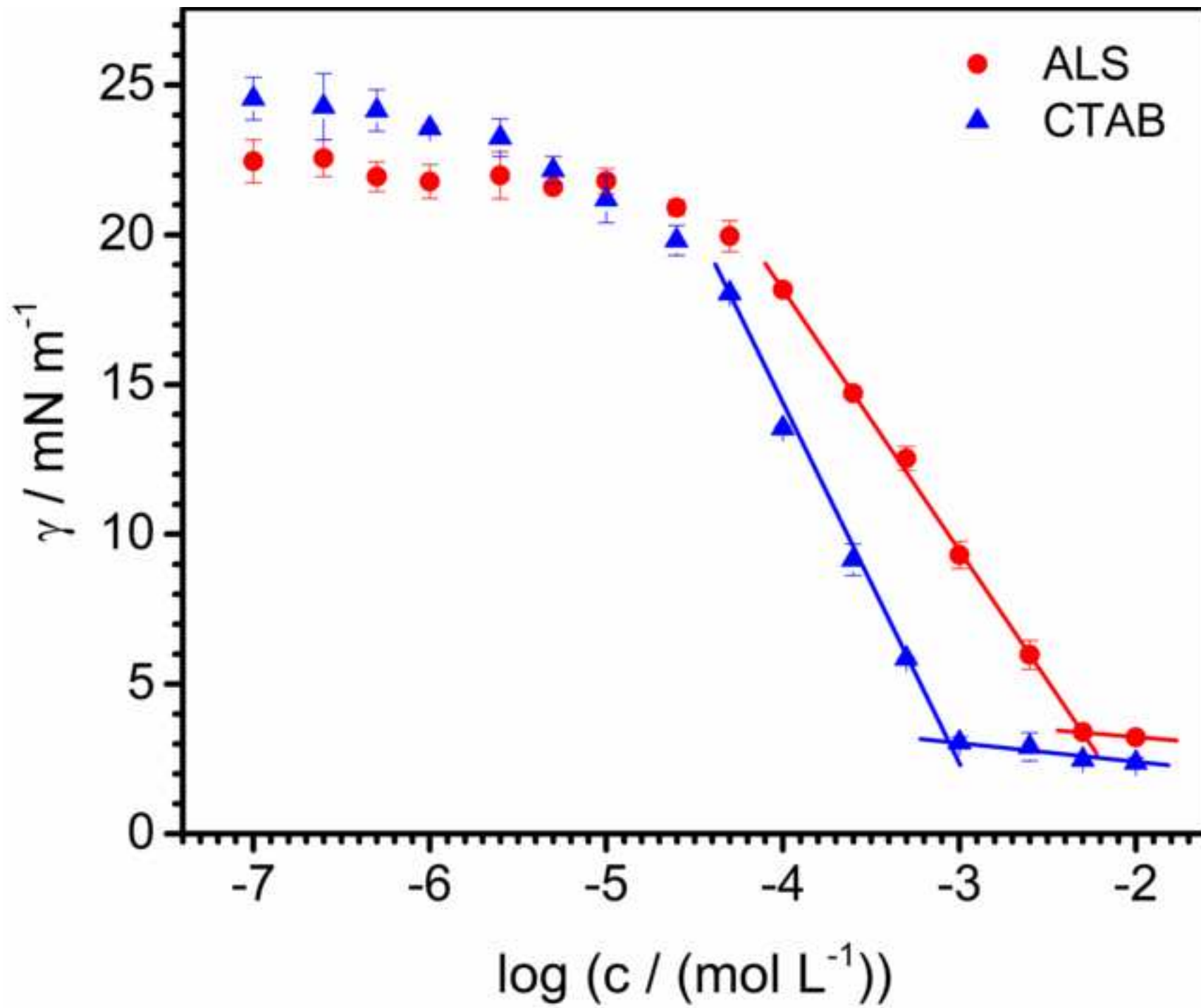
63

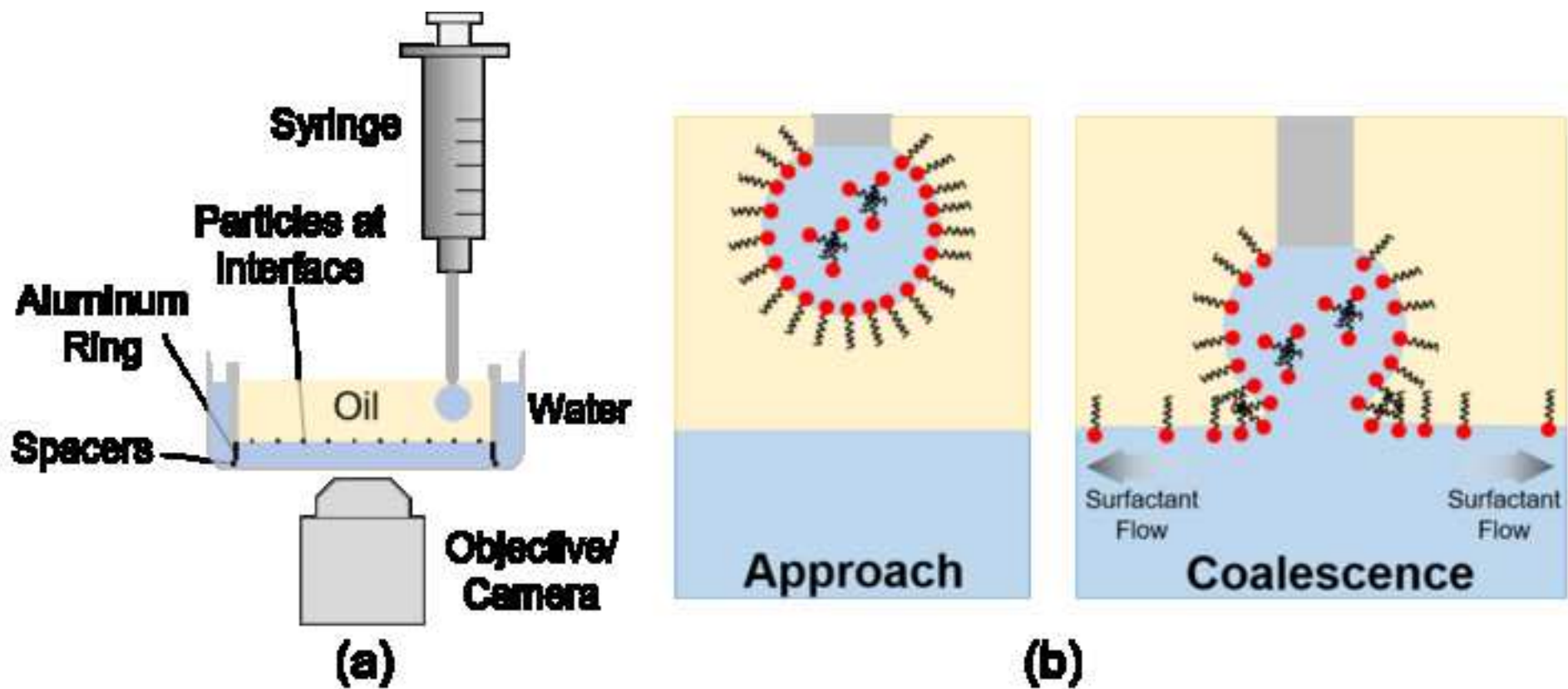
64

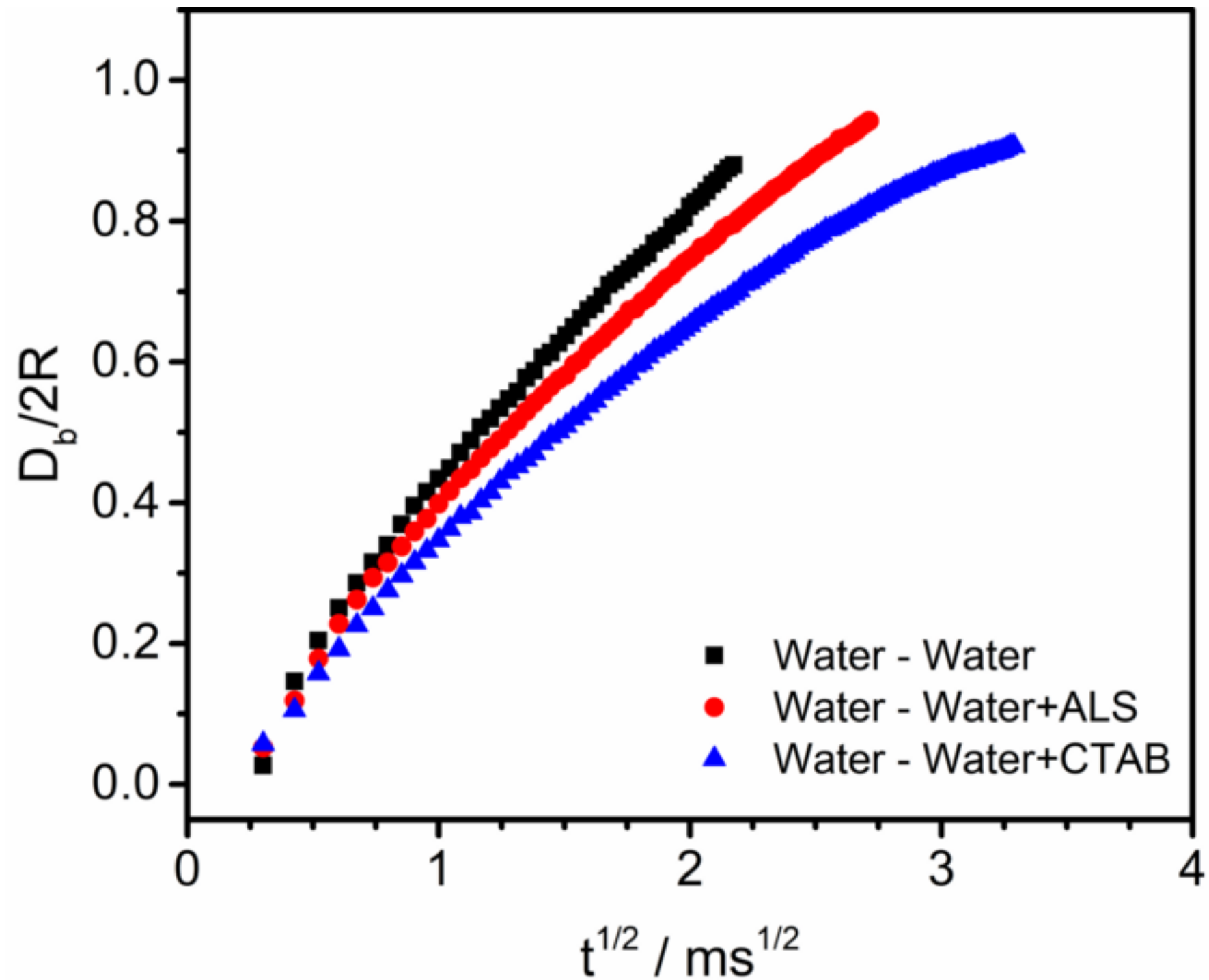
65



5: Figure

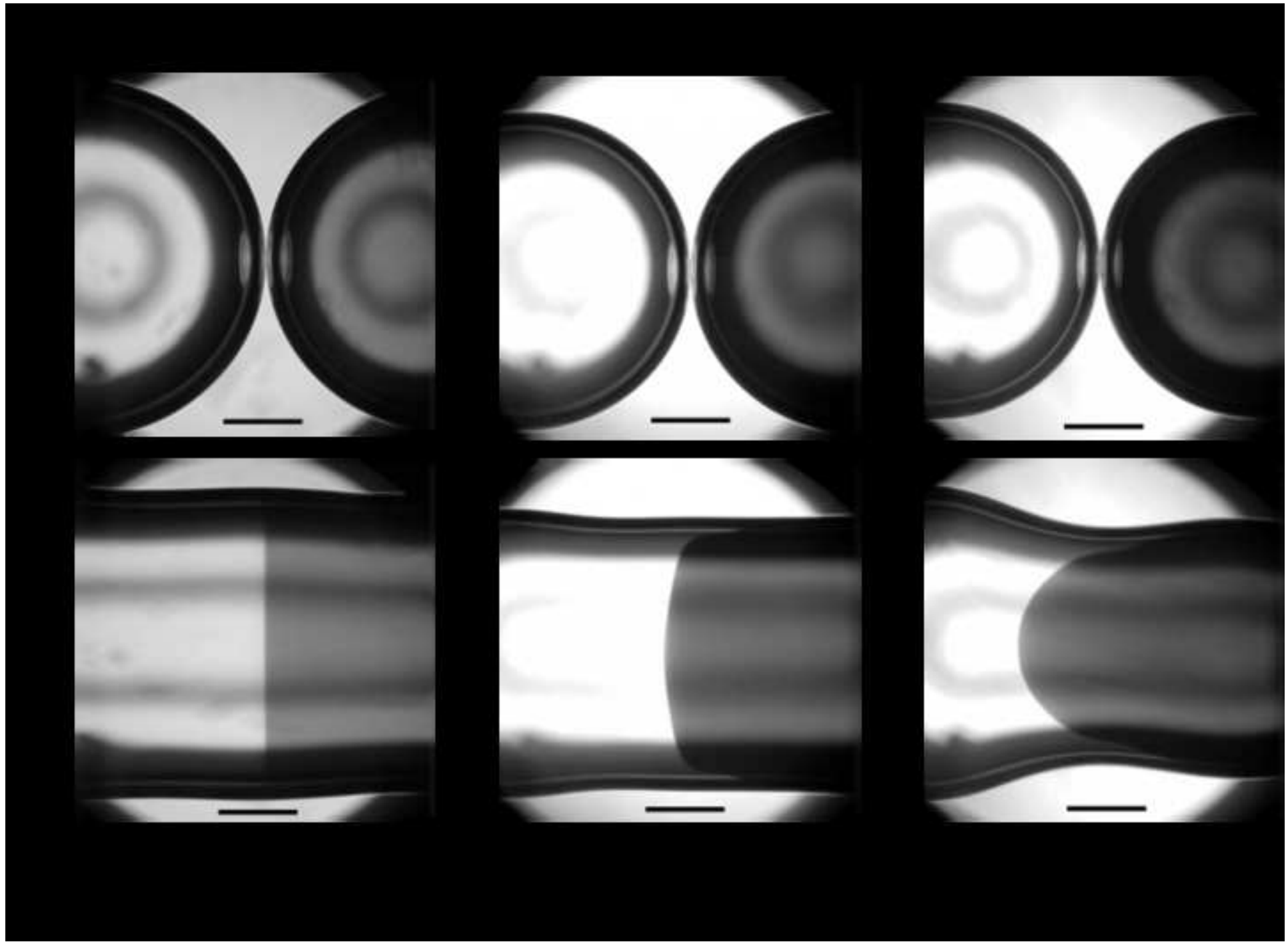
[Click here to download high resolution image](#)





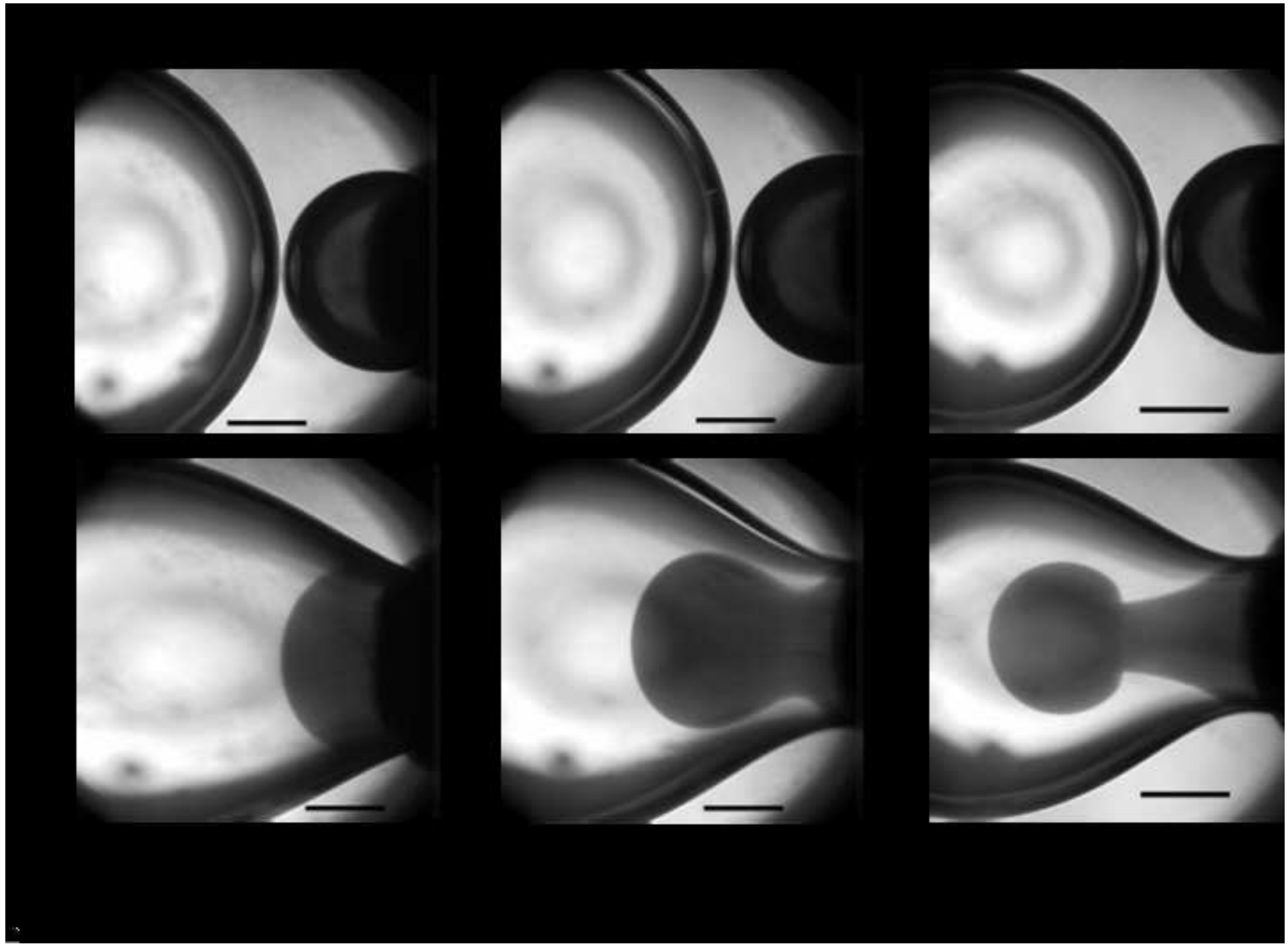
5: Figure

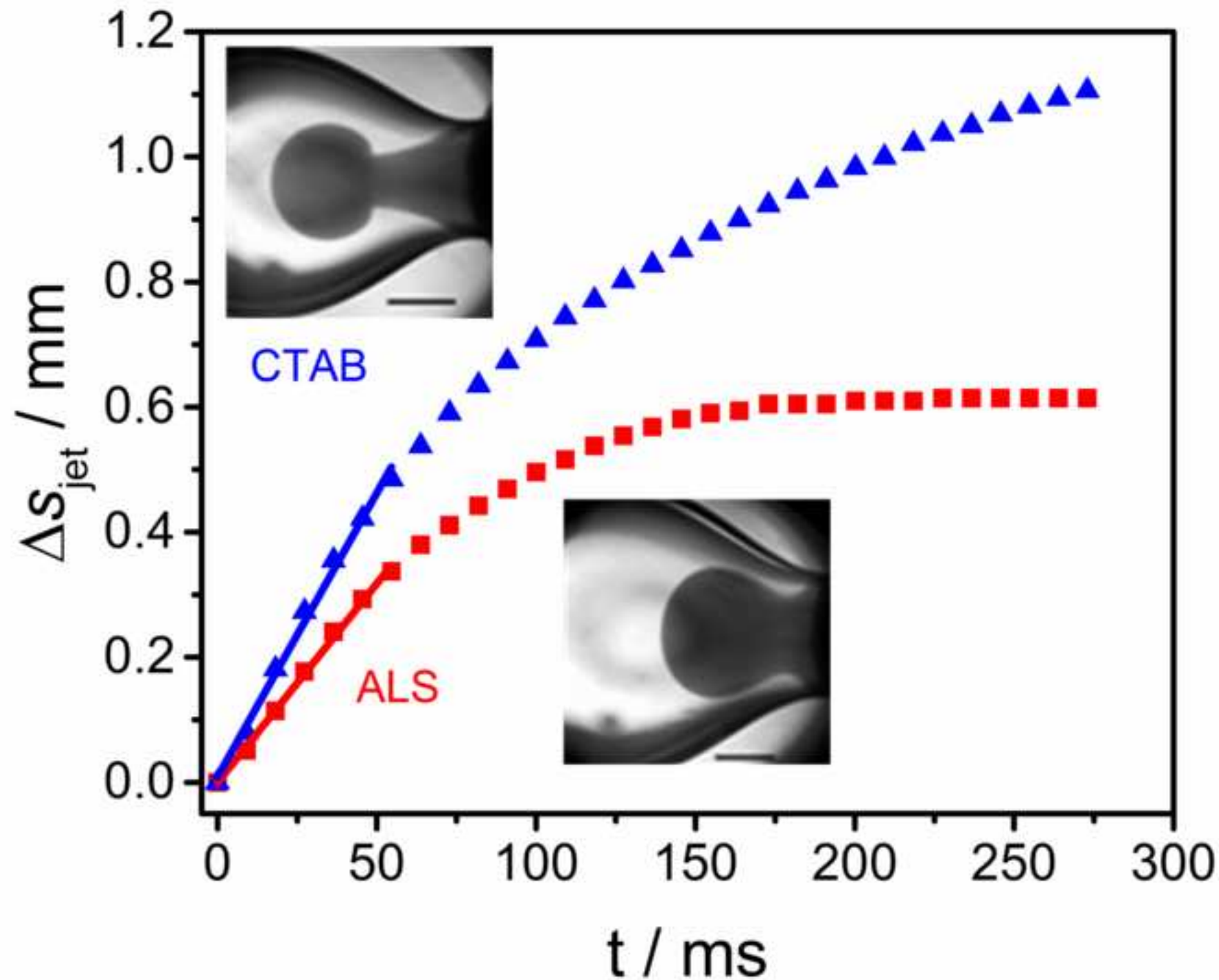
[Click here to download high resolution image](#)



5: Figure

[Click here to download high resolution image](#)





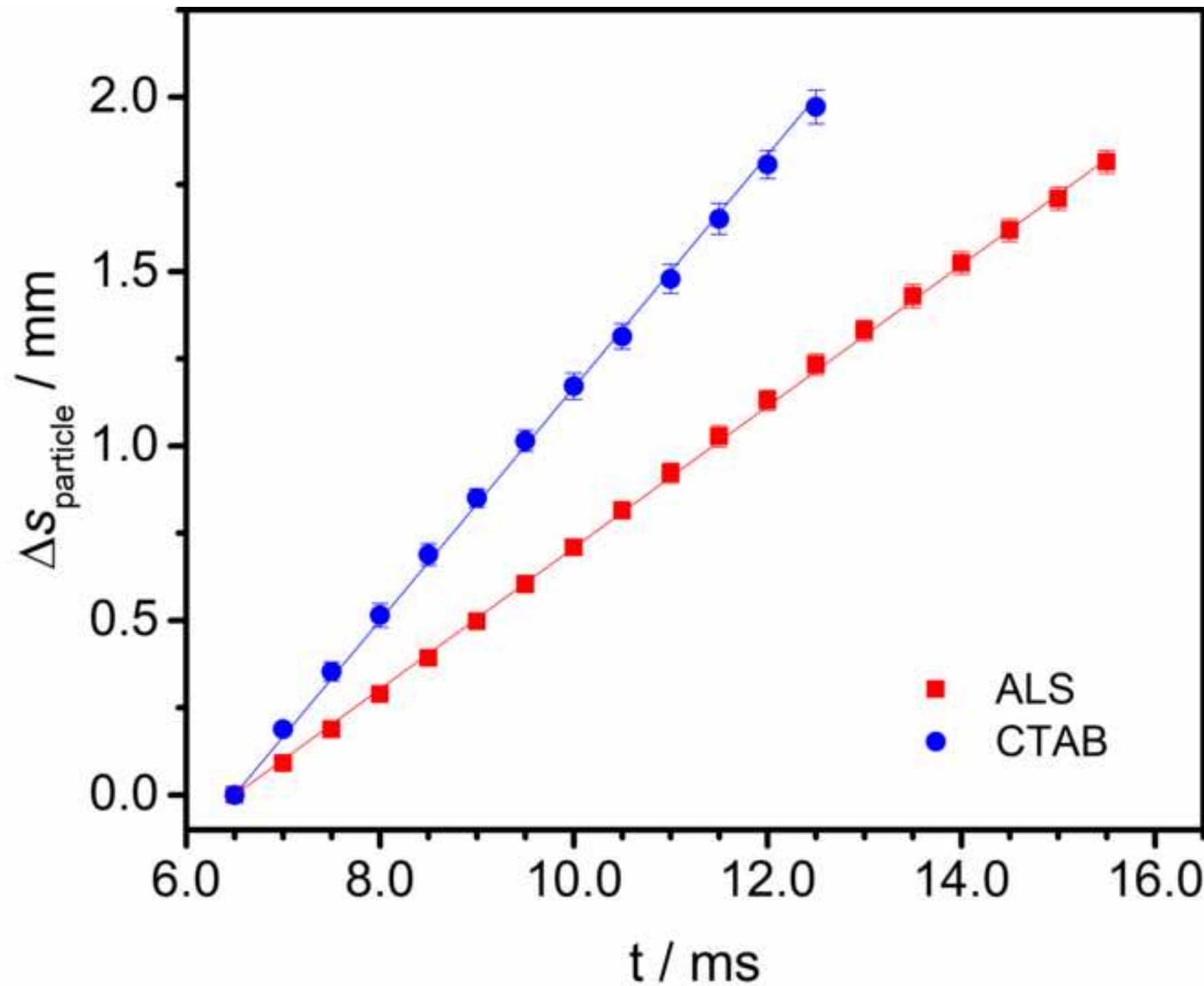


Table 1. Surface excess concentrations and minimum molecular areas calculated for ALS and CTAB at 23 °C at the triglyceride oil-water interface.

Surfactant	Surface Excess Concentration, $\Gamma_m/(10^{-6} \text{ mol m}^{-2})$	Minimum Molecular Area, $A_{\min}/(\text{\AA}^2 \text{ molecule}^{-1})$
Ammonium Lauryl Sulfate (ALS)	0.76	218
Cetyltrimethylammonium bromide (CTAB)	1.07	156